

4-1-2022

Noninvasive *in vivo* Optoacoustic Imaging of Alcohol Use Disorder Using a Mouse Model of Alcohol Use Disorder

Augustine Meombe Mbolle
University of South Florida

Follow this and additional works at: <https://digitalcommons.usf.edu/etd>



Part of the [Bioimaging and Biomedical Optics Commons](#), and the [Neurosciences Commons](#)

Scholar Commons Citation

Meombe Mbolle, Augustine, "Noninvasive *in vivo* Optoacoustic Imaging of Alcohol Use Disorder Using a Mouse Model of Alcohol Use Disorder" (2022). *USF Tampa Graduate Theses and Dissertations*.
<https://digitalcommons.usf.edu/etd/10329>

This Dissertation is brought to you for free and open access by the USF Graduate Theses and Dissertations at Digital Commons @ University of South Florida. It has been accepted for inclusion in USF Tampa Graduate Theses and Dissertations by an authorized administrator of Digital Commons @ University of South Florida. For more information, please contact digitalcommons@usf.edu.

Noninvasive *in vivo* Optoacoustic Imaging of Alcohol Use Disorder Using a Mouse Model of
Alcohol Use Disorder

by

Augustine Meombe Mbolle

A dissertation submitted in partial fulfillment
of the requirements for the degree of
Doctor of Philosophy
Department of Medical Engineering
College of Engineering
University of South Florida

Major Professor: Huabei Jiang, Ph.D.
Robert Frisina Jr., Ph.D.
William Lee III, Ph.D.
George Spirou, Ph.D.
Brendan Walker, Ph.D.

Date of Approval:
March 30, 2022

Keywords: Chronic Alcoholism, Binge Drinking, Low Intensity Focused Ultrasound,
High Alcohol-Preferring Mice, Neuromodulation

Copyright © 2022, Augustine Meombe Mbolle

Dedication

This dissertation is dedicated to the memory of my late father Chief Mbolle Tulu Williams; the mechanical Engineer that never was for cultivating my sense of curiosity from a young age. I consider myself an open-minded and empathetic person, and I believe that is the case thanks to him.

Acknowledgments

I would like to express my sincere gratitude to my advisor Dr. Huabei Jiang for his mentorship and assistance throughout the course of this program. My sincere gratitude also goes to Dr. Brendan Walker of the Department of Psychiatry and behavioral Neuroscience, Morsani College of Medicine for his guidance. I am indebted to all my dissertation committee members for their advice and guidance throughout.

I am indebted to all my professors, my fellow BME graduate students (Fall 2017 intake), and to all my lab mates for their encouragement. I would like to particularly thank Dr. Hao Yang for his willingness to provide advice on pertinent technical issues whenever I asked.

My appreciation is extended to my family and friends, who accepted, without apparent resentment and with barely any audible complaints, my complete self-isolation during the years in which I totally and shamefully neglected them while doing this work and especially my wife, Valerie, for her love, understanding, support and motivation during this work and always. I am particularly indebted to my mom, Mrs. Mbolle Nongo Sarah Sakwe, for vision about education.

Finally, I convey my gratitude to all thank-worthy people who have supported and encouraged me throughout my academic carrier and my life.

Table of Contents

List of Tables	iv
List of Figures	v
Abstract	vii
Chapter 1: Photoacoustic Imaging Background and Literature	1
1.1 Introduction	1
1.1.1 Brief History of Photoacoustic Imaging	1
1.2 Principle of Photoacoustic Imaging	2
1.2.1 Photoacoustic Signal Generation	4
1.2.1.1 Thermal Confinement Holds	5
1.2.1.2 Stress Confinement Holds	5
1.2.2 Photoacoustic Signal Propagation	6
1.2.3 Photoacoustic Image Reconstruction and Quantification	6
1.2.3.1 Time Domain or Back Projection	8
1.2.3.2 Frequency Domain Algorithms	8
1.2.3.3 Time-Reversal Algorithms	9
1.2.3.4 Numerical Model-Based Algorithms	9
1.3 Photoacoustic Imaging Configurations	10
1.4 Photoacoustic Imaging Instrumentation	10
1.4.1 Optical Excitation	11
1.4.2 Ultrasound Detection	11
1.5 Multispectral Photoacoustic Imaging	12
1.5.1 Spectral Unmixing with Known Spectral Source	13
1.6 References	13
Chapter 2: Alcohol Use Disorder: Background and Literature	16
2.1 Introduction	16
2.2 Alcohol Use Disorder Cycle	17
2.2.1 The Reward Stage	17
2.2.2 Development of Alcohol Tolerance	17
2.2.3 Development of Alcohol Use Disorder	18
2.3 The Neurobiology of Alcohol Use Disorder	18
2.3.1 Brain Neural Groups, Neurotransmitters and Receptors in Alcohol Use Disorder	18
2.3.2 Brain Neural Systems Mediating Alcohol Reinforcement	20
2.4 References	21

Chapter 3: Low Intensity Focused Ultrasound, Background and Literature	24
3.1 Introduction.....	24
3.2 Generation and Physical Characteristics of Ultrasound.....	25
3.3 Low Intensity Focused Ultrasound Literature Review	27
3.4 Design of Ultrasound Transducer	30
3.5 Components of Single Transducer Element	31
3.5.1 Piezoelectric Element (PE)	31
3.5.2 Electrical Connection and Driving System.....	32
3.5.3 Backing Layer.....	33
3.6 Types of Transducers.....	34
3.7 Theoretical Lateral Beam Width at Focus and Sonication Parameters.....	35
3.8 Modelling Studies	36
3.8.1 Results.....	38
3.9 References.....	38
 Chapter 4: Significance and Specific Aims of the Research	 41
4.1 Public Health Relevance of the Research	41
4.2 Scientific Premise of the Research	42
4.3 Technological Significance of the Research.....	45
4.4 Specific Aims.....	47
4.4.1 Aim 1	47
4.4.2 Aim 2	48
4.5 References.....	49
 Chapter 5: Manuscripts.....	 55
5.1 Photoacoustic Imaging for <i>In vivo</i> Quantification of Alcohol Induced Structural and Functional Changes in Cerebral Vasculature in High Alcohol Preferring Mice (HAP).....	 56
5.1.1 Abstract.....	56
5.1.2 Introduction.....	57
5.1.3 Materials and Methods.....	59
5.1.3.1 Imaging System	59
5.1.3.2 Animal Model of Ethanol Dependence and Animal Handling.....	 61
5.1.3.3 PAT Imaging of Alcohol-Induced Changes in Cerebral Vessel Diameter	 63
5.1.3.4 Multispectral Photoacoustic Imaging of Alcohol-Induced Changes in Hemoglobin Oxygen Saturation.....	 64
5.1.4 Results.....	65
5.1.4.1 Extraction and Comparison of Cerebral Vessel Diameter in HAP and LAP Mice.....	 65
5.1.4.2 Estimation of Change in Hemoglobin Oxygen Saturation	67
5.1.5 Discussions	68
5.1.6 References.....	72
5.2 Photoacoustic Imaging Guided System for Repetitive Low Intensity Focused Ultrasound Stimulation for the Treatment of Alcohol Use Disorder	 75

5.2.1 Abstract	75
5.2.2 Introduction.....	76
5.2.3 Method	80
5.2.3.1 System Description	80
5.2.3.2 System Testing.....	82
5.2.3.2.1 Ultrasound Field Characterization	82
5.2.3.2.2 Animal Model of Alcohol Use Disorder.....	84
5.2.3.3 PAT Guided LIFU Stimulation of the Nucleus Accumbens	85
5.2.3.3.1 Animal Handling Procedures and PAT Imaging of NAc	85
5.2.3.3.2 Choice of NAc for In vivo PAT Guided LIFU Stimulation.....	86
5.2.3.3.3 <i>In vivo</i> PAT Guided LIFU Stimulation of the Nucleus Accumbens	87
5.2.4 Results.....	88
5.2.4.1 Ethanol and Water Drinking Following LIFU Stimulation of the NAc.....	88
5.2.4.2 Activation of the NAc Following LIFU Stimulation.....	89
5.2.5 Discussion	90
5.2.6 References.....	92
 Chapter 6: Conclusion.....	 100
 Appendix A: Copyright Permissions	 102
 Appendix B: Ethanol and Water Consumption for LIFU Group.....	 104
 Appendix C: IACUC Approvals.....	 107

List of Tables

Table 2.1 Brain neural groups and the receptors they express	20
Table 3.1 Comparison of current clinical and preclinical stimulation techniques.....	25
Table 3.2 Typical values and units of various ultrasound pulse parameters	27
Table 3.3 Parameters used in the numerical solution of the KZK equation to determine the ultrasound pressure field from our 1.3 MHz transducer	37
Table 5.1 Mean blood ethanol concentration for HAP mice	63
Table 5.2 Summary of vessel diameters for various vessels of interest	67
Table B1 Week 1 drinking data	104
Table B2 Week 2 and 3 drinking data	105
Table B3 Week 4 drinking data	106

List of Figures

Figure 1.1 Schematic of the photoacoustic effect.....	3
Figure 1.2 Absorption spectra of various tissue chromophores.....	5
Figure 1.3 A mind map of the principle of photoacoustic imaging showing the optical and acoustic forward problems as well as the respective inverse problems.....	7
Figure 1.4 Block diagram of a photoacoustic imaging system instrumentation.....	11
Figure 3.1 Definition of various ultrasound pulse parameters.....	26
Figure 3.2 Block diagram of the origin and classification of ultrasound physical effect	29
Figure 3.3 Transmission and reception of acoustic waves by piezoelectric element	31
Figure 3.4 Single element transducers in cross section with all components.....	32
Figure 3.5 Spherically focused transducer.....	35
Figure 3.6 Theoretical beam width at focus from transducer geometric characteristics	36
Figure 3.7 Schematic for modelling ultrasound propagation in a 3 layer media.....	37
Figure 3.8 Distribution of acoustic pressure, intensity, and heat around the focus	38
Figure 5.1 Photoacoustic imaging system for non-invasive in vivo imaging of the cerebral vasculature in alcohol preferring mice.....	59
Figure 5.2 Illustration of the connection of the mouse breathing mask used to keep the mouse under water for photoacoustic imaging	61
Figure 5.3 Mean ethanol consumption per day for Hap and LAP mice	62
Figure 5.4 Estimation and comparison of selected blood vessels between HAP and LAP	66
Figure 5.5 Estimation and comparison of percentage change in vessel diameter and hemoglobin oxygen saturation with time for a selected vessel between HAP and LAP	68

Figure 5.6 Block diagram of the Photoacoustic imaging guided system for repetitive low intensity focus ultrasound stimulation for the treatment of alcohol use disorder in cross high alcohol preferring mice	80
Figure 5.7 Characterization of the acoustic field of a low intensity focused ultrasound transducer	82
Figure 5.8 Modelling of low intensity focused ultrasound distribution through intact mouse brain	83
Figure 5.9 Animal preparation for LIFU stimulation	85
Figure 5.10 PAT setup for LIFU guidance	86
Figure 5.11 Fluid consumption and blood ethanol concentration.....	88
Figure 5.12 Change in PAT signal intensity before, during and after LIFU stimulation	89
Figure 6.1 Acoustic effects of the skull	100

Abstract

This research has two parts. The first part focuses on the use of photoacoustic imaging (PAI) to study alcohol-induced effects in the cerebral vasculature of selectively bred alcohol-preferring mice. Part two extends the application of PAI by developing a novel Photoacoustic imaging guided system for repetitive low intensity focused ultrasound (PAI-LIFU) stimulation treatment for alcohol use disorder in crossed high alcohol preferring (cHAP) mice.

Photoacoustic imaging is an emerging hybrid non-invasive optical imaging modality which relies on optical absorption contrast to visualize deep tissue structures and function. It combines the high contrast associated with pure optical imaging and the high resolution associated with pure ultrasonic imaging, to visualize three dimensional tissues structures, vascular morphology as well as provide functional information with high spatial resolution and excellent contrast.

We exploit the significant difference in optical absorption between hemoglobin, deoxyhemoglobin and the surrounding tissues to image and study the direct effects of ethanol on the cerebrovascular system in selectively bred alcohol preferring mice. Alcohol induced effects, including changes in vascular diameter and cerebrovascular perfusion are studied for two alcohol drinking paradigms namely: - binge and chronic alcohol use. In a functional imaging approach, we study physiological changes and functional activities notably alcohol induced hemoglobin oxygen saturation for both drinking paradigms. The results from this study show that both chronic and binge alcohol use are associated with cerebral vascular constriction, as observed in the alcohol preferring mice. More importantly, we have shown that the constriction in cerebral blood vessels and the drop in hemoglobin oxygen saturation following binge drinking is more drastic in

occasional binge drinkers, compared to habitual binge drinkers or individuals with alcohol use disorder.

We developed a novel Photoacoustic imaging guided system for repetitive low intensity focused ultrasound stimulation (PAI-LIFU) for the treatment of alcohol use disorder in crossed high alcohol preferring (cHAP) mice. Results from the treatments using our system suggests that LIFU, targeted to nucleus accumbens (NAc) in the brain of cHAP mice, reduces ethanol consumptions with a marked increase in water consumption in a two-bottled choice paradigm. Furthermore, by analyzing the ratio of volume of ethanol consumed to total volume of fluid consumed, we note a significant drop in ethanol preference ratios in favor of water, following LIFU stimulation of the NAc.

Chapter 1: Photoacoustic Imaging Background and Literature

1.1 Introduction

Photoacoustic imaging (PAI) is an emerging biomedical imaging modality based on the conversion of electromagnetic energy typically from laser light to acoustic energy when tissue is optically irradiated. Besides safety due to the use of nonionizing radiation, PAI overcomes the limitation in optical diffusion associated with pure optical imaging modalities in optically scattering media and thus can achieve high resolution with a range greater than one optical transport mean free path (~1 mm) in tissue. Also, it is associated with a uniquely high contrasts unlike other optical imaging modalities prone to optical scattering. In this chapter, we present a solid background of PAI, as the imaging modality used throughout this research.

1.1.1 Brief History of Photoacoustic Imaging

Photoacoustic imaging (PAI) is based on the photoacoustic (PA) effect, which dates as far back as the 1880s when Alexander Graham Bell first observed the generation of acoustic waves directly from solid samples when they absorbed modulated sunlight [1,8]. After Bell's discovery, no significant scientific research or technological development occurred until the invention of laser systems in the sixties. This lack of research and technological development could be attributed to the unavailability of the peak energy, spectral purity and directionality required by photoacoustic applications. Earlier photoacoustic applications were mostly industrial, exploiting the indirect gas-phase cell type of photoacoustic detection in which acoustic waves were generated by laser-induced surface heating and detected using a microphone.

Though direct laser-induced ultrasound wave detection found applications in non-destructive testing for solid characterization, the idea was not investigated for biomedical imaging applications until the mid-nineties, when the first photoacoustic images began to surface. Between the mid-nineties and the mid-2000s, research in this field witnessed steady progress, culminating with images from the first in-vivo experiments. From the mid-2000s onwards, remarkable progress has been made in the field, in terms of the development of instrumentation and image reconstruction algorithms as well as more advanced applications in structural, functional, and molecular photoacoustic imaging. The imaging modality has equally seen some in-vivo applications in clinical situations and commercial imaging systems are already in the market.

1.2 Principle of Photoacoustic Imaging

In Photoacoustic imaging, laser light is used to generate ultrasound waves from tissue, by irradiating the tissue with typically nanoseconds pulsed laser light [2]. The most used wavelengths for tissue excitation are the visible and near infra-red region, typically in the range 532nm – 1100 nm, with the near infrared (NIR) region from 600nm – 900nm offering penetration depths extending to several centimeters. Once the tissue is irradiated with sufficient light energy of the right wavelength to cause optical excitation, specific tissue chromospheres namely hemoglobin, lipids, water, melanin etc. absorbs the light energy, which is then rapidly converted to heat energy by vibrational and collisional relaxation, producing a small temperature rise within the surrounding tissues [2,3]. The rise in temperature produced by the energy deposition, typically less than 0.1K induces a thermoelastic expansion, accompanied by an initial pressure rise, which launches a pressure wave within the surrounding tissue. The pressure waves propagate to the tissue surface where they are detected by an acoustic transducer as a sequence of time-resolved electrical photoacoustic (PA) signals called A-lines. Depending on the configuration, such time resolved A-

lines can be integrated versus time to yield a time resolved velocity which is then back projected into the tissue to reconstruct the initial energy deposition. Figure 1.1 is a schematic of the phenomena of photoacoustic effect on which PAI is based [2,5].

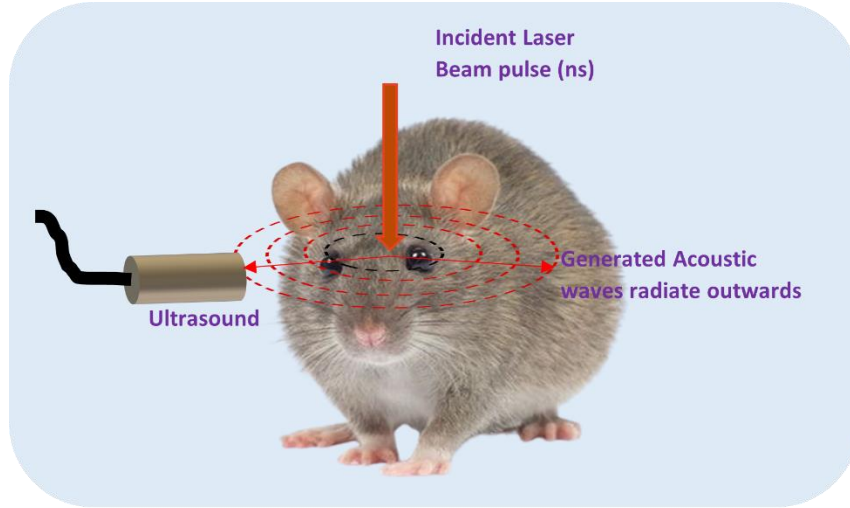


Figure 1.1 Schematic of the photoacoustic effect (*Drawn by author using MS publisher*)

The acoustic pressure $p(\mathbf{r}, t)$ generated after thermoelastic expansion and the thermal energy $H(\mathbf{r}, t)$ are related by equation 1.1:

$$\left(\nabla^2 - \frac{1}{v_s^2} \frac{\partial^2}{\partial t^2}\right) p(\mathbf{r}, t) = -\frac{\beta}{c_p} \frac{\partial H(\mathbf{r}, t)}{\partial t} \quad 1.1$$

where v_s is the speed of sound in tissue, β is the volume thermal expansion and c_p the specific heat capacity at constant pressure. As stated, the laser pulse duration (nanoseconds) is significantly shorter than the thermal diffusion and stress confinement time. Thus, the thermal conduction is often neglected to consider only the thermo-expansion mechanism. The PA image is a representation of the initial pressure $p_0(\mathbf{r})$, since it is reconstructed from a set of PA signals (which encodes this initial pressure) detected by an ultrasound transducer at different spatial locations

[2,5]. Thus, $p_0(\mathbf{r})$, depends on the heating produced by the deposited laser energy and we can say that

$$p_0(\mathbf{r}) = \Gamma H(r, t) \quad 1.2$$

where $\Gamma = \frac{\beta v_s^2}{c_p}$, a dimensionless thermodynamic constant is called the Grüneisen coefficient, provides a measure of the conversion efficiency of heat energy to pressure. β is the volume thermal expansivity, v_s , is the speed of sound in tissue and c_p is the specific heat capacity at constant pressure. The absorbed laser energy distribution $H(\mathbf{r}, t)$ can be expressed as the product of the local optical absorption coefficients $\mu_a(r)$ and the optical fluence $\phi(r, \mu_a, \mu_s, g)$, where μ_a, μ_s are respectively the absorption and reduced scattering coefficients over the illuminated volume of tissue and g is the anisotropy. Equation (1.2) can then be explicitly written in a form which shows the initial optically induced pressure $p_0(\mathbf{r})$ dependent on a variety of optical, mechanical, and thermodynamic parameters as follows

$$p_0(\mathbf{r}) = \Gamma \mu_a(r) \phi(r, \mu_a, \mu_s, g) \quad 1.3$$

A fundamental assumption in PAI is that the thermodynamic and mechanical parameters are sufficiently weakly varying from one tissue type to another and thus spatially invariant. Thus, the overall image contrast depends on the optical parameters namely μ_a, μ_s . Figure 1.2 shows the absorption coefficients spectra of different tissue chromophores.

1.2.1 Photoacoustic Signal Generation

We consider two simplifying assumptions on which the physical basis of photoacoustic signal generation is derived [2]. These assumptions are essential to allow the energy deposition and thus signal generated to be considered as instantaneous.

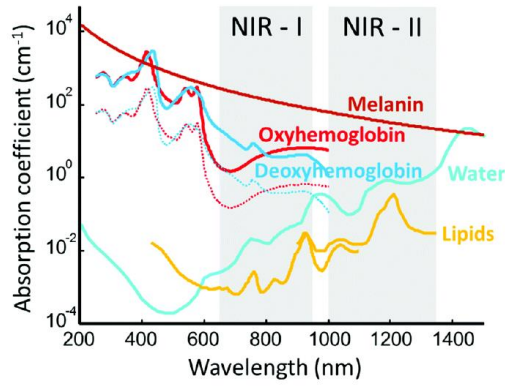


Figure 1.2 Absorption spectra of various tissue chromophores

1.2.1.1 Thermal Confinement Holds

To derive the PA signal, it is necessary to assume that the laser energy deposited on the tissue does not diffuse away from the site where it is deposited during the process of PA signal generation [2,6]. This is often the case if the laser pulse duration is sufficiently less than the tissue thermal relaxation time. This condition is expressed as in equation (1.4) below:

$$\tau_p \ll \tau_{th} = \frac{d_c^2}{\alpha_{th}} \quad 1.4$$

where, τ_p is the laser pulse duration, τ_{th} is the tissue thermal relaxation time, d_c is a characteristic dimension of the imaged tissue and α_{th} is the thermal diffusivity.

1.2.1.2 Stress Confinement Holds

To derive the PA signal, it is necessary to assume that the stress due to thermoelastic expansion does not propagate outwards during the energy deposition process. This is the case if the laser pulse duration is sufficiently less than the tissue stress relaxation time

$$\tau_p \ll \tau_s = \frac{d_c}{v_s} \quad 1.5$$

where, τ_s is the stress relaxation time and v_s is the speed of sound in the medium.

Assuming the thermal and stress confinement conditions above hold, the energy deposition, the photoacoustic excitation pulse, and photoacoustic signal generation can be considered as instantaneous processes, and equation (1.3) then describes the initial pressure increase due to the illuminating pulse at various points in space.

1.2.2 Photoacoustic Signal Propagation

The initial pressure distribution described by equation (1.3) above serves as an initial condition for the acoustic wave equation described in equation (1.1). Applying the initial condition in equation (1.3) to equation (1.1) gives equation 1.6 [9]:

$$\left(\nabla^2 - \frac{1}{v_s^2} \frac{\partial^2}{\partial t^2}\right) p(\mathbf{r}, t) = -\frac{p_0(\mathbf{r})}{v_s^2} \frac{d}{dt} \delta(t) \quad 1.6$$

We can apply Greens's function to equation (1.3), to arrive at an expression for the space-time dependent pressure $p(\mathbf{r}, t)$ as in equation 1.7 [10]

$$p(\mathbf{r}, t) = \frac{1}{4\pi v_s^2} \frac{\partial}{\partial t} \left[\frac{1}{v_s t} \int d\mathbf{r}' p_0(\mathbf{r}') \delta\left(t - \frac{|\mathbf{r}-\mathbf{r}'|}{v_s}\right) \right] \quad 1.7$$

Equation (7) shows that the pressure $p(\mathbf{r}, t)$ at any point in space-time is the integral of the initial pressure distribution $p_0(\mathbf{r})$ over a sphere defined by the time it takes the acoustic wave moving at speed v_s to propagate to that point. The sphere thus has radius $v_s t$, which means that a time-resolved pressure measurement would be a series of integrals over concentric spheres.

1.2.3 Photoacoustic Image Reconstruction and Quantification

The goal in photoacoustic image reconstruction is to recover the initial pressure distribution $p_0(\mathbf{r})$ from the photoacoustic signal $p(\mathbf{r}, t)$, obtained at multiple positions and time over the detection geometry by the detector [6]. The mathematical principles of photoacoustic imaging can be summarized into two forwards problems as shown in Figure 1.3: - An optical and an acoustic forward problem. The optical forward problem relates to the physical processes leading to the initial thermal energy deposition $H(\mathbf{r}, t)$, and relates to the optical (equivalently the

electromagnetic) properties of the tissue (including the distribution of tissue chromophores and their optical absorption coefficients) and the excitation sources. Reconstructing the tissue characteristics involved solving this forward problem in a backward fashion called an inverse optical problem. We consider this inverse optical problem in the next section.

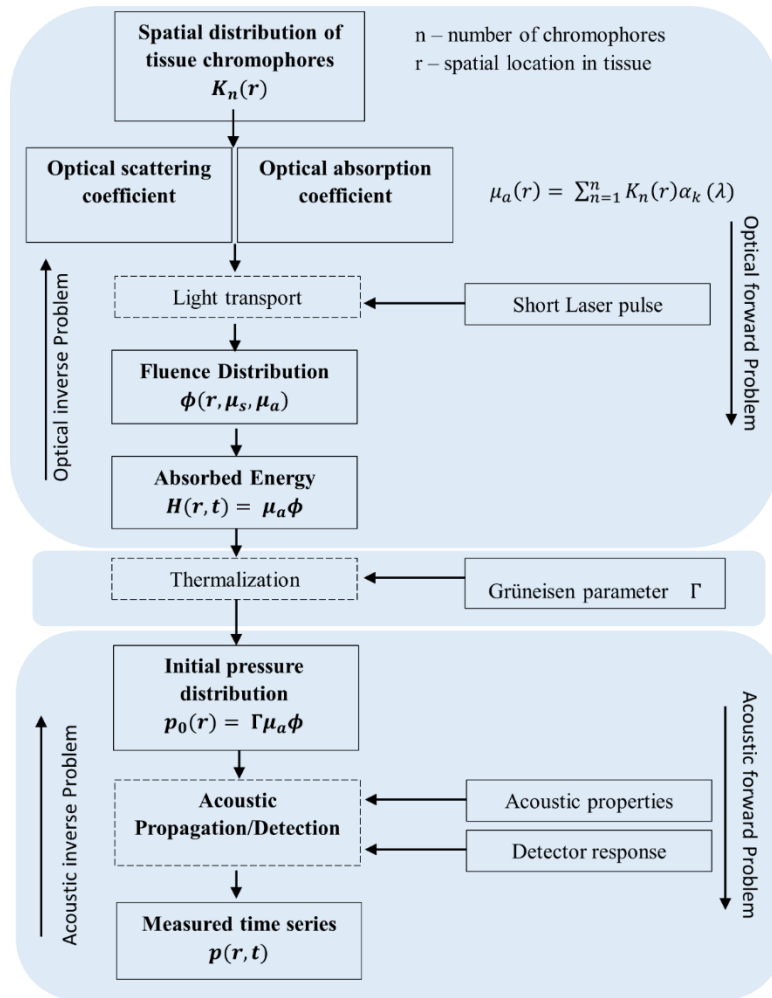


Figure 1.3 A mind map of the principle of photoacoustic imaging showing the optical and acoustic forward problems as well as the respective inverse problems. To reconstruct tissue optical properties involves solving the optical inverse problem. To reconstruct the initial pressure deposited requires solving the acoustic inverse problem. (Drawn by author using MS Words)

The acoustic forward problem relates to the calculation of the acoustic field $p(\mathbf{r}, t)$, in space-time from a known thermal energy distribution $H(\mathbf{r}, t)$, representing the electromagnetic

energy deposited on the tissue, as obtained from the optical forward problem. Reconstructing the initial pressure distribution $p_0(\mathbf{r})$ from the detected photoacoustic signal $p_{dec}(\mathbf{r}, t)$, involves solving this acoustic forward problem in a backward sense, called an Acoustic inverse problem. There are several algorithms employed to reconstruct the initial pressure distribution. Most of these algorithms could be included in one of four categories: Time domain (back projection/delay and sum), frequency domain, numerical time reversal and numerical model-based algorithms. We consider each in the following section

1.2.3.1 Time Domain or Back Projection

This approach exploits the fact that the pressure at any point in space-time are integrals of the initial pressure distribution over the detection geometry. The detected pressure however doesn't exactly correspond to the mathematical description given by equation (1.7) owing to difference in ultrasonic detector aperture and bandwidths (temporal resolution). Instead, analytical formualars similar in form to equation (1.7) but incorporating specific detector properties are used to implement fast image reconstruction computer algorithms. A typical analytical formular for the detected pressure [11,12] is shown in equation (1.8) below.

$$p_{dec}(\mathbf{r}, t) = h(t) * \int_S p(\mathbf{r}, t) D(\mathbf{r}) dS \quad 1.8$$

In equation (1.8), S is the surface over which the pressure is detected, $D(\mathbf{r})$ is the detector's sensitivity distribution and $h(t)$ is the temporal impulse response of the detector. Each 1D acoustic signal is projected onto 3D space in a way consistent to the time of flight [13].

1.2.3.2 Frequency Domain Algorithms

These algorithms are based on solving the inverse problem in the frequency domain using the Fourier transform method and then transforming the solution back to the space -time domain [13]. Given that, for $t > 0$, the acoustic forward problem can be described by a homogenous wave

equation, its acoustic field can be written as an infinite sum of known products functions in 4D space as follows:

$$p(\mathbf{r}, t) = \sum_n a_n f_{1,n}(r_1) f_{2,n}(r_2) f_{3,n}(r_3) f_{4,n}(t) \quad 1.9$$

where r_1, r_2, r_3 are the three spatial variables which define the reconstruction geometry and t is the time coordinate. Equation 1.9 represents an abstract general representation of equation 1.7, where the sum over n could also be interpreted as an integration over a surface. Equation 1.9 is at the heart of most frequency domain techniques used in photoacoustic tomography. Since the functions $f_{1,n}$ through $f_{4,n}$ are predetermined, a solution to $p(\mathbf{r}, t)$ per equation 1.9 reduces to knowing the coefficients a_n .

1.2.3.3 Time-Reversal Algorithms

These algorithms exploit the fact that the pressure distribution $p(\mathbf{r}, t)$ can be time-reversed (propagated backward) for some $t > 0$. This can be achieved by solving the acoustic wave equation 1.1 to obtain the initial pressure distribution, which indirectly tells us about the optoacoustic source. To apply time reversal will then require knowing the pressure $p(\mathbf{r}, t)$ at some time $t > 0$ for all positions. This is however not easily possible since the photoacoustic signal is collected over a surface. Xu et al [14] and Finch et al [15] implemented the first time reversal algorithm, which were based on a Green's function implementation. The Green's function was subjected to a Dirichlet boundary condition. However, under the far-field approximation, their implementation was reduced to a back-projection as in section 1.2.3.1.

1.2.3.4 Numerical Model-Based Algorithms

These algorithms exploit the linear connection between the measured acoustic field and the photoacoustic source to discretize the forward acoustic problem into a matrix form as follows:

$$[p] = [K][r] \quad 1.10.$$

where $[p]$ is a column vector of the acoustic field measured at a given position in time, $[r]$ is a column vector of the energy density on the grid and $[K]$ is the model matrix. Equation 1.10 reduces the inverse problem into a simpler algebraic problem. Finite element algorithms are based on the model based algorithms [16].

1.3 Photoacoustic Imaging Configurations

Photoacoustic imaging is currently done in one of two major imaging configurations: Photoacoustic Tomography (PAT) and Photoacoustic microscopy (PAM). There are however different variants of these configurations, some of which are a result of different imaging instruments. In PAT, a large diameter (large enough to illuminate the tissue volume of interest) laser beam is used to irradiate a tissue. As light penetrates the tissue volume, it is scattered, resulting to a larger tissue volume being illuminated with diffused light. Chromophores within the tissue absorb this light, and the tissue gets impulsively heated resulting in thermoelastic expansion and subsequent emission of broad band ultrasound waves [8]. The waves propagate to the tissue surface where they are detected by a mechanically scanned single transducer [17] or a transducer array [18]. With a known speed of sound, the time varying acoustic signals detected can then be spatially resolved and reconstructed into the three-dimensional tissue image using a reconstruction algorithm as in section 1.2.3.

In Photoacoustic microscopy, a photoacoustic image is obtained by mechanically scanning either a focused ultrasound detector or a focused laser beam and forming the image from the acquired A-lines without the use of a reconstruction algorithm. Mechanically scanning a focused ultrasound detector results in acoustic resolution photoacoustic microscopy (AR-PAM), while scanning a focused laser beam results in optical resolution photoacoustic microscopy (OR-PAM).

1.4 Photoacoustic Imaging Instrumentation

A basic PAI system require two major parts. An optical excitation part and an ultrasound detection part [6].

1.4.1 Optical Excitation

There are two major optical excitation schemes. A time-varying and a pulsing scheme. Though time-varying schemes have been used, the most prominent excitation scheme for photoacoustic tomography is a pulsing scheme, which employs a short-pulsed laser (typically nano seconds). Typical pulse repetition frequencies are in tens of Hertz, which results in short frame rates. Wavelengths are typically in the near infrared (NIR) to visible regions of the electromagnetic spectrum).

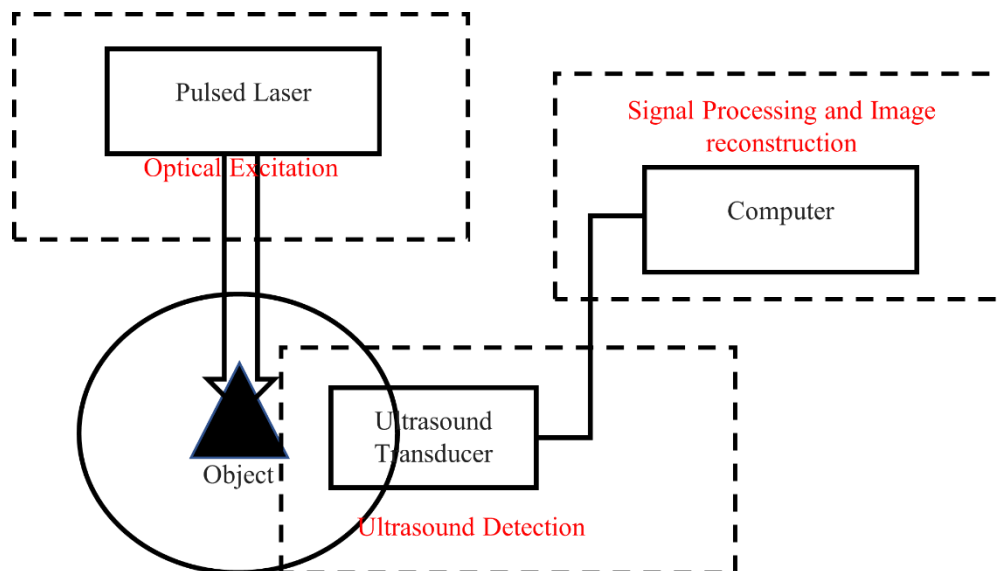


Figure 1.4 Block diagram of a photoacoustic imaging system instrumentation (*Drawn by author using MS Words*)

1.4.2 Ultrasound Detection

This part detects the time-resolved pressure signals in the ultrasound frequency range, generated following the optical excitation of the tissue. The detection is the function of specialized piezoelectric transducers of the type used in conventional ultrasound imaging. The detection system can be implemented by either mechanically scanning a single ultrasound transducer across

multiple spatial sampling locations or by using a multielement transducer array which measures at multiple locations in parallel. The detected photoacoustic signal is broadband in nature, but single piezoelectric transducers typically have a short bandwidth. Thus, using a single detector severely limits the detection bandwidth which results in image artifacts and severe loss of frequencies outside the detection bandwidth [2-9]. This severely affects the imaging axial resolution. As a result, modern photoacoustic imaging systems usually use multielement transducer arrays rather than a single frequency piezoelectric element, in order to capture all frequencies in the broadband photoacoustic signal. The choice of detection geometry also has a great influence on imaging quality (mostly lateral resolution) and performance since the image reconstruction accuracy relies on whether the spatial ultrasound pressure field is sufficiently sampled. A poor or wrong choice of detection geometry would lead to poor spatial sampling of the pressure field and a consequent poor lateral resolution. Typical detection geometries include a circular, spherical, and cylindrical.

1.5 Multispectral Photoacoustic Imaging

Equation 1.2 and 1.3 show that the initial acoustic pressure distribution depends on the optical energy deposition, which in turn depends on optical absorption and fluence. Thus, the photoacoustic imaging contrast can be said to depend on the optical absorption. This means that, materials which strongly absorb light will produce excellent photoacoustic contrast. As seen from Figure 1.2, light absorbers are typically tissue chromophores such as hemoglobin, melanin, lipids, water etc. To enhance imaging contrast, exogenous chromophores such as organic dyes, to certain nanoparticles are sometimes injected into tissue to absorb light. Thus, it is often not directly possible to pinpoint the exact source of optical absorption, to attribute a particular signal. However, at certain wavelengths (Figure 1.2) certain chromophores are more dominantly light absorbing than others. For example, hemoglobin is the predominant absorber at around 700nm

Multispectral photoacoustic imaging is a form of optical absorption spectroscopy [19] which attempts to identify the source of photoacoustic imaging contrast by exciting tissue at multiple wavelengths and identifying various contrast sources by means of their known optical absorption spectra. The selected wavelengths are such that the different absorber can be distinguished from each other. After multiwavelength imaging, the resulting set of PAT images at each single wavelength are fed into a spectral unmixing algorithm, where they are converted to sets of images of specific absorbers. The manuscript in section 5.1 is based in part to multispectral imaging which uses spectral unmixing for known optical absorption spectra to distinguish hemoglobin absorbance from deoxyhemoglobin.

1.5.1 Spectral Unmixing with Known Spectral Source

If the dominant absorbers within the imaged tissue are known, together with their absorption spectra, the images at each specific wavelength can be analyzed on a per-pixel base and the result fitted to a linear combination of the known source spectra as follows.

$$p_0(\lambda_i) = k \sum_{j=1}^n \varepsilon_j(\lambda_i) c_j \quad 1.11$$

In equation 2.11, $p_0(\lambda_i)$ is the photoacoustic pixel value (equivalent to initial pressure distribution) at each wavelength λ_i , $i = 1 \dots N$ and c_j are the concentrations of each of the n absorbers within the tissue, each with a known absorption spectrum $\varepsilon_j(\lambda_i)$. See section 5.1.

1.6 References

1. Bell, Alexander Graham. "The photophone." *Science* 11 (1880): 130-134.
2. Xia, Jun, Junjie Yao, and Lihong V. Wang. "Photoacoustic tomography: principles and advances." *Electromagnetic waves (Cambridge, Mass.)* 147 (2014): 1.
3. Nasiriavanaki, Mohammadreza, Jun Xia, Hanlin Wan, Adam Quentin Bauer, Joseph P. Culver, and Lihong V. Wang. "High-resolution photoacoustic tomography of resting-state functional connectivity in the mouse brain." *Proceedings of the National Academy of Sciences* 111, no. 1 (2014): 21-26.

4. Razansky, Daniel, Andreas Buehler, and Vasilis Ntziachristos. "Volumetric real-time multispectral optoacoustic tomography of biomarkers." *Nature protocols* 6, no. 8 (2011): 1121-1129.
5. Li, Changhui, Andres Aguirre, John K. Gamelin, Anastasios Maurudis, Quing Zhu, and Lihong V. Wang. "Real-time photoacoustic tomography of cortical hemodynamics in small animals." *Journal of biomedical optics* 15, no. 1 (2010): 010509.
6. Ho, Aaron Ho Pui, Donghyun Kim, and Michael G. Somekh. *Handbook of photonics for biomedical engineering*. Springer Netherlands, 2017.
7. Cox, Benjamin T., Jan G. Laufer, Paul C. Beard, and Simon R. Arridge. "Quantitative spectroscopic photoacoustic imaging: a review." *Journal of biomedical optics* 17, no. 6 (2012): 061202.
8. Bell, Alexander Graham. "The production of sound by radiant energy." *Science* 48 (1881): 242-253.
9. Xu, Minghua, and Lihong V. Wang. "Photoacoustic imaging in biomedicine." *Review of scientific instruments* 77, no. 4 (2006): 041101.
10. Blackstock DT. *Fundamentals of physical acoustics*. New York: D.T., John Wiley & Sons, 2000.
11. Wang, Kun, Sergey A. Ermilov, Richard Su, Hans-Peter Brecht, Alexander A. Oraevsky, and Mark A. Anastasio. "An imaging model incorporating ultrasonic transducer properties for three-dimensional optoacoustic tomography." *IEEE transactions on medical imaging* 30, no. 2 (2010): 203-214.
12. Haltmeier, Markus, and Gerhard Zangerl. "Spatial resolution in photoacoustic tomography: effects of detector size and detector bandwidth." *Inverse Problems* 26, no. 12 (2010): 125002.
13. Rosenthal, Amir, Vasilis Ntziachristos, and Daniel Razansky. "Acoustic inversion in optoacoustic tomography: A review." *Current Medical Imaging* 9, no. 4 (2013): 318-336.
14. Xu, Yuan, and Lihong V. Wang. "Time reversal and its application to tomography with diffracting sources." *Physical review letters* 92, no. 3 (2004): 033902.
15. Finch, David, and Sarah K. Patch. "Determining a function from its mean values over a family of spheres." *SIAM journal on mathematical analysis* 35, no. 5 (2004): 1213-1240.
16. Yao, Lei, and Huabei Jiang. "Finite-element-based photoacoustic tomography in time domain." *Journal of Optics A: Pure and Applied Optics* 11, no. 8 (2009): 085301.
17. Zhang, Qizhi, Zhao Liu, Paul R. Carney, Zhen Yuan, Huanxin Chen, Steven N. Roper, and Huabei Jiang. "Non-invasive imaging of epileptic seizures in vivo using photoacoustic tomography." *Physics in Medicine & Biology* 53, no. 7 (2008): 1921.

18. Wang, Bo, Liangzhong Xiang, Max S. Jiang, Jianjun Yang, Qizhi Zhang, Paul R. Carney, and Huabei Jiang. "Photoacoustic tomography system for noninvasive real-time three-dimensional imaging of epilepsy." *Biomedical optics express* 3, no. 6 (2012): 1427-1432.
19. Ntziachristos, Vasilis, and Daniel Razansky. "Molecular imaging by means of multispectral optoacoustic tomography (MSOT)." *Chemical reviews* 110, no. 5 (2010): 2783-2794.
20. Burgholzer, P., J. Bauer-Marschallinger, and M. Haltmeier. "Breaking the resolution limit in photoacoustic imaging using non-negativity and sparsity." *Photoacoustics* 19 (2020): 100191.

Chapter 2: Alcohol Use Disorder: Background and Literature

2.1 Introduction

The excessive use of alcohol is known to be amongst the ten leading causes of injury and disease, accounting for over 5.3% of deaths worldwide [1]. Despite these harmful effects, an estimated 15 million Americans were dependent on Alcohol in 2017 [2]. In the United States alone, the high prevalence of problematic drinking is estimated to cause nearly 88000 preventable deaths annually, with huge costs associated with excess morbidity [3]. The principal psychoactive component of alcoholic drinks is ethanol [4]. While most other psychoactive drugs are illegal, alcohol is peculiar in that, it is legal and socially accepted in most societies of the world [5]. Although responsible drinking is a euphoric act, associated with some health benefits due to the medicinal values of ethanol, chronic drinking, beside exerting harmful effects on almost all body systems is positively and negatively reinforcing and [34] and associated with the risk of developing alcohol use disorder (AUD); widely described as a condition whereby abstinence from alcohol results in the development of undesired side effects, which only subside after alcohol drinking is resumed [6,7]. There exist considerable differences between individuals in the ensuing intoxication following alcohol consumption and whether an AUD is developed [8]. In the United States for example, only 6% of alcohol drinkers aged 18 and older develop AUD. The reason outlined for this is that only genetically predisposed individuals experiencing alcohol related socioenvironmental cues end up developing an addiction [5,6]. Such genetic predisposition, and socioenvironmental factor are thought to account for the differences in the ensuing intoxication and the development of an AUD following chronic drinking. Several risk factors, including sex,

age, hormonal status, stress, environmental impoverishment, mental disorder, aggression, relief of withdrawal symptoms etc. increase vulnerability to alcohol, with some risk factors necessarily interacting with others to result in an additive vulnerability [9-12]. Such additive vulnerability increases the predictability that repeated exposure to alcohol will lead to the development of AUD.

2.2 Alcohol Use Disorder Cycle

Under normal circumstances, most people drink alcohol responsibly, never getting a binge (0.08 gm% in a 2-hour period) and not allowing alcohol take control of their lives. However, certain environmental cues including learned behavior, stress, dysfunctional family, lack of emotional social support and other risky habit may cause people to drink more alcohol than usual, resulting in high blood alcohol levels [13-15]. Generally, the sequence of events from responsible drinking to the development of AUD can be divided into three stages as follows: The reward stage, the development of tolerance and the development of AUD

2.2.1 The Reward Stage

This indicates the first stage of the cycle, where the subject is first introduced to alcohol due to some environmental cue such as peer pressure, emotional trauma. Stress etc. Once the initial contact with alcohol is pleasurable, then drinking may expand in a social context, with a more frequent use. [13-15]. This may be done through repeated episodic heavy drinking or setting aside periods of times for intense heavy drinking. The primary motivation for drinking at this stage is due to the hedonic value derived from alcohol consumption, hence the reinforcement is said to be positive [16,17]

2.2.2 Development of Alcohol Tolerance

Consistent alcohol use either through repeated episodic heavy drinking or setting aside periods of times for intense heavy drinking may result in the development of alcohol tolerance, a

situation where the consumption of constant amount of alcohol produces a lesser hedonic effect, warranting the consumption of increasingly higher amounts of alcohol to get the same pleasurable effect [18,19] Such alcohol tolerance usually results in the consumption of huge amounts of alcohol, contributing to alcohol dependence, especially in genetically predisposed individuals. The alcohol-induced pleasure effect following tolerance also initiates a state of negative affection, that is a motivation for compulsive drinking [20-22]

2.2.3 Development of Alcohol Use Disorder

Repeated alcohol drinking due to tolerance may result in an advanced state of tolerance whereby withdrawal from further alcohol consumption results in the development of certain undesired side effects such as headaches, seizures intense craving and even death. Such withdrawal symptoms normalize when alcohol consumption is resumed. At this level, the resumption of alcohol consumption is for survival purposes rather than any form of reward and consumption could be considered negatively reinforcing [19,23,24,34].

2.3 The Neurobiology of Alcohol Use Disorder

For the past several decades, advancements in neuroimaging techniques and the development of animal models of addiction have led to a drift in understanding of alcohol use disorder towards its neurological basis. It is now well established that, alcohol acts on specific brain structures, transiently or permanently changing their structure and function in the process [25-27]. In this section, we describe the major brain neural networks implicates in addiction as well as their neural structures (nodes).

2.3.1 Brain Neural Groups, Neurotransmitters and Receptors in Alcohol Use Disorder

The reward and aversive effects of alcohol are driven by a complex network of neurons, their synapses, specific receptors, as well as various neurotransmitters which make up the central

nervous system. A neuron is a specialized electrically excitable cell capable of processing and transmitting information via electrochemical signaling while ensuring the release of chemical substances called neurotransmitters. Neurons communicate at interneural gaps called synaptic cleft, where the presynaptic neuron (neuron before the synapse in the communication direction) transfers information to the post synaptic neuron (neuron after the synapse in the communication direction) through specialized protein receptors. Neurotransmitters bind to their protein receptors like a key to a lock, to activate neuronal transmission. Depending on the neurotransmitter involved, the postsynaptic neuron is either activated or inhibited.

There are two types of neurotransmitter receptors namely ligand-gated ion channels, with the responsibility of allowing the rapid flow of ions directly across the outer cell surface membrane and G-protein-coupled receptors, specialized in setting into motion the chemical signaling process. Brain networks include the following types of neurons, named according to the neurotransmitter they carry. They include dopaminergic neurons (Dopamine neurotransmitter), GABAergic neurons (gamma-aminobutyric acid), opioidergic neurons (opioid), glutamatergic neurons (glutamate), cholinergic neurons (acetylcholine) and serotonergic neurons and together form multiple synapses [28-30]. Dopaminergic neurons originate from the ventral tegmental area (VTA) extending to the nucleus accumbens (NAc) and the prefrontal cortex (PFC) [31]. They receive inhibitory innervations from GABAergic interneurons and post synaptic GABA receptors, stimulatory innervations from glutamatergic neurons and post synaptic glutamic receptors (NMDA- N-methyl-D-aspartate receptor, AMPA-alpha-amino-3-hydroxy-5-methyl-4-isoxazolepropionic acid receptor, and kainate receptors), as well as cholinergic neurons and postsynaptic receptors [31,32]. Table 2.1 summarizes the various neural groups and the receptors they express.

2.3.2 Brain Neural Systems Mediating Alcohol Reinforcement

A neural system (also called circuit) consists of a series of interconnected neurons which relay information related to a specific brain function. These neurons connect the nodes (neural structures) of the circuit and information is passed from one neuron to another through electrochemical signaling, as described in section 2.3.1.

Table 2.1 Brain neural groups and the receptors they express. (Abbreviations: A2R – adenosine receptor type 2, CCKR – Cholecystokinin B receptor, CB1R- cannabinoid receptor 1, CRF1R- corticotrophin receptor, MOR- mu-opioid receptor, DOR- delta-opioid receptor, KOR- kappa opioid receptor, mGluR1-metabotropic glutamate receptor type 1, mAChR-metabotropic acetylcholine receptor)

Neural group	Receptor expresses by neurons (Their anticipated function)
Dopaminergic	GABA _A R (inhibitory), KOR (aversive), D2R (behavioral inhibition), AMPAR (drug seeking), A2R (neuroadaptation), mGluR1 (Ca ²⁺ mobilization), and CB1R (alcohol preference)
GABAergic	CB1R (alcohol preference), MOR, DOR, KOR (opioid response), CRF1R (stress/anxiety-like behavior), mGluIR (direct GABA release), and mGlu _I & _{III} R (K ⁺ stimulated GABA release)
Glutamatergic	KOR (Glu release), mAChR _{3, 2/3} (regulate Glu release), and GABA _B R (inhibitory/stimulatory)
Opioidergic	CB2 (stimulatory), DARs (stimulatory), NMDAR (inhibitory), and CCKR (inhibitor)
Serotonergic	GABA _A R (inhibitory), NMDAR & AMPAR (excitatory), CRF1R (anxiety), and 5-HTR (autoinhibition)

Alcohol's acute reinforcing effects results from an interaction between alcohol and various neurotransmitter systems in two major brain system: -The reward and stress systems. Following chronic exposure, such interactions may result in changes in neuronal functions which underline

the development of alcohol use disorder. These systems are discussed in Chapter 5.2.M2 (second manuscript) and therefore not repeated here.

2.4 References

1. World Health Organization. *Global status report on alcohol and health 2018*. World Health Organization, 2019.
2. Welty, L., A. Harrison, K. Abram, N. Olson, D. Aaby, and K. McCoy. "Substance Abuse and Mental Health Services Administration. (2017). Key substance use and mental health indicators in the United States: Results from the 2016 National Survey on Drug Use and Health (HHS Publication No. SMA 17-5044, NSDUH Series H-52). Rockville, MD: Center for Behavioral Health Statistics and Quality." *Substance Abuse and Mental Health Services Administration. Retrieved. College of Health Sciences* 106, no. 5 (2019): 128.
3. Stahre, Mandy, Jim Roeber, Dafna Kanny, Robert D. Brewer, and Xingyou Zhang. "Peer reviewed: Contribution of excessive alcohol consumption to deaths and years of potential life lost in the United States." *Preventing chronic disease* 11 (2014).
4. Peele, Stanton. "Promoting positive drinking: Alcohol, necessary evil or positive good." *Alcohol and pleasure: A health perspective* (1999): 375-389.
5. Artero, Ana, Arturo Artero, Juan J. Tarín, and Antonio Cano. "The impact of moderate wine consumption on health." *Maturitas* 80, no. 1 (2015): 3-13.
6. Samokhvalov, Andriy V., Hyacinth Irving, Satya Mohapatra, and Jürgen Rehm. "Alcohol consumption, unprovoked seizures, and epilepsy: A systematic review and meta-analysis." *Epilepsia* 51, no. 7 (2010): 1177-1184.
7. Stahre, Mandy, Jim Roeber, Dafna Kanny, Robert D. Brewer, and Xingyou Zhang. "Peer reviewed: Contribution of excessive alcohol consumption to deaths and years of potential life lost in the United States." *Preventing chronic disease* 11 (2014).
8. Quinn, Patrick D., and Kim Fromme. "Individual differences in subjective alcohol responses and alcohol-related disinhibition." *Experimental and clinical psychopharmacology* 24, no. 2 (2016): 90.
9. Tarter, Ralph E., Arthur I. Alterman, and Kathleen L. Edwards. "Vulnerability to alcoholism in men: a behavior-genetic perspective." *Journal of Studies on Alcohol* 46, no. 4 (1985): 329-356.
10. Carroll, Marilyn E., Justin J. Anker, and Jennifer L. Perry. "Modeling risk factors for nicotine and other drug abuse in the preclinical laboratory." *Drug and alcohol dependence* 104 (2009): S70-S78.
11. Goeders, N. E. "The impact of stress on addiction [Электронный ресурс]/Nick E. Goeders." *European Neuropsychopharmacology* (2003).

12. Miczek, Klaus A., Jasmine J. Yap, and Herbert E. Covington III. "Social stress, therapeutics and drug abuse: preclinical models of escalated and depressed intake." *Pharmacology & therapeutics* 120, no. 2 (2008): 102-128.
13. Saatcioglu, Omer, Rahsan Erim, and Duran Cakmak. "Role of family in alcohol and substance abuse." *Psychiatry and Clinical Neurosciences* 60, no. 2 (2006): 125-132.
14. Keyes, K. M., M. L. Hatzenbuehler, Bridget F. Grant, and Deborah S. Hasin. "Stress and alcohol: epidemiologic evidence." *Alcohol research: current reviews* (2012).
15. Petit, Géraldine, Charles Kornreich, Paul Verbanck, Agnieszka Cimochovska, and Salvatore Campanella. "Why is adolescence a key period of alcohol initiation and who is prone to develop long-term problem use?: A review of current available data." *Socioaffective neuroscience & psychology* 3, no. 1 (2013): 21890.
16. Koob, George F. "Addiction is a reward deficit and stress surfeit disorder." *Frontiers in psychiatry* 4 (2013): 72.
17. Koob, George F., and Nora D. Volkow. "Neurocircuitry of addiction." *Neuropsychopharmacology* 35, no. 1 (2010): 217-238.
18. Goldberg, Leonard. "Quantitative Studies on Alcohol Tolerance in Man. The Influence of Ethyl Alcohol on Sensory, Motor and Psychological Functions Referred to Blood Alcohol in Normal and Habituated Individuals." *Acta Physiologica Scandinavica* 5, no. Supplement XVI (1943).
19. Holland, Michael G., and Robin E. Ferner. "A systematic review of the evidence for acute tolerance to alcohol—the “Mellanby effect”." *Clinical toxicology* 55, no. 6 (2017): 545-556.
20. Koob, George F. "Alcoholism: allostasis and beyond." *Alcoholism: Clinical and Experimental Research* 27, no. 2 (2003): 232-243.
21. Koob, George F. "Neuroadaptive mechanisms of addiction: studies on the extended amygdala." *European neuropsychopharmacology* 13, no. 6 (2003): 442-452.
22. Koob, George F., and Michel Le Moal. "Addiction and the brain antireward system." *Annu. Rev. Psychol.* 59 (2008): 29-53.
23. Volkow, Nora D., Yu-Shin Ding, Joanna S. Fowler, Gene-Jack Wang, Jean Logan, John S. Gatley, Stephen Dewey et al. "Is methylphenidate like cocaine? Studies on their pharmacokinetics and distribution in the human brain." *Archives of general psychiatry* 52, no. 6 (1995): 456-463.
24. Ron, Dorit, and Segev Barak. "Molecular mechanisms underlying alcohol-drinking behaviours." *Nature Reviews Neuroscience* 17, no. 9 (2016): 576-591.

25. Squeglia, Lindsay M., Joanna Jacobus, and Susan F. Tapert. "The effect of alcohol use on human adolescent brain structures and systems." *Handbook of clinical neurology* 125 (2014): 501-510.
26. Abernathy, Kenneth, L. Judson Chandler, and John J. Woodward. "Alcohol and the prefrontal cortex." *International review of neurobiology* 91 (2010): 289-320.
27. Crews, Fulton T., Ryan P. Vetreno, Margaret A. Broadwater, and Donita L. Robinson. "Adolescent alcohol exposure persistently impacts adult neurobiology and behavior." *Pharmacological reviews* 68, no. 4 (2016): 1074-1109.
28. Clapp, Peter, Sanjiv V. Bhave, and Paula L. Hoffman. "How adaptation of the brain to alcohol leads to dependence: a pharmacological perspective." *Alcohol Research & Health* 31, no. 4 (2008): 310.
29. Volkow, Nora D., and Marisela Morales. "The brain on drugs: from reward to addiction." *Cell* 162, no. 4 (2015): 712-725.
30. Volkow, Nora D., and Marisela Morales. "The brain on drugs: from reward to addiction." *Cell* 162, no. 4 (2015): 712-725.
31. Pavuluri, Mani, Kelley Volpe, and Alexander Yuen. "Nucleus accumbens and its role in reward and emotional circuitry: A potential hot mess in substance use and emotional disorders." *AIMS Neuroscience* 4, no. 1 (2017): 52-70.
32. Yamaguchi, Tsuyoshi, Hui-Ling Wang, Xueping Li, Tsz H. Ng, and Marisela Morales. "Mesocorticolimbic glutamatergic pathway." *Journal of Neuroscience* 31, no. 23 (2011): 8476-8490.
33. Yager, Lindsay M., Aaron F. Garcia, Amanda M. Wunsch, and Susan M. Ferguson. "The ins and outs of the striatum: role in drug addiction." *Neuroscience* 301 (2015): 529-541
34. Walker, Brendan M. "Conceptualizing withdrawal-induced escalation of alcohol self-administration as a learned, plasticity-dependent process." *Alcohol* 46, no. 4 (2012): 339-348.

Chapter 3: Low Intensity Focused Ultrasound, Background and Literature

3.1 Introduction

The international neuromodulation society defines neuromodulation as “Changing nerve activity by electrical stimulation or chemical substances to target areas of the body, with the aim of normalizing or modulating nerve function. Vagal stimulation, Transcranial magnetic stimulation (TMS), Transcranial electrical stimulation (tES), Deep Brain stimulation (DBS), High intensity focused ultrasound (HIFU) and low intensity focused ultrasound (LIFU) are listed as the main neuromodulation methods. While each method is unique in many ways (see Table 3.1 below), they all share the common characteristic of attempting to induce a physical, behavioral, or physiological change by stimulating a specific region through primary and secondary activation. The overall effect produced by the stimulation depends mainly on the parameters of the stimulant used [1]. Major setbacks of these technologies are either a low spatial resolution or entailing an invasive procedure.

Following its successes as a diagnostic tool, ultrasound has been proposed as an amenity to deal with these setbacks, due to its capability as a mechanical wave to transfer energy from point to point within tissue via molecular vibrations [2]. More so, the ability to focus ultrasound into a small region of interest through various tissues has led scientist to consider its potential therapeutic uses in functional neuromodulation and tumor ablation. There are two configurations currently used in the literature [1, 3]: - High Intensity focuses ultrasound (HIFU) and low intensity focused ultrasound (LIFU). HIFU is already an approved technique for tissue ablation of specific brain targets in the treatment of essential tremors and chronic pain. LIFU on its part is unique amongst

other neuromodulation methods in combining exceptional spatial resolution (mm scale) with the potential to target sub-cortical structures (deeper than 10cm) through intact skull. Guided by an imaging modality like fMRI, its potential to induce neuronal excitation or suppression without evidence of tissue damage as well as its neuromodulation effects have also been reported [3-5].

Table 2.1 compares the various currently know neuromodulation techniques.

Table 3.1 Comparison of current clinical and preclinical stimulation techniques

Parameter for comparison	DBS	tDCS	TMS	(LIFU)
Invasiveness	Invasive	Noninvasive	Noninvasive	Noninvasive
Spatial Resolution	~1mm	Undetectable	~3-5cm	Frequency dependent ~1-5mm
Depth of stimulation	Unlimited	Undetectable	~1-1.5 cm unless H-coil is used	10-15 cm or more
Duration of reversible effect	~5 s	24 h	~5 s	~10-40 min
fMRI Brain Mapping	Difficult	Difficult	Very Difficult	Easily possible

3.2 Generation and Physical Characteristics of Ultrasound

Ultrasound is a mechanical wave, which means that it requires a medium for propagation. It is generated by mechanical vibrations, which results in a rhythmical variation in pressure and density. As it propagates, regions of increase pressure or density in the medium of propagation are called regions of compression, while regions of decreased pressure are called regions of rarefaction. The period of an ultrasound wave is the time (in seconds) required to complete one cycle. It is determined by the source of the ultrasound. The ultrasound frequency is the complete

cycles produced in unit time. It is the reciprocal of the period and is measured in units of Hertz (Hz) and higher units. The frequency is determined by the source of the ultrasound and lies above the human audible range (20kHz). Ultrasound intensity is the amount of ultrasound energy concentrated per unit area. Measured in units of Watt per centimeters squared (W/cm²), other synonyms include power and amplitude. The intensity does not depend on the source but can be altered (increased or decreased) by the operator of the ultrasound device. Ultrasound wavelength is the distance covered by one ultrasound cycle. It is measure in units of meters and its derivatives. The ultrasound speed of propagation is the rate at which the ultrasound travels in a medium. It is highly medium dependent and measured in units of meters per second. For a given medium where ultrasound wavelength is λ and frequency is f , the ultrasound speed is determined by the product of the wavelength and frequency ($f\lambda$). Ultrasound is typically delivered to tissue either in pulse or continuous mode. An ultrasound pulse is a collection of ultrasound wave cycles that travel together. The time from the start of a pulse to when the pulse ends is called the pulse duration (i.e. the actual time for which the pulse is on).

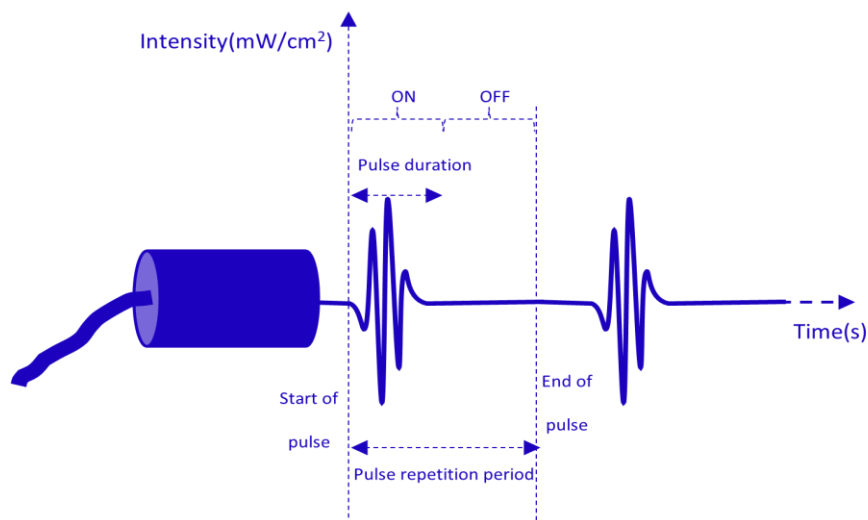


Figure 3.1 Definition of various ultrasound pulse parameters

The spatial pulse length (SPL) is the distance occupied by the entire pulse, from its starts to when it ends. The pulse repetition period (PRP) is the time from the start of one pulse to the start of the next pulse. It includes one pulse duration and one “listening time”. The pulse repetition frequency, the reciprocal of PRP is the number of pulses created by the system in one second. The duty factor is the percentage or fraction of time for which the system transmits ultrasound. During a pulse duration, the average pulse intensity is called the Pulse Average (PA). When measured at the focal point of the transducer (for a focused transducer), it is termed the Spatial Peak Pulse Average Intensity (I_{SPPA}). The focal point is a point of spatial peak intensity. During the entire pulse repetition period, the average pulse intensity is called Temporal Average pulse Intensity. When measured at the focal point of the transducer, it is termed the Spatial Peak Temporal Average Pulse Intensity (I_{SPTA}). Typical values and units of various ultrasound pulse parameters and units

Table 3.2 Typical values and units of various ultrasound pulse parameters

Parameter	Basic unit	Units	Adjustable	Determined by	Typical value
Pulse duration	time	μs	no	source	0.5-3.0 μs
Spatial pulse length	distance	mm	no	Source and medium	0.1-1.0 mm
Pulse repetition period	time	ms	yes	source	0.1 -1.0 ms
Pulse repetition frequency	1/time	Hz	yes	source	1-10kHz
Duty factor	none	none	yes	source	< 1%

3.3 Low Intensity Focused Ultrasound Literature Review

As a mechanical wave, the ability of ultrasound to penetrate deep tissues has resulted in a significant interest in its therapeutic application. Advancements in ultrasound transducer

technology has enabled the alteration of ultrasound beam geometry to enhance various therapeutic application of ultrasound. As early as the late 50s Fry et al. [6] observed the partial suppression in electrophysiological responses recorded from the primary visual cortex of craniotomized cat when focused ultrasound was transmitted to the lateral geniculate nucleus (LGN). Elsewhere, Mazoue et al. [7] reported that US could induce increased excitability of neuronal tissue. Several other studies later demonstrated the effect of ultrasound on the neural fibers in hippocampal slice cultures as well as the alteration in bioelectrical activities in various mammalian brains [8-10]. Other interesting studies include the examination of network scale of neuromodulation in neural activity in cortical and subcortical regions in rats. The direct stimulation of the cortex, thalamus, hippocampus as well as caudate nucleus in rats has been shown to induce steady changes in potential while inducing spreading depression in the cortex and deeper brain structures [11]. Low intensity sonication (1-100mW/cm²) led to activation of bioelectrical activities while higher intensities (1-100W/cm²) caused a decrease in the amplitude of electrocorticogram [12]. Also, non-cortical areas exposed to ultrasound radiation have been shown to alleviate seizure and abnormal EEG activities in chemically induced epileptic rats [13]. Groundbreaking studies by Tyler et al. 2008 showed that US could generate action potential in central neurons, intracellular influx of Calcium and sodium ions as well as a potentiated synaptic transmission in the central nervous system [14]. After this groundbreaking work, several other in vivo studies were performed to investigate the excitatory and inhibitory effects of ultrasound on various brain regions of anesthetized animals using various imaging technologies to monitor the effects. Results from fMRI and electrophysiology studies confirmed the activation and selective suppression effects of LIFU on craniotomized rabbit brain function [15]. In anesthetized rats, LIFU application to the thalamus has been shown to significantly reduce the time for animals to recover from ketamine/xylazine

induced anesthesia [16]. The development of this application has been suggested for extension in the treatment of disorders of consciousness. In human, focused ultrasound has been shown to induce tactile sensation, itching, tickling and various forms of pain.

Acoustic waves interact with the medium in which they are propagating through the motion of particles and pressure variations. While certain applications of diagnostic or therapeutic ultrasound can be considered to lie in the linear propagation regime, as the acoustic intensity increases, nonlinear phenomena become increasingly prominent. This interaction yields several different physical effects, which can be classified into thermal effects and nonthermal effects. Thermal effects are mostly related to the medium’s temperature increase, due to the conversion of acoustic energy into heat. The nonthermal effects are mechanical in nature and include radiation force, pressure and torque, acoustic streaming and the formation and cavitation of microbubbles. Figure 3.2 depicts this categorization.

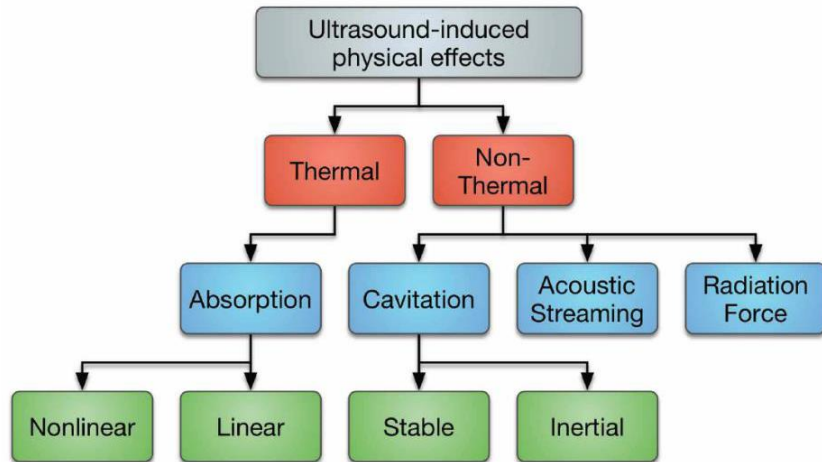


Figure 3.2 Block diagram of the origin and classification of ultrasound physical effect

For thermal effects, when acoustic waves propagate through a medium, they experience a continuous loss of energy because of attenuation which is converted to thermal energy and results in that medium’s temperature increase. Furthermore, when nonlinear propagation is considered,

this energy loss becomes even more pronounced due to the faster generation and attenuation of higher harmonics. This effect is called the absorption effect and is the main source of thermal energy during the propagation of acoustic waves within a material or tissue. There nonthermal effects are due mainly to acoustic cavitation, acoustic streaming, and radiation force effects.

3.4 Design of Ultrasound Transducer

The fundamental principle of ultrasound transducer design is the piezoelectric effect. It involves a bidirectional conversion of two forms of energy: - Electrical and mechanical energy. The piezoelectric effect is observed in piezoelectric materials such as quartz and tourmaline, though quartz and tourmaline are typically not used in the design of ultrasound transducers due to their weak piezoelectricity. Instead, piezoelectric ceramics such as barium titanate, lead metaniobate, and perhaps the most used material is lead zirconate titanate (PZT) are used in medical ultrasound devices for the generation and detection of ultrasound waves

When a mechanical deformation is applied to a piezoelectric element – the dipole moment associated with that element changes and a voltage, linearly proportional to that deformation, is generated. This phenomenon is called the direct piezoelectric effect and involves the conversion of mechanical energy into electrical. The polarity of the generated voltage depends on the direction and nature of the applied deformation. When a compression along the polarization axis or tension perpendicular to that axis is applied, a voltage with the same polarity as the original poling voltage is generated. On the other hand, a tension along that axis or a compression perpendicular to it produces a voltage with a reverse polarity. It is this property of piezoelectric materials that allows them to facilitate both the generation and detection of waves that are mechanical in nature, such as ultrasonic waves

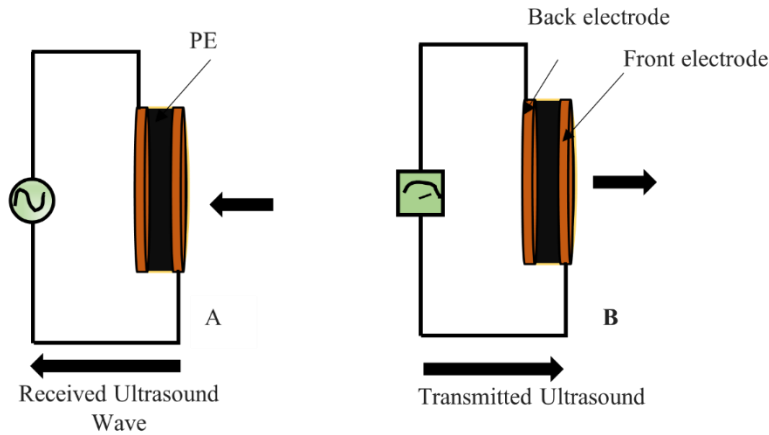


Figure 3.3 Transmission and reception of acoustic waves by piezoelectric element. The piezoelectric element has two electrodes with opposing faces. An acoustic wave is generated when the element is supplied with an AC voltage (B). An acoustic wave impinging on the element would generate a measurable AC voltage (A).

3.5 Components of Single Transducer Element

3.5.1 Piezoelectric Element (PE)

Transducers used in medical applications are generally made of piezoelectric elements with several shapes and sizes. The fundamental ultrasonic transducer consists of only one such piezoelectric element. Such a transducer is called a single element transducer and that is what we employ in this work.

To construct a single element transducer, two conductive electrodes are attached to the piezoelectric element (the core component of the transducer) to facilitate the transfer of electrical energy. To maximize the output of acoustic energy, the two electrodes are bonded to a backing and a matching layer, and the entire assembly is placed in a plastic housing. A focusing lens is typically attached to the matching layer to make the device to focus a beam of acoustic waves. This setup can be seen in Figure 3.5.

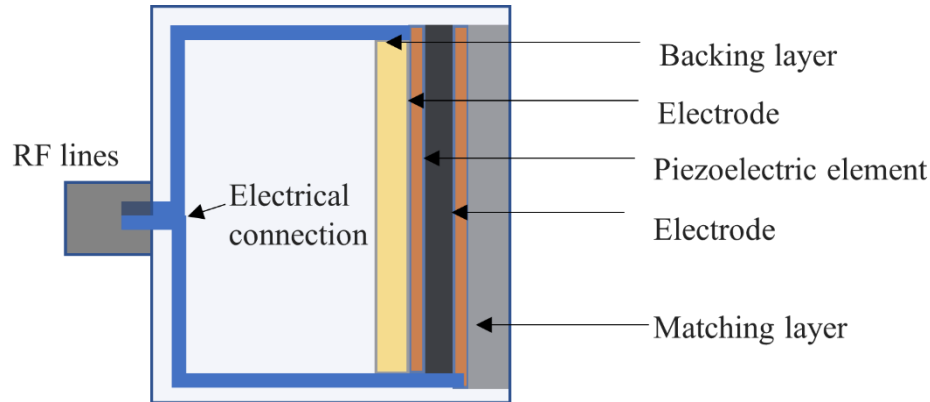


Figure 3.4 Single element transducers in cross section with all components

The frequency at which the piezoelectric element vibrates with maximum efficiency is called the fundamental frequency of the transducer. This is the frequency at which the transducer emits ultrasound waves. The choice of this frequency requires a care choice of the piezoelectric material thickness. For most medical ultrasound transducer, this element exhibits a large extent, with a large lateral extent relative to its thickness, with an aspect ratio greater than 10. Typically, the resonating frequencies are related to the piezoelectric material thickness by the expression

$$f_r = \frac{nc_p}{2L_p} \quad 3.1$$

where f_r , c_p , L_p are respectively the fundamental frequencies (Hz), speed of sound (m/s) in the piezoelectric material and the material thickness (m) while n is an integer which specifies the various frequencies. ($n=1$ is the fundamental or center frequency).

3.5.2 Electrical Connection and Driving System

When a transducer is used to generate acoustic wave, it is said to be operating in transmit mode. When used to receive acoustic signals, it operates in receive mode. The PE of a single element transducer is usually coated with two thin films of electrically conductive materials (gold or silver) which facilitates the bidirectional transfer of energy. A radiofrequency (RF) line used to mediate the transfer of electrical signals is connected to the electrodes (Fig. 3.5). When the

piezoelectric element is operating in transmit mode, the RF line transmits electrical stimulus to the element which leads to the generation of acoustic waves. In transmit mode, the RF line transfers the signal generated by the element in the presence of impinging ultrasonic waves. The back electrode is used to transfer the electrical energy while the front electrode is grounded to protect the patient from electrical shocks.

In the case of transmit mode operation, the generation of an RF signal is achieved using several hardware components which are external to the transducer and are referred to as the transducer's driving system. An AC current at the operating frequency of the transducer, and with a given amplitude and phase, is generated by a typical RF signal generator. That signal is then amplified by an RF amplifier and transferred to the transducer through a circuit network matching the electrical impedance of the amplifier to that of the transducer. Thus, maximum power transfer efficiency is achieved while driving the piezoelectric element. When the transducer is operating in receive mode, the signal generated by the piezoelectric element is first amplified, and then routed to a measurement device, such as an oscilloscope, which measures and stores the generated signal.

3.5.3 Backing Layer

To maximize the acoustic energy output from the piezoelectric element towards the front face of the transducer, two layers are bonded to the piezoelectric element – The Backing and Matching layers (Fig 3.5). While the backing layer forces the generated acoustic energy to be radiated towards the front face with minimal energy loss, the matching layer ensures a gradual transition in acoustic impedance from the piezoelectric element to the tissue. In an ideal matching layer, the characteristic acoustic impedance Z is the geometric average of the impedances of the two media and has a thickness of one quarter the acoustic wavelength in the layer (element water interface).

$$Z_{matching} = \sqrt{Z_{element}Z_{water}} \quad 3.2$$

3.6 Types of Transducers

The transducer type is depicted by the shape of the piezoelectric element used. Planar transducers use a flat piezoelectric element. Focused transducers use a piezoelectric element shaped like a hollow segment of either a sphere or a cylinder. Such transducers are referred to as either spherically focused(sphere) or cylindrically focused, in the case of a cylinder.

Spherically focused transducers produce acoustic waves that naturally tend to converge to a single focal point and then diverge again as they continue to propagate. This point is referred to as the geometric focus of the transducer and lies at the center of the imaginary sphere the piezoelectric element is a portion of. Naturally, the focal point location with respect to the transducer's face, depends on the aperture width of that spherical segment, i.e., curvature radius R and the diameter d . Because of this geometric dependence, the geometrical focusing of such a transducer is described by the transducer's f -number, which is the ratio of R and d , i.e., f -number = R/d . Clearly, increasing the curvature radius of such a transducer 'pushes' the focal point further away from the transducer

The resulting acoustic field at the focal point is technically named the focal spot or focal region but may also be referred to as the transducer's focus for the sake of simplicity. In the case of spherically focused transducers, the focal spot has the shape of a long, narrow ellipsoid with dimensions dependent on the transducer's F -number and the acoustic frequency. The size of the focal spot is inversely proportional to the transducer's diameter d and at the same time proportional to the product of the acoustic wavelength λ and the transducer's f -number [17]. The above properties also apply to cylindrically focused transducers, with the only difference being that the

latter produce a continuous line of such focal spots and thus are often referred to as line-focused transducers.

When employing focused transducers, the convergence of the acoustic waves at the focal point produces an acoustic pressure far higher than the pressure at the face of the transducer, the ratio of which is termed focal gain. Due to this, it is possible to produce acoustic waves with intensities that will induce the different thermal and nonthermal physical effects discussed in Section 3.3 at the focal spot, without inducing any effects on the overlaying tissues. This attribute of focused ultrasound is the cornerstone of its applications in therapy.

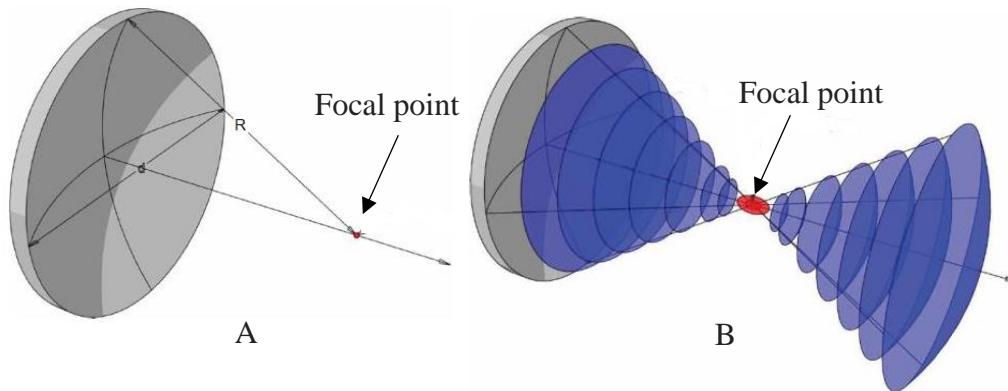


Figure 3.5 Spherically focused transducer. A Main geometric characteristic. B Acoustic field

3.7 Theoretical Lateral Beam Width at Focus and Sonication Parameters

We designed a focused ultrasound transducer of frequency 1.3MHz and a -6dB bandwidth for our application. (0.8 – 1.5 MHz). Using a speed of sound in soft tissue of 1540m/s, we estimated the theoretical beam width at focus as follows:

$$\text{Diameter } d = 64 \text{ mm, focal length } F = 51 \text{ mm, } f_{number} = \frac{F}{d} = \frac{51}{64} = 0.78$$

therefore, the theoretical Beam width at focus

$$BW_f = 1.4 \times \frac{\lambda \times F}{d} = 1.4 \times \frac{1540 \frac{m}{s} \times 61}{1.3 \times 10^6 \times 64} = 1.32 \text{ mm} \quad 3.3$$

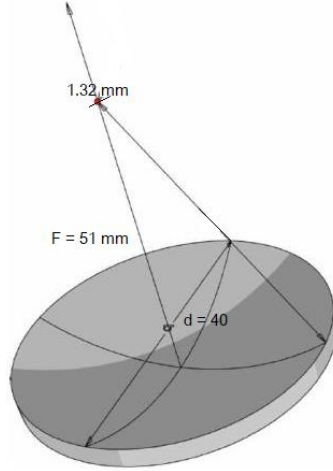


Figure 3.6 Theoretical beam width at focus from transducer geometric characteristics

3.8 Modelling Studies

Modelling predicts some important properties of the LIFU beam such as the intensity and maximum heating effect at focus as the beam propagates through tissue to the target ROI. There are many of such modelling solutions in the literature. The one employed in this study integrates a high-order parabolic approximation of the axis symmetric Westervelt equation (typically called the Khokhlov-Zabolotkaya – Kuznetsova KZK) equation from the frequency domain [18].

$$\frac{\partial^2 p}{\partial t^2} - c^2 \nabla^2 p + 2c \frac{\partial}{\partial t} [\alpha(\omega) * p(\omega)] = \frac{\beta}{\rho c^2} \frac{\partial^2 p^2}{\partial t^2} \quad 3.4$$

where p (Pa) is the acoustic pressure, t (s) is time, c (m/s) is small angle acoustic speed, α is the attenuation or dispersion function, β (dimensionless) is the nonlinear parameter and ρ (kg/m³) is the density of the medium of propagation.

The result is a spatial distribution of pressure of each harmonic, considering beam diffraction, interference effects, power-law frequency-dependence of attenuation and corresponding phase velocity dispersion, fraction of energy lost that is converted to heat. The power density and temporal average intensity are computed from the pressure field. Using the

power density as source, the bioheat transfer equation is integrated to determine the thermal dose field. The parameters used in our modelling are those used in a numerical solution to the KZK equation in the frequency domain. Table 3.3 shows these parameters while figure 3.5 shows the simulation schematic

Table 3.3 Parameters used in the numerical solution of the KZK equation to determine the ultrasound pressure field from our 1.3 MHz transducer.

Material	Parameter	value	units
Transducer	Frequency	1.3	MHz
	Radius (diameter)	32	Mm
	Focal Length	51	mm
Water	Speed of sound	1482	m/s
	Mass density	1000	Kg/m ³
	Absorption coefficient at 1.3 MHz	0.217	dB/m
	Nonlinear coefficient	2	-
Mouse Brain	Speed of sound	1540	m/s
	Mass density	1045	Kg/m ³
	Absorption coefficient at 1.3 MHz	80	dB/m
	Nonlinear coefficient	1.35	-

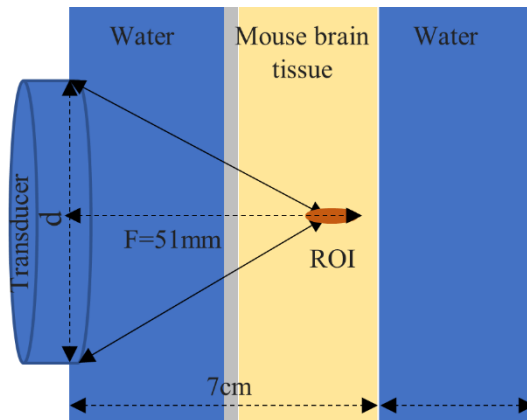


Figure 3.7 Schematic for modelling ultrasound propagation in a 3 layer media. The thin mouse skull shown in grey is negligible in the simulation

3.8.1 Results

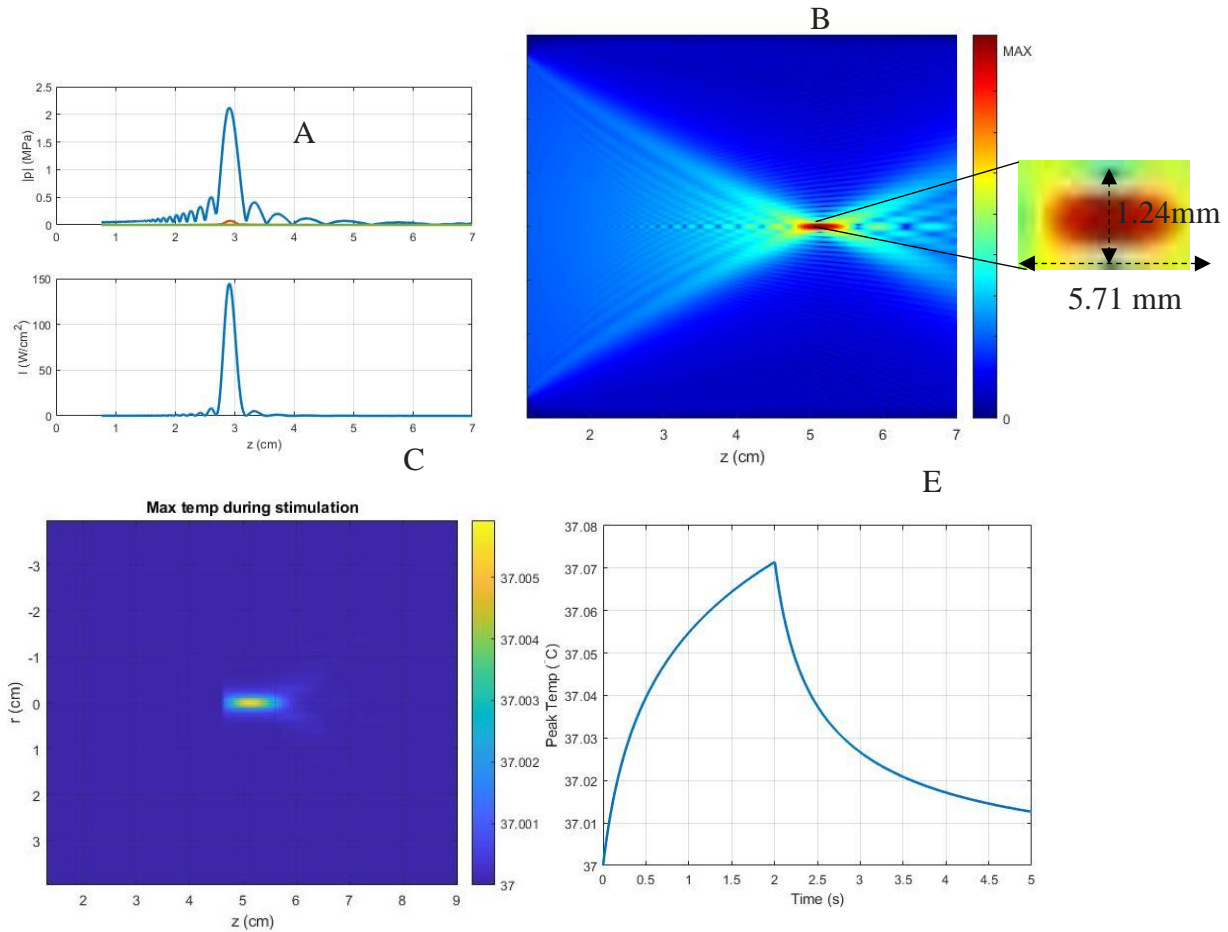


Figure 3.8 Distribution of acoustic pressure, intensity, and heat around the focus. A. Distribution of axial acoustic pressure and intensity. B. Distribution and Analysis of intensity distribution at focus. The lateral beam width at focus is estimated to be 1.24 mm while the axial beam width is 5.71 mm C/E Distribution of temperature at focus after 2 s of sonication. Tissue temperature rises by 0.08 $^{\circ}\text{C}$, less than 0.1 $^{\circ}\text{C}$

3.9 References

1. Baek, Hongchae, Ki Joo Pahk, and Hyungmin Kim. "A review of low-intensity focused ultrasound for neuromodulation." *Biomedical Engineering Letters* 7, no. 2 (2017): 135-142.
2. Rezayat, Ehsan, and Iman Ghodrati Toostani. "A review on brain stimulation using low intensity focused ultrasound." *Basic and clinical neuroscience* 7, no. 3 (2016): 187.

3. Legon, Wynn, Leo Ai, Priya Bansal, and Jerel K. Mueller. "Neuromodulation with single-element transcranial focused ultrasound in human thalamus." *Human brain mapping* 39, no. 5 (2018): 1995-2006.
4. Lee, Wonhye, Stephanie D. Lee, Michael Y. Park, Lori Foley, Erin Purcell-Estabrook, Hyungmin Kim, Krisztina Fischer, Lee-So Maeng, and Seung-Schik Yoo. "Image-guided focused ultrasound-mediated regional brain stimulation in sheep." *Ultrasound in medicine & biology* 42, no. 2 (2016): 459-470.
5. Gavrilov, L. E. O. N. I. D. "Focused ultrasound stimulation of the peripheral nervous system: Physical basis and practical applications." *International Journal of Modern Physics: Advances in Theory and Application* 1 (2016): 45-118.
6. Legon, Wynn, Tomokazu F. Sato, Alexander Opitz, Jerel Mueller, Aaron Barbour, Amanda Williams, and William J. Tyler. "Transcranial focused ultrasound modulates the activity of primary somatosensory cortex in humans." *Nature neuroscience* 17, no. 2 (2014): 322-329.
7. Fry, F. J., H. W. Ades, and W. J. Fry. "Production of reversible changes in the central nervous system by ultrasound." *Science* 127, no. 3289 (1958): 83-84.
8. Mazoue, H., P. Chauchard, and R. G. Busnel. "Nervous excitation with high frequency ultrasonics." *Journal de physiologie* 45, no. 1 (1953): 179-182.
9. TAKAGI, SADAYUKI F., S. Y. O. J. I. Higashino, T. A. T. S. U. A. K. I. Shibuya, and N. O. B. U. T. A. K. A. Osawa. "The actions of ultrasound on the myelinated nerve, the spinal cord and the brain." *The Japanese Journal of Physiology* 10, no. 2 (1960): 183-193.
10. Rinaldi, Patricia C., Joie P. Jones, Frederick Reines, and LeRoy R. Price. "Modification by focused ultrasound pulses of electrically evoked responses from an in vitro hippocampal preparation." *Brain research* 558, no. 1 (1991): 36-42.
11. Bachtold, Michael R., Patricia C. Rinaldi, Joie P. Jones, Frederick Reines, and LeRoy R. Price. "Focused ultrasound modifications of neural circuit activity in a mammalian brain." *Ultrasound in medicine & biology* 24, no. 4 (1998): 557-565.
12. Koroleva, V. I., N. I. Vykhodtseva, and V. A. Elagin. "Cortical and subcortical spreading depression in rats produced by focused ultrasound." *Neurophysiology* 18, no. 1 (1986): 43-48.
13. Velling, V. A., and S. P. Shklyaruk. "Modulation of the functional state of the brain with the aid of focused ultrasonic action." *Neuroscience and behavioral physiology* 18, no. 5 (1988): 369-375.
14. Manlapaz, J. S., K. E. Åström, H. T. Ballantine Jr, and P. P. Lele. "Effects of ultrasonic radiation in experimental focal epilepsy in the cat." *Experimental neurology* 10, no. 4 (1964): 345-356.

15. Tyler, William J., Yusuf Tufail, Michael Finsterwald, Monica L. Tauchmann, Emily J. Olson, and Cassandra Majestic. "Remote excitation of neuronal circuits using low-intensity, low-frequency ultrasound." *PloS one* 3, no. 10 (2008): e3511.
16. Yoo, Seung-Schik, Alexander Bystritsky, Jong-Hwan Lee, Yongzhi Zhang, Krisztina Fischer, Byoung-Kyong Min, Nathan J. McDannold, Alvaro Pascual-Leone, and Ferenc A. Jolesz. "Focused ultrasound modulates region-specific brain activity." *Neuroimage* 56, no. 3 (2011): 1267-1275.
17. Velling, V. A., and S. P. Shklyaruk. "Modulation of the functional state of the brain with the aid of focused ultrasonic action." *Neuroscience and behavioral physiology* 18, no. 5 (1988): 369-375.
18. Rinaldi, Patricia C., Joie P. Jones, Frederick Reines, and LeRoy R. Price. "Modification by focused ultrasound pulses of electrically evoked responses from an in vitro hippocampal preparation." *Brain research* 558, no. 1 (1991): 36-42.

Chapter 4: Significance and Specific Aims of the Research

4.1 Public Health Relevance of the Research

Alcohol use disorder (AUD) is a chronically relapsing neurological disorder characterized by the compulsion to seek and consume alcohol, loss of control in limiting alcohol intake, and the emergence of a negative emotional state when access to alcohol is discontinued [1]. Despite the well-defined negative consequences of chronic alcohol consumption, the prevalence of heavy and binge alcohol use remains high in the United States, especially among adolescent and young adult populations [2]. Although there are a number of treatment options for AUD – including pharmacotherapeutic, psychiatric, and behavioral interventions – attempts to quit drinking often fail and rates of relapse after cessation from alcohol remain high. AUD is also a major global risk factor for disability and premature loss of life, affecting an estimated 76 million people worldwide with enormous health and socioeconomic burden [3-5]. In the United States alone, more than \$249 billion in economic costs is attributable to AUD [6,7]. The current treatment modalities, primarily based on behavioral therapies and medications, are associated with a low success rate, with a 40%-70% relapse rate one to three years after standard treatment [8,9]. The three FDA-approved medications for AUD (Acamprosate, Disulfiram and Naltrexone) are either associated with unpleasant side effects (drowsiness, weakness, fatigue, dizziness etc.), or are ineffective in preventing the withdrawal symptoms that drive relapse to alcohol [8,10]. In addition, existing therapeutic interventions require long-term inpatient treatments that are both time- and cost-prohibitive, such that only ~10% of patients with AUD receive treatment [9, 11]. Furthermore, successful abstinence occurs in less than 50% of patients who undergo treatment for AUD [12].

Thus, there is an unmet need to develop novel, non-invasive, non-pharmaceutical treatment modalities that would support and maintain alcohol abstinence by preventing both cravings and withdrawal symptoms.

4.2 Scientific Premise of the Research

Despite the heavy socioeconomic burden, advancements in research towards understanding the etiology and pathophysiology of AUD were impeded for a long time by the notion of AUD being a moral, and thus psychological deficiency, rather than a chronically relapsing neurobiological brain disease [13,14]. With advances in technology and development of animal models of alcohol use disorder, more rigorous research is progressively unraveling the neural circuits, systems and processes involved in the development of an AUD. It is now widely accepted that chronic alcohol exposure induces neuroadaptive changes in a variety of neural circuits, including those that control motivation, arousal, and the stress response. In fact, alcohol can act on almost all neurotransmitter receptors in the brain, including those for dopamine (DA), opioids, gamma-aminobutyric acid (GABA), glutamate, and the glucocorticoids [14-16]. The overall effect of these changes is the development of an incentive sensitization to alcohol's effects which motivates the individual to continually seek alcohol [17]. Initial alcohol-seeking is driven by motivation from its anxiolytic and rewarding properties. However, with continued use, the brain habituates to alcohol, and the motivation shifts to an avoidance of withdrawal symptoms characterized by dysphoria, extreme stress, and anxiety when alcohol is discontinued. Thus, the individual is caught in a self-perpetuating cycle of continually seeking increasing quantities of alcohol to achieve the positive effects associated with alcohol and to avoid the negative affect associated with withdrawal.

The incredibly poor rates of alcohol abstinence may be due to neural dysfunction that current pharmacotherapies fail to correct. Specifically, AUD may evolve from biological dysfunctions within the DA-mediated midbrain reward circuit. DA is an essential signal within the brain reward system that is thought to mediate both pleasure and motivation within everyday life [18,19] and to underlie the rewarding effects of alcohol. In support of this, behavioral manipulations that induce DA release from the nucleus accumbens (NAc), a central component of the reward circuit, can lead to electrical self-stimulation, self-administration of drugs, and place preference conditioning [20-22]. This is likely due to alcohol's ability to reinforce consummatory behavior through midbrain DA neurons within the reward system into the prefrontal cortex (PFC) and limbic system [23-25]. This excitation of DA release is indirect, and is mediated by both glutamate and GABA neurotransmitter systems upstream of DA neurons [26]. Low levels of endogenous DA or DA receptors may produce an increased sensitivity to the reinforcing effects of alcohol [27,28]. After the initial exposure, alcohol use is reinforced and escalates. The chronic consumption of alcohol then induces a series of pathological neural changes, largely in the midbrain DA system, in transcription factor activity, gene expression, receptor density, and neural activation [29]. These changes lead to a semi-permanent shift in the hedonic set point of the reward circuit, leading to persistent alcohol consumption [30]. It has been demonstrated that the alcohol-preferring P rat has fewer dopaminergic neurons projecting from the ventral tegmental area (VTA) to the NAc but higher levels of DA neurotransmission (i.e., burst firing) even prior to alcohol exposure [31,32], and that chronic alcohol exposure increases the reinforcing effects of alcohol in the VTA of the P rat [33]. Similarly, the high-alcohol preferring (HAP) mouse, similar to the cHAP mouse used in this research, demonstrates reduced spontaneous burst firing in the reward circuit compared to non-alcohol preferring mice [34].

If AUD results from pathological neural function in the midbrain DA system, then treatments that reduce or block such pathological activity should also reduce alcohol consumption. Deep brain stimulation (DBS), the high frequency stimulation of select neural regions in order to correct pathological conditions, has been hypothesized to act by inhibiting the pathological neural activity that underlies conditions such as Parkinson's Disease. DBS induces changes in both glutamatergic and GABAergic neurotransmission, producing hyperpolarization of somatic membranes and depolarization of axonal membranes [35-37]. These neural changes result in a decoupling of neurons, reducing the pathological activity of local neurons and the systems to which they are both prodromically and antidromically coupled. DBS has been shown to decrease consumption of alcohol and drugs of abuse in both animal models and in patients. DBS of the NAc in a patient comorbid for affective disorders produced an immediate and long-lasting suppression of alcohol consumption [38]. DBS of the NAc shell also decreased the reinstatement of cocaine-seeking in rats [39]. Most important to the current hypothesis, DBS of the NAc produces a sharp reduction in alcohol intake in alcohol-preferring and alcohol-non-preferring rats, and this effect is selective for alcohol, as water intake is not decreased by accumbal DBS [40,41]. Finally, in the first study using DBS to treat alcoholics with no co-occurring pathologies, two of three patients achieved complete abstinence from alcohol immediately after DBS surgery and at a one-year follow up, while the third patient demonstrated drastically reduced alcohol intake at both time-points [42]. However, DBS is an invasive procedure with high risk of adverse outcomes such as hemorrhage and infection and the need for regular maintenance. Furthermore, its use is limited to treatment-refractory individuals who are otherwise healthy, and it requires a dedicated medical team. Thus, there is an urgent need for a non-invasive, less-costly intervention that can mimic the neurobiological effects of DBS.

4.3 Technological Significance of the Research

To address the unmet need of developing a non-invasive, non-pharmaceutical treatment modality, low intensity focused ultrasound (LIFU)-based neuromodulation; the targeted alteration of nerve activity through the controlled delivery of LIFU neurostimulations to a specific region of interest (ROI) within the brain [8], offers a novel route for the treatment of AUD. LIFU provides a way of mechanically inducing neuroplasticity through the localized application of an ultrasound stimulus to a suitable ROI in high spatial resolution (millimeter scale) along with the ability to target subcortical structures.

The concept of neuromodulation-based treatment for AUD is not entirely new. In 2007, Kuhn et al [43] reported the unintended remission of long-term comorbid alcohol consumption by a patient following DBS of the NAc for treating an anxiety disorder. Subsequently, data from both animal and human studies involving DBS of the NAc showed reduced alcohol consumption [43-48]. Repetitive transcranial magnetic stimulation (rTMS) to the dorsolateral prefrontal cortex (DLPFC) has been shown to reduce alcohol-related cravings or consumption, post active rTMS treatment [45, 48-54]. Transcranial direct current stimulation (tDCS) has equally shown promise in reducing alcohol related cravings and consumption [55-60]. However, DBS is prone to risks of infection and neural immune system reactions [61]. Also, both TMS and tDCS fail to provide the required spatial resolution to target deep brain regions of interest and are unable to stimulate such regions without exerting undesired effects to the surrounding tissues, even with the integration of H-coils into modern TMS machines in a bit to focus more precisely [62]. LIFU, on the other hand, combines exceptional millimeter scale spatial resolution with the potential to target subcortical structures (deeper than 10 cm) through intact skull [63]. We have so far seen its successful applications in promoting bone fracture healing[64], acceleration of soft tissue regeneration [65],

opening ion channels and synaptic activation[66], suppression of induced epileptic behavior [67], preventing a rise in morphine place preference in opioid dependent rats[68] amongst several other applications. An ideal neuromodulation strategy would be noninvasive, cost effective safe, and have high spatial resolution to precisely modulate the target neural circuits; LIFU has all these features. The ability of LIFU to target subcortical structures allows the noninvasive stimulation of the reward circuit, including the VTA and NAc, mimicking a strategy that has previously only been available with the much riskier procedure of implanting electrodes for DBS.

A key feature in a LIFU stimulation is to use a suitable imaging modality to guide the focused ultrasound beam to the neural target of interest. Imaging guidance typically has a single important role: to ensure that the ultrasound reaches the desired ROI. Most previous studies have used variants of MRI for guiding LIFU stimulation [63]. While MRI can provide high resolution tissue structures and functional MRI can image hemodynamics during/after the stimulation, MRI scanners still suffer from their perennial cost-ineffectiveness, bulkiness, coupled with a long scanning time. In addition, MRI does not provide tissue mechanical/acoustic properties that are essential for a precise, noninvasive delivery of focused ultrasound beam to the target ROI. We have used photoacoustic tomography (PAT) along with finite element (FE) modeling to serve as a novel integrated platform for optimal LIFU guidance. PAT provides both structural and functional/hemodynamic information in high spatiotemporal resolution (submillimeter-millisecond scale) [69], while FE modeling ensures a precise delivery of focused ultrasound to the target region in the brain.

To test the functionality and repeatability of the PAI-LIFU system we developed, we have used it to ultrasonically stimulate the NAc or VTA *in vivo* in crossed high alcohol preferring (cHAP) mice. Animal models such as rodents are by far the most used in this area. Use of larger

animals (such as non-human primates, ewes, etc.) and human subjects is often limited due to limited supply of these animals, lack of genetically-engineered strains and most importantly, by ethical constraints when large sample sizes are required, and a multitude of confounding variables exist. The use of a high-alcohol-preferring mouse line allowed us to control for genetic variability and to run studies that are sufficiently powered to examine age and sex as biological variables as well as to examine changes in neural structures (NAc or VTA). In addition, the use of this animal model allowed us to determine whether LIFU produces any secondary effects on the neuronal environment, such as inflammatory and oxidative stresses.

4.4 Specific Aims

4.4.1 Aim 1

This aim is concerned with demonstrating the capabilities of PAI in brain imaging using a mouse model of alcohol use disorder and showcase it as a cost effective and safer alternative for alcohol use disorder imaging. It has to do with the experimental and instrumentation part of this research. To achieve this aim, we designed, and built a PAI system to image both cortical and deep tissues of the brain, as well as functional activities in crossed alcohol preferring mice. To better image deep brain and cortical structures like vasculature and their associated functional activities like blood flow and oxygen saturation using PAI, enough optical energy must be delivered to the tissue to generate strong ultrasound signals from it. We therefore improved an existing PAI system for optimal light delivery to the brain region. As explained elsewhere, the skull is associated with severe optical attenuation owing to light absorption and scattering. This greatly affects light penetration to cortical and deep brain tissues located below the skull, with a consequent reduction in optical fluence and the overall image quality. Thus, it was essential to optimize light delivery to compensate for light absorbed and/scattered by the skull and still leave enough light energy for

cerebral structures. Light absorption by tissue depends on the wavelength. While the optical absorption coefficient of the skull is higher at some wavelengths (typically the lower near infrared (NIR $\lambda < 700nm$), it is relatively lower at others (typically the upper NIR $700nm < \lambda < 1000nm$). The optical absorption coefficient of cortical tissues including blood vessels also greatly varies in this wavelength range. We therefor studied the optical absorption spectra of skull and all other tissues to optimize wavelength. The end goal here is a PAI system with optimized light delivery capable of imaging both deep and surface structures as well as associated functional activities in small animals

4.4.2 Aim 2

Aim 2 is concerned with developing and testing the efficacy of a novel photoacoustic imaging guided system for repetitive low intensity focused ultrasound (PAI-LIFU) brain stimulation for the treatment of alcohol use disorder. Data from a plethora of experimental models strongly suggest that a low intensity dose of ultrasound can reversibly modulate physiological activities in peripheral nerve neurons, the spinal cord as well as intact brain circuitries. More specifically, low intensity ultrasound acts on mechanosensitive ion channels to reversibly modulate their activity. For this to happen, ultrasound must accurately and precisely be delivered to the required ROI with high resolution. With this in mind, we aimed at developing instrumentation and testing its functionality and repeatability by using it to precisely deliver a low intensity focused ultrasound beam onto specific neural structures in the mouse brain using a newly developed Photoacoustic imaging guided low intensity focused ultrasound (PAI-LIFU) system for treating alcohol use disorder, while observing and correlating how such response affect the overall addictive behavior of the animal

4.5 References

1. Koob, George F., and Michel Le Moal. "Drug abuse: hedonic homeostatic dysregulation." *Science* 278, no. 5335 (1997): 52-58.
2. Abuse, Substance. "Mental Health Services Administration (SAMHSA). 2001 National Household Survey on Drug Abuse Summary Findings." *Office of Applied Studies: Rockville, MD* (2002).
3. J. Rehm, C. Mathers, S. Popova, et al., Global burden of disease and injury and economic cost attributable to alcohol use and alcohol use disorders, *Lancet* 373 (2009) 2223–2233.
4. J. Rehm, K.D. Shield, Alcohol, and mortality: global alcohol-attributable deaths from cancer, liver cirrhosis and injury in 2010, *Alcohol Res. Curr. Rev.* 35 (2013) 174–183.
5. WHO—World Health Organization, Global Status Report on Alcohol and Health, WHO Library Cataloguing-in-Publication Data 2014.
6. Sacks, Jeffrey J., Katherine R. Gonzales, Ellen E. Bouchery, Laura E. Tomedi, and Robert D. Brewer. "2010 national and state costs of excessive alcohol consumption." *American journal of preventive medicine* 49, no. 5 (2015): e73-e79.
7. Stahre, Mandy, Jim Roeber, Dafna Kanny, Robert D. Brewer, and Xingyou Zhang. "Peer reviewed: contribution of excessive alcohol consumption to deaths and years of potential life lost in the United States." *Preventing chronic disease* 11 (2014).
8. De Ridder, Dirk, Patrick Manning, Gavin Cape, Sven Vanneste, Berthold Langguth, and Paul Glue. "Pathophysiology-based neuromodulation for addictions: an overview." *Neuropathology of Drug Addictions and Substance Misuse* (2016): 14-24.
9. Swift, Robert M. "Medications and alcohol craving." *Alcohol Research & Health* 23, no. 3 (1999): 207.
10. Kuhn, Jens, Christian P. Bührle, Doris Lenartz, and Volker Sturm. "Deep brain stimulation in addiction due to psychoactive substance use." *Handbook of clinical neurology* 116 (2013): 259-269.
11. Leggio, Lorenzo, and Mary R. Lee. "Treatment of alcohol use disorder in patients with alcoholic liver disease." *The American journal of medicine* 130, no. 2 (2017): 124-134.
12. Moos, Rudolf H., and Bernice S. Moos. "Rates and predictors of relapse after natural and treated remission from alcohol use disorders." *Addiction* 101, no. 2 (2006): 212-222.
13. Tabakoff, Boris, and Paula L. Hoffman. "The neurobiology of alcohol consumption and alcoholism: an integrative history." *Pharmacology Biochemistry and Behavior* 113 (2013): 20-37.

14. Domi, Esi, Ana Domi, Louise Adermark, Markus Heilig, and Eric Augier. "Neurobiology of alcohol seeking behavior." *Journal of Neurochemistry* (2021).
15. Koob, G. F., and N. D. Volkow. "Neurobiology of addiction: a neurocircuitry analysis. *Lancet Psychiatry*. 2016; 3 (8): 760–73."
16. Koob, George F., S. Barak Caine, Petri Hyytia, Athina Markou, Loren H. Parsons, Amanda J. Roberts, Gery Schulteis, and Friedbert Weiss. "Neurobiology of drug addiction." (1999).
17. Klenowski, Paul M. "Addictive Behaviors Emerging role for the medial prefrontal cortex in alcohol-seeking behaviors."
18. Fibiger, H.C. and A.G. Phillips, *Mesocorticolimbic dopamine systems and reward*. Ann N Y Acad Sci, 1988. 537: p. 206-15.
19. Gardner, E.L., *Brain reward mechanisms*, in *Substance Abuse: a Comprehensive Textbook*, J. Lowinson, et al., Editors. 1997, Williams & Wilkins: Baltimore. p. 61-85.
20. Eiler, W.J., 2nd, et al., *Amphetamine lowers brain stimulation reward (BSR) threshold in alcohol-preferring (P) and -nonpreferring (NP) rats: regulation by D-sub-1 and D-sub-2 receptors in the nucleus accumbens*. *Exp Clin Psychopharmacol*, 2006. 14(3): p. 361-76.
21. Nelson, A.M., G.A. Larson, and N.R. Zahniser, *Low or high cocaine responding rats differ in striatal extracellular dopamine levels and dopamine transporter number*. *J Pharmacol Exp Ther*, 2009. 331(3): p. 985-97.
22. You, Z.B., Y.Q. Chen, and R.A. Wise, *Dopamine and glutamate release in the nucleus accumbens and ventral tegmental area of rat following lateral hypothalamic self-stimulation*. *Neuroscience*, 2001. 107(4): p. 629-39.
23. Diana, M., M. Melis, and G.L. Gessa, *Increase in meso-prefrontal dopaminergic activity after stimulation of CB1 receptors by cannabinoids*. *Eur J Neurosci*, 1998. 10(9): p. 2825-30.
24. Hertel, P., et al., *Effects of D-amphetamine and phencyclidine on behavior and extracellular concentrations of neurotensin and dopamine in the ventral striatum and the medial prefrontal cortex of the rat*. *Behav Brain Res*, 1995. 72(1-2): p. 103-14.
25. Tanda, G., F.E. Pontieri, and G. Di Chiara, *Cannabinoid and heroin activation of mesolimbic dopamine transmission by a common mu1 opioid receptor mechanism*. *Science*, 1997. 276(5321): p. 2048-50.
26. Cami, J. and M. Farre, *Drug addiction*. *N Engl J Med*, 2003. 349(10): p. 975-86.
27. Vengeliene, V., et al., *Neuropharmacology of alcohol addiction*. *Br J Pharmacol*, 2008. 154(2): p. 299-315.

28. Volkow, N.D., et al., *Brain DA D2 receptors predict reinforcing effects of stimulants in humans: replication study*. Synapse, 2002. 46(2): p. 79-82.
29. Koob, G.F., *The neurobiology of addiction: a neuroadaptational view relevant for diagnosis*. Addiction, 2006. 101 Suppl 1: p. 23-30.
30. Koob, G.F. and M. Le Moal, *Drug abuse: hedonic homeostatic dysregulation*. Science, 1997. 278(5335): p. 52-8.
31. Morzorati, S.L. and R.L. Marunde, *Comparison of VTA dopamine neuron activity in lines of rats selectively bred to prefer or avoid alcohol*. Alcohol Clin Exp Res, 2006. 30(6): p. 991-7.
32. Morzorati, S.L., *VTA dopamine neuron activity distinguishes alcohol-preferring (P) rats from Wistar rats*. Alcohol Clin Exp Res, 1998. 22(4): p. 854-7.
33. Rodd, Z.A., et al., *Prolonged increase in the sensitivity of the posterior ventral tegmental area to the reinforcing effects of ethanol following repeated exposure to cycles of ethanol access and deprivation*. J Pharmacol Exp Ther, 2005. 315(2): p. 648-57.
34. Juarez, B., et al., *Midbrain circuit regulation of individual alcohol drinking behaviors in mice*. Nature Communications, 2017. 8(1): p. 2220.
35. McIntyre, C.C., et al., *Uncovering the mechanism(s) of action of deep brain stimulation: activation, inhibition, or both*. Clin Neurophysiol, 2004. 115(6): p. 1239-48.
36. Gubellini, P., et al., *Deep brain stimulation in neurological diseases and experimental models: from molecule to complex behavior*. Prog Neurobiol, 2009. 89(1): p. 79-123.
37. Montgomery, E.B., Jr. and J.T. Gale, *Mechanisms of action of deep brain stimulation(DBS)*. Neurosci Biobehav Rev, 2008. 32(3): p. 388-407.
38. Kuhn, J., et al., *Remission of alcohol dependency following deep brain stimulation of the nucleus accumbens: valuable therapeutic implications?* J Neurol Neurosurg Psychiatry, 2007. 78(10): p. 1152-3.
39. Vassoler, F.M., et al., *Deep brain stimulation of the nucleus accumbens shell attenuates cocaine priming-induced reinstatement of drug seeking in rats*. J Neurosci, 2008. 28(35): p. 8735-9.
40. Knapp, C.M., et al., *Deep brain stimulation of the nucleus accumbens reduces ethanol consumption in rats*. Pharmacol Biochem Behav, 2009. 92(3): p. 474-9.
41. Henderson, M.B., et al., *Deep brain stimulation of the nucleus accumbens reduces alcohol intake in alcohol-preferring rats*. Neurosurg Focus, 2010. 29(2): p. E12.

42. Muller, U.J., et al., *Successful treatment of chronic resistant alcoholism by deep brain stimulation of nucleus accumbens: first experience with three cases*. *Pharmacopsychiatry*, 2009. 42(6): p. 288-91.
43. Kuhn, Jens, Doris Lenartz, Wolfgang Huff, SunHee Lee, Athanasios Koulousakis, Joachim Klosterkoetter, and Volker Sturm. "Remission of alcohol dependency following deep brain stimulation of the nucleus accumbens: valuable therapeutic implications" *Journal of Neurology, Neurosurgery & Psychiatry* 78, no. 10 (2007): 1152-1153.
44. Muller UJ, Sturm V, Voges J, Heinze HJ, Galazky I, Heldmann M, et al. Successful treatment of chronic resistant alcoholism by deep brain stimulation of nucleus accumbens: first experience with three cases. *Pharmacopsychiatry*. 2009;42(6):288-91.
45. Knapp, Clifford M., Lisa Tozier, Arlene Pak, Domenic A. Ciraulo, and Conan Kornetsky. "Deep brain stimulation of the nucleus accumbens reduces ethanol consumption in rats." *Pharmacology Biochemistry and Behavior* 92, no. 3 (2009): 474-479.
46. Henderson, Michael B., Alan I. Green, Perry S. Bradford, David T. Chau, David W. Roberts, and James C. Leiter. "Deep brain stimulation of the nucleus accumbens reduces alcohol intake in alcohol-preferring rats." *Neurosurgical focus* 29, no. 2 (2010): E12.
47. Wilden, Jessica A., Kurt Y. Qing, Sheketha R. Hauser, William J. McBride, Pedro P. Irazoqui, and Zachary A. Rodd. "Reduced ethanol consumption by alcohol-preferring (P) rats following pharmacological silencing and deep brain stimulation of the nucleus accumbens shell." *Journal of neurosurgery* 120, no. 4 (2014): 997-1005.
48. Hadar, R., V. Vengeliene, E. Barroeta Hlusicke, S. Canals, H. R. Noori, F. Wieske, J. Rummel et al. "Paradoxical augmented relapse in alcohol-dependent rats during deep-brain stimulation in the nucleus accumbens." *Translational psychiatry* 6, no. 6 (2016): e840-e8
49. Höppner, Jacqueline, Thomas Broese, Lutz Wendler, Christoph Berger, and Johannes Thome. "Repetitive transcranial magnetic stimulation (rTMS) for treatment of alcohol dependence." *The World Journal of Biological Psychiatry* 12, no. sup1 (2011): 57-62.
50. Maatoug, Redwan, Kévin Bihan, Philibert Duriez, P. Podevin, L. Silveira-Reis-Brito, Amine Benyamina, Antoni Valero-Cabré, and Bruno Millet. "Non-invasive and invasive brain stimulation in alcohol use disorders: A critical review of selected human evidence and methodological considerations to guide future research." *Comprehensive psychiatry* 109 (2021): 152257.
51. Haaranen, Mia, Giulia Scuppa, Stefano Tambalo, Vilja Järvi, Sine M. Bertozzi, Andrea Armirotti, Wolfgang H. Sommer, Angelo Bifone, and Petri Hyytiä. "Anterior insula stimulation suppresses appetitive behavior while inducing forebrain activation in alcohol-preferring rats." *Translational psychiatry* 10, no. 1 (2020): 1-11.
52. Schluter, Renée S., Ruth J. van Holst, and Anna E. Goudriaan. "Effects of ten sessions of high frequency repetitive transcranial magnetic stimulation (HF-rTMS) add-on treatment on impulsivity in alcohol use disorder." *Frontiers in neuroscience* 13 (2019): 1257.

53. Pettorruso, Mauro, Massimo di Giannantonio, Luisa De Risio, Giovanni Martinotti, and George F. Koob. "A light in the darkness: repetitive transcranial magnetic stimulation (rTMS) to treat the hedonic dysregulation of addiction." *Journal of addiction medicine* 14, no. 4 (2020): 272-274.
54. Perini, Irene, Robin Kämpe, Theodor Arlestig, Hanna Karlsson, Andreas Löfberg, Michal Pietrzak, Abraham Zangen, and Markus Heilig. "Repetitive transcranial magnetic stimulation targeting the insular cortex for reduction of heavy drinking in treatment-seeking alcohol-dependent subjects: a randomized controlled trial." *Neuropsychopharmacology* 45, no. 5 (2020): 842-850.
55. Wietschorke, Katharina, Julian Lippold, Christian Jacob, Thomas Polak, and Martin J. Herrmann. "Transcranial direct current stimulation of the prefrontal cortex reduces cue-reactivity in alcohol-dependent patients." *Journal of neural transmission* 123, no. 10 (2016): 1173-1178.
56. den Uyl, Tess E., Thomas E. Gladwin, and Reinout W. Wiers. "Transcranial direct current stimulation, implicit alcohol associations and craving." *Biological psychology* 105 (2015):
57. Trojak, Benoit, Agnès Soudry-Faure, Nicolas Abello, Maud Carpentier, Lysiane Jonval, Coralie Allard, Foroogh Sabsevari et al. "Efficacy of transcranial direct current stimulation (tDCS) in reducing consumption in patients with alcohol use disorders: study protocol for a randomized controlled trial." *Trials* 17, no. 1 (2016): 1-8.
58. Witkiewitz, Katie, Elena R. Stein, Victoria R. Votaw, Adam D. Wilson, Corey R. Roos, Stevi J. Gallegos, Vincent P. Clark, and Eric D. Claus. "Mindfulness-based relapse prevention and transcranial direct current stimulation to reduce heavy drinking: A double-blind sham-controlled randomized trial." *Alcoholism: Clinical and Experimental Research* 43, no. 6 (2019): 1296-1307.
59. Klauss, Jaisa, Quézia S. Anders, Luna V. Felipe, Michael A. Nitsche, and Ester M. Nakamura-Palacios. "Multiple sessions of transcranial direct current stimulation (tDCS) reduced craving and relapses for alcohol use: a randomized placebo-controlled trial in alcohol use disorder." *Frontiers in pharmacology* 9 (2018): 716.
60. Kim, Hyun Joon, and Nyeonju Kang. "Bilateral transcranial direct current stimulation attenuated symptoms of alcohol use disorder: A systematic review and meta-analysis." *Progress in Neuro-Psychopharmacology and Biological Psychiatry* 108 (2021): 110160.
61. Bronstein, Jeff M., Michele Tagliati, Ron L. Alterman, Andres M. Lozano, Jens Volkmann, Alessandro Stefani, Fay B. Horak et al. "Deep brain stimulation for Parkinson disease: an expert consensus and review of key issues." *Archives of neurology* 68, no. 2 (2011): 165-165.
62. Parasuraman, Raja, James Christensen, and Scott Grafton. "Neuroergonomics: The brain in action and at work." *Neuroimage* 59, no. 1 (2011): 1-3.

63. Rezayat, Ehsan, and Iman Ghodrati Toostani. "A review on brain stimulation using low intensity focused ultrasound." *Basic and clinical neuroscience* 7, no. 3 (2016): 187.
64. Pounder, Neill M., and Andrew J. Harrison. "Low intensity pulsed ultrasound for fracture healing: a review of the clinical evidence and the associated biological mechanism of action." *Ultrasonics* 48, no. 4 (2008): 330-338.
65. Best, Thomas M., Kevin E. Wilk, Claude T. Moorman, and David O. Draper. "Low intensity ultrasound for promoting soft tissue healing: a systematic review of the literature and medical technology." *Internal medicine review (Washington, DC: Online)* 2, no. 11 (2016).
66. Tyler, William J., Yusuf Tufail, Michael Finsterwald, Monica L. Tauchmann, Emily J. Olson, and Cassondra Majestic. "Remote excitation of neuronal circuits using low-intensity, low-frequency ultrasound." *PloS one* 3, no. 10 (2008): e3511.
67. Li, Xin, Huifang Yang, Jiaqing Yan, Xingran Wang, Yi Yuan, and Xiaoli Li. "Seizure control by low-intensity ultrasound in mice with temporal lobe epilepsy." *Epilepsy research* 154 (2019): 1-7.
68. Deveci, Erdem, Alperen Kılıç, Onur Yılmaz, Aynur Nabi, Arif Sanlı Ergün, Ayhan Bozkurt, Ayşe Kurtulmuş et al. "The effects of focused ultrasound pulsation of nucleus accumbens in opioid-dependent rats." *Psychiatry and Clinical Psychopharmacology* 29, no. 4 (2019): 748-759.
69. Attia, Amalina Binte Ebrahim, Ghayathri Balasundaram, Mohesh Moothanchery, U. S. Dinish, Renzhe Bi, Vasilis Ntziachristos, and Malini Olivo. "A review of clinical photoacoustic imaging: Current and future trends." *Photoacoustics* 16 (2019): 100144.

Chapter 5: Manuscripts

This chapter contains two manuscripts based on this research: - (5.1, 5.2). A Third and fourth manuscript are in progress. 5.2, titled “Photoacoustic imaging for in vivo quantification of alcohol-induced structural and functional changes in cerebral vasculature in high alcohol preferring mice (HAP)”.is published in a peer-review journal Elsevier Alcohol. It is based on the application of the structural and functional imaging capabilities of photoacoustic imaging to study alcohol-induced changes in cerebral blood vessels in alcohol preferring mice. I am the first author in this paper. The paper appears here in the original form in which it was written.

The second manuscript, 5.2 is titled “Photoacoustic imaging guided system for low intensity focused ultrasound stimulation for the treatment of alcohol use disorder” is under peer review. It is based on the design, development, and application of a low intensity focused ultrasound system for noninvasive in vivo brain stimulation in small animals. While the system is primarily design for treatment of alcohol use disorder, it can be used for any process requiring the noninvasive delivery of substances to the deep brain in small animals. The system is applied in the stimulation of the nucleus accumbens, a region within the deep brain highly implicated in alcohol addiction. The third manuscript is based on the application of the photoacoustic imaging guided low intensity focused ultrasound system in 5.2 to stimulate the ventral tegmental area, a key neural structure implicated in alcohol use disorder. This paper is still in progress. The fourth manuscript is a minireview article on the application of high resolution imaging in the study of addiction in small animals. It is also in progress

5.1 Photoacoustic Imaging for *In vivo* Quantification of Alcohol Induced Structural and Functional Changes in Cerebral Vasculature in High Alcohol Preferring Mice (HAP)

5.1.1 Abstract

Alcohol-induced structural and functional changes were studied *in vivo* by photoacoustic tomography (PAT) of the cerebrovascular system in selectively bred alcohol-preferring mice. High (HAP) and low (LAP) alcohol-preferring mice are replicate lines of mice selectively bred to prefer 10% (v/v) ethanol to water and water to ethanol, respectively, in a free-access two-bottle choice scenario. A cohort of 15 singly-housed alcohol-preferring mice (five HAP mice for the experimental group, five LAP mice for the control group, and five other LAP mice set aside) were given free-access two-bottle choice 10% ethanol (v/v) and water in 50-mL graduated drinking bottles mounted on each of their cages for 4 weeks prior to PAT brain scanning. A daily log of the volume of ethanol consumed over a 24-h period was kept. At the end of the fourth week, blood samples were collected from the HAP mice and blood ethanol concentrations (BECs) were measured to ascertain their levels of ethanol intoxication. The mice were then grouped into five weight-matched pairs of HAP and LAP for comparison purposes, and noninvasive *in vivo* PAT imaging was performed on each weight-matched pair. To mimic a binge drinking paradigm, mice were rearranged into four weight-matched groups of three animals each: an HAP mouse and two LAP mice. For each group, one HAP mouse and one LAP mouse received a 20% ethanol solution via intraperitoneal (i.p.) injection after 24 h of ethanol abstinence, in weight-based doses of 3 g/kg prior to imaging, while the last LAP mouse received a sham i.p. injection. PAT images of the brain were collected for 30 min thereafter. Cerebral vascular diameters for selected vessels of interest were extracted from the PAT images and compared between HAP mice and LAP mice. For the binge scenario, changes in vessel diameter and hemoglobin oxygen saturation were extracted from

PAT images and studied over a 30-min duration. Vascular diameter was significantly smaller in HAP mice compared to LAP mice in weight-matched pairs. Hemoglobin-oxygen saturation and vessel diameter dropped more quickly in LAP mice than in HAP mice following a 20% ethanol i.p. injection (3 g/kg), with a 32% reduction in cerebrovascular diameter in a 30-min period. This study demonstrates the effectiveness of PAT in alcohol use disorder imaging and diagnosis, and its feasibility in studying alcohol-induced changes in vascular structure and perfusion. It also adds to other bodies of evidence to suggest that the effects of binge drinking are more adverse in occasional drinkers than habitual drinkers.

5.1.2 Introduction

The current understanding of the neurobiology and pathophysiology of alcohol use disorder has been largely due to advancements in imaging studies and technology. Often, the knowledge has been acquired indirectly from rodent models of addiction, owing to their similarities to humans in the manner and route of ingestion of various drugs of addiction. Although rodent models can never perfectly replicate conditions in humans, they allow researchers to easily account for and control genetic and environmental factors that are believed to significantly contribute to the predisposition of alcohol use disorder. Thus, they can produce an excellent face validity that enables easy clinical translation [30].

Computerized tomography (CT) [4,5] and variants of magnetic resonance imaging (MRI) [27,31] are currently the gold standards for alcohol use disorder imaging. While CT is radiation-based, MRI is associated with a huge cost, mostly unaffordable for the often-frequent clinical visits associated with alcohol use disorder treatment and rehabilitation. Photoacoustic imaging (PAI) is an emerging hybrid optical imaging modality that relies on optical absorption contrast to visualize tissue structures up to several centimeters deep, with scalable ultrasonic resolution. It does this by

detecting outgoing broadband ultrasound signals generated from laser-illuminated biological tissue [3,25]. PAI has been proposed as a safe optical imaging approach and is particularly promising for frequent use situations such as routine clinical and preventive examinations [32]. Thus, it could be a candidate for the frequent clinical visits associated with alcohol use disorder treatment and rehabilitation. It has also been suggested as an imaging tool to detect functional changes in the brain of small animal models of drug abuse and addiction [13]. There seemingly exists an agreement in the literature on the vasoactive properties of alcohol as well as the etiology and mechanism of brain damage associated with AUD [4,5,27, 31], with most studies focusing on deep brain regional damage. Studies on cerebral vasculature [11,17,23] focus more on the alcohol-induced changes in cerebral blood flow and cerebral blood volume. Studies that quantify the alcohol-induced changes in cerebral vascular diameter and functional changes such as hemoglobin oxygen saturation, and those involving photoacoustic imaging, are quite limited or non-existent. The current study thus has a dual aim: 1) to demonstrate the feasibility of PAI in brain imaging and to propose it as a cost effective and safe alternative for AUD imaging, and 2) to exploit the rich optical absorption contrast differences between oxyhemoglobin and deoxyhemoglobin to noninvasively image alcohol-induced changes in cerebral hemoglobin oxygen saturation and quantify changes in cerebral vascular diameter in high (HAP) and low (LAP) alcohol-preferring mice using PAT. The quantification of vascular diameter from medical images can have far-reaching applications in the diagnosis of pathologies related to diabetes, hypertension, and related cardiovascular disorders, which have direct effects on blood vessels as well as in disease staging. Selected blood vessels of interest (VOI) that supply the mesolimbic brain pathway implicated in AUD are isolated and compared between HAP mice and control LAP mice based on their diameters. We also quantitatively study how cerebral vessel diameter and hemoglobin oxygen

saturation change over a 30-min period following a 20% ethanol intoxication via intraperitoneal injection. Our choice of cerebral vessels is largely due to their roles in supplying blood and oxygen to major brain areas.

5.1.3 Materials and Methods

5.1.3.1 Imaging System

We used a 2D multispectral photoacoustic imaging system shown in Figure 5.1. A short-pulse laser beam was generated from a portable fast-tuning Phocus mobile OPO laser system (OPOTEK LLC; Carlsbad, California, United States; pulse width: 7 ns; repetition rate: 20 Hz). A custom-made fiber optic bundle coupled the beam (Ceram Optec GmbH, Germany) through interlocked ports and delivered it to the mouse brain tissue. The fiber bundle had an output end with a large circular aperture (numerical aperture: 0.37) that covered the entire mouse head and provided uniform illumination to the entire brain region.

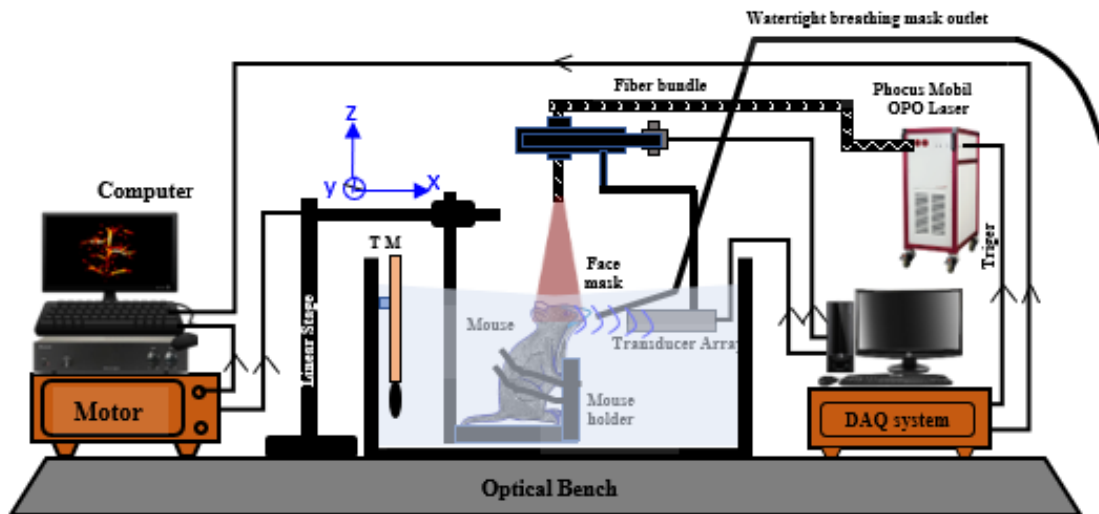


Figure 5.1 Photoacoustic imaging system for non-invasive in vivo imaging of the cerebral vasculature in alcohol preferring mice. TM-Thermoelectric thermometer with water heater, TLS-Translational linear stage.

The photoacoustic signals generated were detected by a semi-circular cylindrically focused transducer array with 256 elements (Japan Probe Co. Ltd.; Japan). The array had a radius of 65 mm with a center frequency of 4 MHz and a bandwidth greater than 80%. It was coupled with a custom-made 256 channel data acquisition system, which had an integrated amplifier system with an adjustable gain of 40–91 dB (Photosound Technologies Inc.; Houston, Texas, United States; sampling rate: 40 mega-samples per second; resolution: 12 bits; frame rate: 50 Hz). A 3.0 USB cable transferred the signal to the computer in real time.

For a 20-Hz single-pulse imaging, our system collected one complete frame of data in approximately 0.05 s. A custom-made device of the same length as the array kept track of its focal zone and marked the position of the animal head as well as the depth of imaging for all animals.

By moving the linear stage to which the mouse holder was attached along the z direction, scanning was performed above and below the initial position, to get different planes of the mouse cerebral cortex. A major difference between our imaging system design and traditional PAT imaging systems is the fact that our animals used a custom-made transparent breathing mask fabricated by 3D printing a stereo lithographically formatted model obtained via reverse engineering [29]. This allowed us to completely immerse the animal holder into water, while supplying life support gases via the inlet and allowing expiration via the outlets. This breathing system was equally used to deliver a low dose of anesthesia, which kept the animal in deep sleep throughout the experiment. Traditional PAT designs place the animal beneath the water tank and use a plastic membrane with ultrasound gel for coupling [13,25,33]. Such designs are often associated with acoustic coupling interference issues, which results in artifacts.

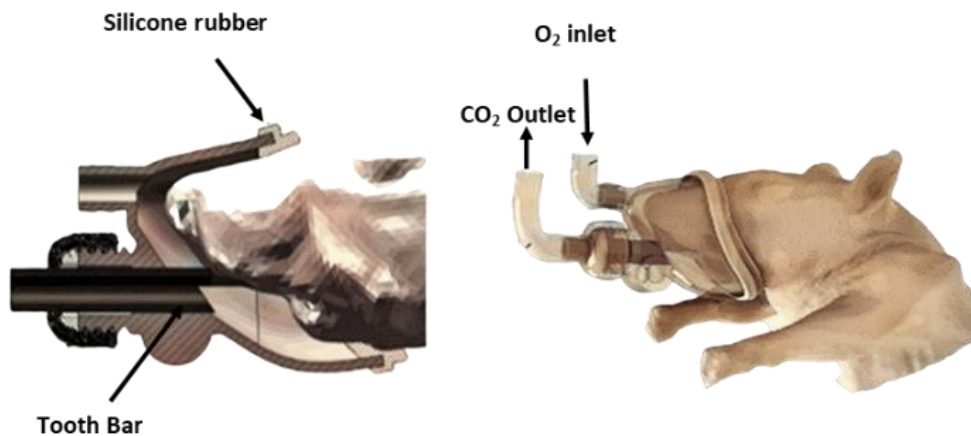


Figure 5.2 Illustration of the connection of the mouse breathing mask used to keep the mouse under water for photoacoustic imaging. The silicon rubber seal ensures a tight non-leaky mask.

5.1.3.2 Animal Model of Ethanol Dependence and Animal Handling

The HAP and control LAP mice used in this study were obtained from Indiana University, Purdue University, Indianapolis (Indianapolis, Indiana, United States) [19,24]. These are crossed replicate lines of mice selectively bred to prefer 10% (v/v) ethanol over water (HAP) and water over ethanol (LAP). Upon arrival at the University of South Florida (USF), mice were housed in a reversed 12:12-h light–dark cycle colony room, with lights off at 8:00 AM, at the University of South Florida, Department of Psychology (PSY) animal facility. All mice had free access to two-bottle choice 10% ethanol (v/v), water, and rodent chow *ad libitum* for a period of 4 weeks, prior to the imaging experiments. Water and ethanol were provided using 50-mL graduated test tubes mounted on each cage. At the end of the fourth week, blood samples were drawn from the tail at midday when animals were expected to be at peak drinking [18,19]. After plasma supernatant extraction using a Pasteur pipette, blood ethanol concentration (BEC) was measured by means of a benchtop Analox Alcohol Analyzer. This procedure was meant to check that the experimental HAP mice were drinking to intoxication as the daily ethanol consumption data revealed. Table 5.1 summarizes the BEC data, while Fig. 5.3 shows the drinking pattern for the best-drinking HAP

mice 30 days prior to imaging. Details of the animal model generation and line selection can be seen in these works [10,18,19,21,24].

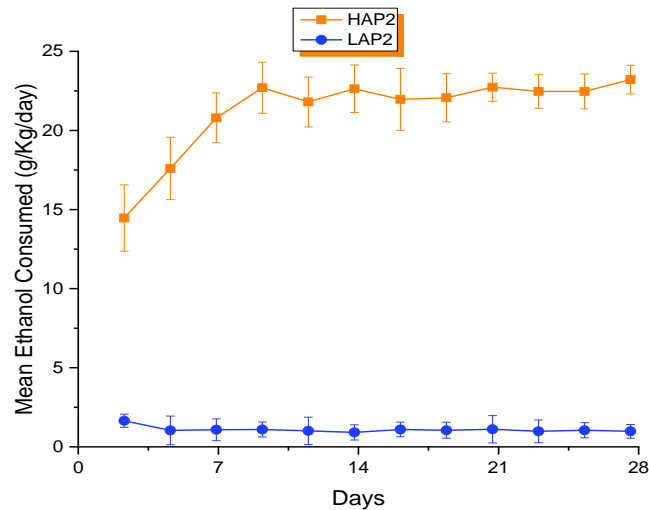


Figure 5.3 Mean ethanol consumption per day for HAP and LAP mice. This data is for the five best alcohol drinkers (HAP) and the five worst drinkers (LAP) used for our imaging experiment. The mice were paired based on their weights for comparison.

The rodent manipulation procedures were in accordance with a laboratory animal use protocol approved by the University of South Florida Institutional Animal Care and Use Committee (USF-IACUC). All experimental animal procedures were performed in conformity with the guidelines of the US National Institute of Health Guide for the Care and Use of Laboratory Animals [22]. HAP mice and control LAP mice were paired according to similarity in their weights at the time of imaging, and animals with similar weights were scanned and compared during the same scanning session using the 2D multispectral photoacoustic imaging system described earlier. The animal was affixed to a custom-made mouse holder (Fig. 5.1) and held in place by loosely tied rubber bands. System settings, including laser energy (12 mJ/cm^2), distance from fiber bundle to animal head (10 cm), as well as the location of the animal's head remained the same from animal to animal. We used a custom-made plastic device to keep track of the head location. After weighing, each animal was administered 4% isoflurane gas anesthesia using an isoflurane

anesthetic setup, to induce sleep. While in deep sleep, hair was removed from the scalp region using a rodent clipper and hair removal cream was used afterward to depilate the remaining hair. The breathing mask was then fitted to the mouse face and the tooth bar was used to pull the mouse face until the mask was completely fitted and tight. The oxygen pipe was then connected to the mask's oxygen inlet (Fig. 5.2). The oxygen flew through 1.0–1.5% isoflurane anesthesia to keep the animal asleep throughout the scanning. Scanning was done with the skull and scalp intact. At the end of the scanning, euthanasia was done with an overdose of isoflurane followed by cervical dislocation

Table 5.1 Mean blood ethanol concentration for HAP mice.

Subject (HAP)	S1	S2	S3	S4	S5
Mean BEC (mg/dl)	214.9	220.2	229.1	217.7	233.8
Error (\pm)	15.55	19.81	13.95	16.55	12.59

5.1.3.3 PAT Imaging of Alcohol-Induced Changes in Cerebral Vessel Diameter

In the first phase of imaging, no additional ethanol was infused into the mice. Our goal was to mimic a free-choice alcohol use disorder. Thus, the only ethanol the animals were exposed to was ingested by free choice. For the second phase, mice were arranged into four weight-matched groups of three animals each: an HAP mouse and two LAP mice. For each group, an HAP mouse and one LAP mouse received 145–150 μ L of 20% ethanol solution (prepared from ACS grade 190 proof ethanol and sterile 0.9% physiological saline) via intraperitoneal injection (i.p.) after 24 h of ethanol abstinence in weight-based doses of 3 g/kg prior to imaging, while the last LAP received a sham IP injection. The goal was to induce a single ethanol binge [6,15] and to reduce the variability across subjects observed with ethanol ingestion by free choice (Fig. 3). PAT images

were then acquired for 30 min at an isosbestic wavelength of 800 nm, at which the relative photoacoustic signal change reflects the change in total hemoglobin concentration (HbT).

PAT signal for a single 2D image in 0.05 s, a time shorter than that for one mouse heartbeat. We have neglected heat conduction, since our OPO laser's nanosecond pulse duration is shorter than the thermal diffusion time, to ensure thermal and stress confinement [32]. Thus, considering only the thermo-expansion mechanism, the photoacoustically generated acoustic field within mouse tissue can be described by the following:

$$\left[\nabla^2 - \frac{1}{c^2} \frac{\partial^2}{\partial t^2} \right] p(\mathbf{r}, t) = \frac{\beta}{c_p} \frac{\partial}{\partial t} [\varphi(\mathbf{r}) I(t)] \quad 5.1$$

where β , C_p , c , $p(\mathbf{r}, t)$ and $\varphi(\mathbf{r})$ are, respectively, the thermal coefficient of expansion, the specific heat capacity at constant pressure, the speed of sound, the acoustic pressure at position r and time t , and the optical energy absorbed in the mouse tissue. Our goal was to recover $\varphi(\mathbf{r})$ from the detected PA signals. We acquired several data frames over a 30-min time span and reconstructed the images using a delay and sum algorithm with temperature-based speed of sound calibration [35].

5.1.3.4 Multispectral Photoacoustic Imaging of Alcohol-Induced Changes in Hemoglobin Oxygen Saturation

For the hemoglobin oxygen saturation imaging we used the same binge animals as described in section 5.1.2.3, and acquired PA signals at 720nm and 840nm wavelengths, based on the molar extinction coefficient spectra of oxyhemoglobin (HbO) and deoxyhemoglobin (HbR) [16]; using the switchable OPO laser system described earlier. At these wavelengths, HbO and HbR are the predominant optical energy absorbing chromophores with significantly different molar extinction coefficients [14]. The system collects a single frame of multispectral data in 0.1 seconds. The laser energy was instantaneously deposited within the mouse cerebral cortex and assuming invariance in the sound speed and density, the

initial acoustic pressure $P_0(\lambda_i, x, y)$ for the i -th ($i=1,2$) wavelength can be thought to represent the reconstructed PAT images $I(\lambda_i, x, y)$ at that wavelength, which itself represents the absorbed energy $E(\lambda_i, x, y)$ but for a constant factor [14]. Our choice of wavelengths (720 nm and 840 nm) around an isosbestic wavelength ensures that the difference $\delta\mu_a$ in absorption coefficients between each image $I(\lambda_i, x, y)$ is small and the high sensitivity of our imaging system results in significantly low noise in each of the images $I(\lambda_i, x, y)$ as well as the difference image δI , resulting in negligible uncertainty in sO_2 due to noise. We thus neglected fluence correction [28]. After image reconstruction, we employed a least square linear spectral fitting technique to obtain the distribution of HbO and HbR [14]. $E(\lambda_i, x, y)$ can be expressed as follows:

$$P_0(\lambda_i, x, y) \cong E(\lambda_i, x, y) = \Phi(\lambda_i)\mu_a(\lambda_i, x, y) \cong \Phi(\lambda_i) \left(\varepsilon_{\lambda_i}^{HbO_2} C_{HbO_2}^{\lambda_i} + \varepsilon_{\lambda_i}^{HbR} C_{HbR}^{\lambda_i} \right) \quad 5.2$$

where $\Phi(\lambda_i)$ is the fluence and μ_a is the optical absorption coefficient. From equation 5.2, the oxygen saturation sO_2 map was calculated as follows

$$sO_2 = \frac{C_{HbO}(x,y)}{(C_{HbO}(x,y) + C_{HbR}(x,y))} \quad 5.3$$

where $(C_{HbO}(x, y) + C_{HbR}(x, y))$ is the total hemoglobin HbT .

5.1.4 Results

5.1.4.1 Extraction and Comparison of Cerebral Vessel Diameter in HAP and LAP Mice

The significant difference in optical absorption between hemoglobin, deoxyhemoglobin; and the surrounding tissues [12] results in good contrast which enables cerebral blood vessels in HAP and LAP mice to be clearly identifiable in PAT images. As shown in Figure 5.4 (A), we extracted the vessels diameter (Strictly speaking vessel intensity) of the blood vessels by fitting a normalized Gaussian curve, of the form given in equation 5.4 to a blood vessel's cross-sectional profile along the y direction. Since the Gaussian function never vanishes at the edges, the exact boundaries of the curve cannot be measured directly with exactness. Thus, we have evaluated the

full width at half maximum (FWHM) of the Gaussian [9,26,34]. It gives the width of the curve at the point where the value of the function is equal to half of its maximum value.

$$y = y_0 + \frac{Ae^{\left(\frac{-(x-x_c)^2}{2\sigma^2}\right)}}{\sigma\sqrt{2\pi}} \quad 5.4$$

where $\sigma = \frac{A}{w\sqrt{2\pi}}$ defines the spread of the Gaussian, A is a constant which gives a measure of the PA signal intensity and w is the full width at half maximum. x_c is the center of the Gaussian and y_0 is its base.

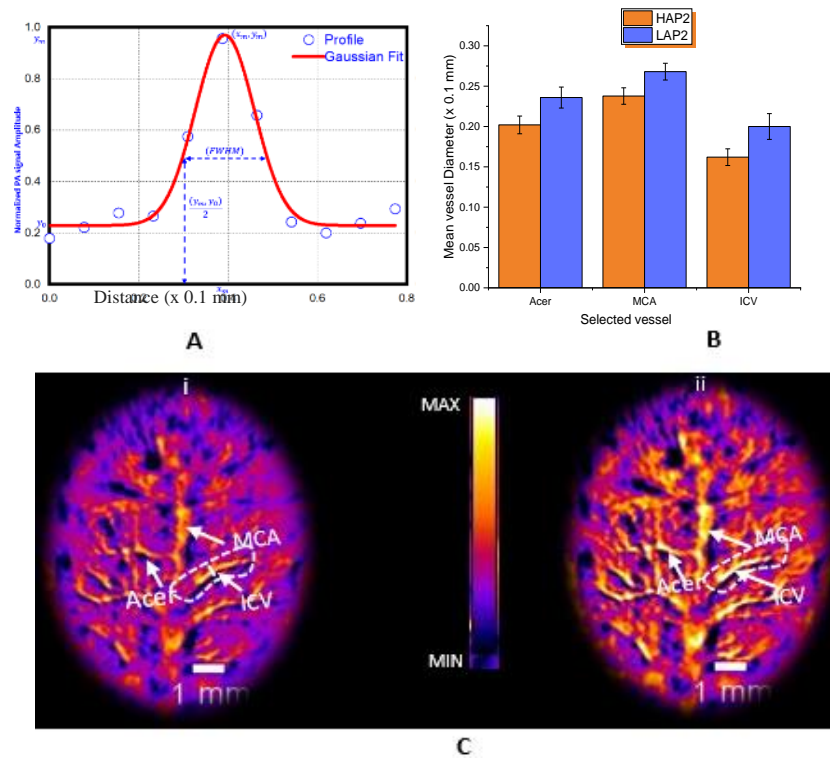


Figure 5.4 Estimation and comparison of selected blood vessels between HAP and LAP. A, Details of a Normalized Gaussian fit for one of the vessels of interest from which full width at half maximum (FWHM) is estimated (ICV- Inferior cerebral vein, MCA- Middle cerebral artery, Acer: -Anterior Cerebral Artery). B, Results of statistical analysis and comparison between selected vessels for 5 HAP and 5 LAP (3 x 5 vessels for each animal model). The error bars indicated the standard deviation in the calculation. With a p value of $p < 0.002$, ($F = 40.38$), the vessels diameter for HAP is significantly smaller than for LAPs. C(i) and C(ii), Typical PAT image of HAP and LAP mouse cerebral cortex respectively at 800nm wavelength.

The Gaussian height y_m occurs at the center where $x = x_c$ and is given by:

$$y_m = \frac{A}{\sigma\sqrt{2\pi}} \quad 5.5$$

The full width at half maximum occurs when the Gaussian takes half of its maximum value as shown in Figure 5.4 (A). Upon substitution, rearranging, and solving for $x = w$, we get the full width at half maximum to be:

$$FWHM = w = 2\sigma\sqrt{2\ln 2} \quad 5.6$$

which depends only on σ , the spread of the Gaussian.

We then performed a generalized linear mixed model ANOVA on the mean of vessel diameter with animal type as class variable using the SAS software (SAS Institute, Cary, NC) for HAP and LAP, with a α -value of 0.05. With a p value of 0.0002, $F=40.8$, the results show that vessel diameter is statistically and significantly larger in low alcohol preferring mice, compared to their high alcohol preferring counterparts. Table 5.2 summarizes the data.

Table 5.2 Summary of vessel diameters for various vessels of interest.
(Acer: anterior cerebral artery; ICV: inferior cerebral vein; MCA: middle cerebral artery).

<i>Mice</i>	<i>Vessel (VOI)</i>	<i>Number</i>	<i>Mean Diameter</i>	<i>Std. Dev.</i>	<i>Std. Err.</i>	<i>Min.</i>	<i>Max.</i>
LAP	MCA	5	0.268	0.010	0.004	0.255	0.280
	Acer	5	0.236	0.013	0.005	0.220	0.245
	ICV	5	0.201	0.015	0.007	0.181	0.220
HAP	MCA	5	0.238	0.010	0.004	0.225	0.244
	Acer	5	0.202	0.011	0.005	0.188	0.215
	ICV	5	0.162	0.010	0.005	0.150	0.175

5.1.4.2 Estimation of Change in Hemoglobin Oxygen Saturation

From the time series images for binge drinking described in 5.1.2.3, we extracted the change in vessel diameter over time for HAPs and LAPs. We further extracted the change in hemoglobin oxygen saturation from the multispectral images for HAP and LAP as described in

5.1.2.4 and compared the results. Figure 5.5 (a -c) shows the oxygen saturation maps over time as well as the comparison of percentage change in vessel diameter and hemoglobin oxygen saturation.

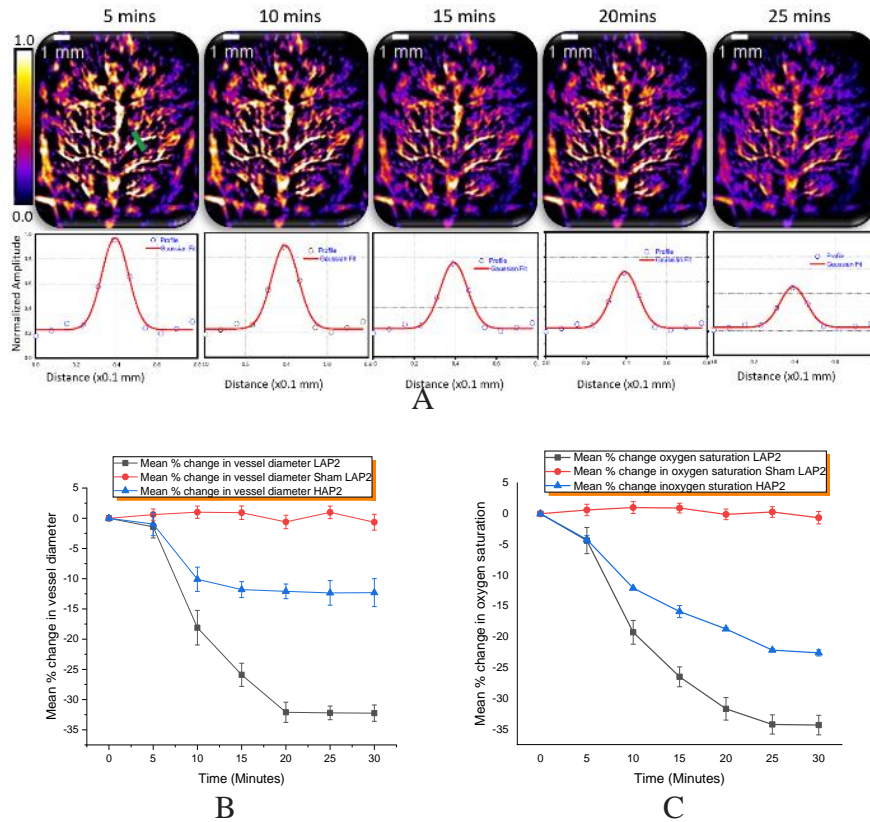


Figure 5.5 Estimation and comparison of percentage change in vessel diameter and hemoglobin oxygen saturation with time for a selected vessel between HAP and LAP. Both acutely ingest 20% ethanol (3g/kg), after 24 hours of EtOH abstinence. A: Demonstration of drop in vessel diameter for the selected vessels. B: Comparison of the change in vessel diameter for HAP and LAP, C: Corresponding change in hemoglobin oxygen saturation for the same vessel.

5.1.5 Discussions

We have studied the effect of alcohol dependence on cerebral blood vessels for two drinking paradigms, namely chronic and binge drinking, using photoacoustic tomography (PAT). PAT is an emerging hybrid optical imaging modality that relies on optical absorption contrast to visualize tissue. We have exploited the significant difference in optical absorption between hemoglobin, deoxyhemoglobin, and the surrounding tissues to image and study the direct effects

of ethanol on the cerebrovascular system in selectively bred alcohol-preferring mice. HAP mice selectively bred to prefer ethanol to water in a two-bottle free-choice scenario and consume huge amounts of ethanol were used as the experimental subjects. LAP mice selectively bred to consume very little ethanol, or no ethanol served as controls.

Both animal species belong to the same cohort, were born on the same day, and were bred under the same conditions. Our comparison groups in this study consist of weight-matched HAP and LAP mice. This ensures that we minimize errors that may result from differences in biological clocks in different animals. We have modeled vessel diameter by fitting a Gaussian curve to the cross-sectional profile across the blood vessels. We calculated and equated the Gaussian full width at half maximum (FWHM) to the diameter, which strictly speaking is the vessel's photoacoustic intensity at the point of evaluation. Oxyhemoglobin and deoxyhemoglobin, the proteins responsible for transporting oxygen in blood, are the predominant chromophores that absorb the incident optical energy in this study. Thus, the photoacoustic signal intensity (equivalently the amplitude) is a direct measure of the amount of optical energy absorbed, which indirectly gives a measure of the volume (amount or size) of the absorber or its container (blood vessel). Thus, the alcohol-induced drop in signal intensity for HAP mice, compared to their LAP counterparts, observed in this study is evidence of the drop in container volume/content, namely blood vessel diameter/blood volume. Many other studies have reported such alcohol induced changes in blood volume [11,17,23].

The vasoactive properties of alcohol are well known in pharmacology to be dependent on the dose and manner of alcohol consumption. In this study, we used HAP mice that had been made dependent on ethanol at a dose of 10% v/v for their entire life by free choice. We used this unique phenomenon to study the chronic effects of ethanol on cerebral blood vessels by simply imagining

and comparing corresponding cerebral blood vessels in HAP and LAP mice of the same weight and age. The LAP mice are genetically bred to consume very little or no ethanol. To study binge drinking and acute alcohol-induced changes in cerebral oxygen saturation, we administered a weight-based dose of 20% v/v ethanol to both HAP and LAP mice and studied how the vessels' diameter and hemoglobin oxygen saturation changed over time using the functional capabilities of photoacoustic imaging. We then compared the results to weight-matched LAP mice that had received a sham IP injection. This approach reduces the variability in drinking observed with the free-choice drinking and ensures the animals acutely receive a huge dose of ethanol, as in binge drinking.

The exact mechanism of alcohol induced vascular constriction is not clear in the literature. However, from basic physiology the major determinant of vascular diameter and thus of resistance and flow rate is the contractile state of the vascular smooth muscle which is the vascular tone of the vessel. Thus, we have shown using PAT that alcohol exerts its effect directly on vascular smooth muscles to influence their tone. Though blood flow is not strictly laminar, a simple form of Poiseuille's law [8], can be used to model blood flow. The resistance to blood flow can be written as $R = 8\eta L / (\pi r^4)$; where L is the vessel's length, r , its radius, while η and π are constants. The blood flow rate F can be written as $F = \delta P \pi r^4 / (8\eta L)$, where δP is the pressure difference across a segment of the blood vessel. Thus, vessel diameter has an inverse effect on resistance and a direct effect on flow rate. Therefore, for a given blood volume, vascular constriction results in increase resistance and decrease flow to the brain, resulting in a drop in photoacoustic intensity with time. In particular, the equation shows the dramatic influence vessel diameter has on resistance and flow rate. Blood flow to the brain delivers oxygen used in oxidative metabolism [2]. Because cerebral neurons are limited in their capacity to undergo anaerobic respiration [36], the

brain relies on oxidative metabolism for most of its ATP. Thus, blood flow to the brain is crucial for normal brain function. Such alcohol induced drops in vascular diameter and the resulting resistance to and drop in flow as we have demonstrated could be responsible for acute ischemic stroke [20] and aneurysmal hemorrhage reported to be associated with binge drinking, with episodes reported to occur with 24 hours of drinking in humans [1] Constriction of vessels diameters observed in this study may also result in such increase in blood pressure reported to be associated with heavy ethanol consumption

The results from this study show that chronic alcohol dependence is associated with cerebral vessel constriction, as we observed in the HAP mice. Also, binge drinking that involves drinking a huge dose of alcohol at a single instant constricts cerebral vessels as well. More importantly, we have shown that the constriction of cerebral blood vessels and the drop in hemoglobin oxygen saturation following binge drinking is more drastic in occasional binge drinkers, compared to habitual binge drinkers or alcohol addicts. The observed difference in ethanol's effect between HAP mice and LAP mice following a 20% binge ethanol intoxication may result from differences in ethanol tolerance between the two lines of mice. Genetic differences in ethanol metabolism (faster breakdown in HAP mice – more tolerant, due to genetically higher ethanol metabolic enzymes; slower breakdown in LAPs – less tolerant due to genetically fewer ethanol metabolic enzymes) or differences related to adaptation over time, owing to the manner of ethanol consumption (chronic binge in HAP mice, as opposed to episodic binge drinking in LAP mice) between the two lines may account for the observed difference in tolerance.

In conclusion, we have demonstrated the feasibility of using PAT to study changes in vascular structure and perfusion in AUD imaging and diagnosis. The results show that chronic alcohol dependence is associated with cerebral vascular constriction. Additionally, binge drinking

is associated with cerebral vascular constriction and rapid drop in hemoglobin oxygen saturation, with the effect being more drastic in occasional binge drinkers than in habitual binge drinkers. The findings also demonstrate the potential health benefits of identifying and intervening with individuals who binge drink and report tolerance, even when they do not meet current alcohol use disorder diagnostic criteria.

5.1.6 References

1. Altura, B. M., Altura, B. T., & Gebrewold, A. (1983). Alcohol-induced spasms of cerebral blood vessels: relation to cerebrovascular accidents and sudden death. *Science (New York, N.Y.)*, 220(4594), 331–333.
2. Bélanger, M., Allaman, I., & Magistretti, P. J. (2011). Brain energy metabolism: focus on astrocyte-neuron metabolic cooperation. *Cell metabolism*, 14(6), 724–738. <https://doi.org/10.1016/j.cmet.2011.08.016>
3. Bell A. G., (1880) On the production of sound by light, *Am. J. Sci.* 20,305. <https://doi.org/10.2475/ajs.s3-20.118.305>
4. Cala L. A., Jones B., Mastaglia F. L., Wiley B. (1978). Brain Atrophy and intellectual impairment in heavy drinkers- A clinical psychometric and computerized tomography study, *Aust. NZ. J. Med.* 8, 147. <https://doi.org/10.1111/j.1445-5994.1978.tb04502.x>
5. Cala L. A., Mastaglia F. L. (1981). Computerized tomography in chronic alcoholics, *Alcohol Clin. Exp. Res.* 5(2), 283. <https://doi.org/10.1111/j.1530-0277.1981.tb04902.x>.
6. Chen, M. M., Palmer, J. L., Ippolito, J. A., Curtis, B. J., Choudhry, M. A., & Kovacs, E. J. (2013). Intoxication by intraperitoneal injection or oral gavage equally potentiates postburn organ damage and inflammation. *Mediators of inflammation*, 2013. <https://doi.org/10.1155/2013/971481>
7. Christoph G. A. Hoelen and Frits F. M. de Mul, (2000). Image reconstruction for photoacoustic scanning of tissue structures, *Appl. Opt.* 39, 5872-5883. <https://doi.org/10.1364/AO.39.005872>
8. Fantini, S., Sassaroli, A., Tgavalekos, K. T., & Kornbluth, J. (2016). Cerebral blood flow and autoregulation: current measurement techniques and prospects for noninvasive optical methods. *Neurophotonics*, 3(3), 031411. <https://doi.org/10.1117/1.NPh.3.3.031411>
9. Fischer M. J., Uchida S., Messlinger K. (2010). Measurement of meningeal blood vessel diameter in vivo with a plug-in for ImageJ *Microvascular Research* 80(2):258-66. <https://doi.org/10.1016/j.mvr.2010.04.004>.

10. Grahame N. J, Li T. K, Lumeng L. (1999) Selective breeding for high and low alcohol preference in mice. *Behav Genet.* 29(1):47-57. [https://doi: 10.1023/a:1021489922751](https://doi.org/10.1023/a:1021489922751).
11. Gundersen H, van Wageningen H, Grüner R. (2013). Alcohol-induced changes in cerebral blood flow and cerebral blood volume in social drinkers. *Alcohol Alcohol.* 48(2).
12. Jacques S. L. (2013). Optical properties of biological tissues: a review. *Phys Med Biol.* 58(11): R37-61. <https://doi.org/10.1088/0031-9155/58/11/R37>.
13. Jo J., Yang X. (2011). Detection of cocaine induced rat brain activation by photoacoustic tomography. *J Neurosci Methods.* 195(2): 232-5. [https://doi: 10.1016/j.jneumeth.2010.12.006](https://doi:10.1016/j.jneumeth.2010.12.006).
14. Li, M., Tang, Y., & Yao, J. (2018). Photoacoustic tomography of blood oxygenation: A mini review. *Photoacoustic*, 10, 65–73. <https://doi.org/10.1016/j.pacs.2018.05.001>
15. Ma, H., Yu, L., Byra, E. A., Hu, N., Kitagawa, K., Nakayama, K. I., ... & Ren, J. (2010). Aldehyde dehydrogenase 2 knockout accentuates ethanol-induced cardiac depression: role of protein phosphatases. *Journal of molecular and cellular cardiology*, 49(2), 322-329. <https://doi:10.1016/j.yjmcc.2010.03.017>.
16. Matcher SJ, Elwell CE, Cooper CE, Cope M, Delpy DT (1995) Performance comparison of several published tissue near-infrared spectroscopy algorithms. *Anal Biochem* 227:54–68. <https://doi.org/10.1006/abio.1995.1252>.
17. Mathew R. J., Wilson WH. (1986). Regional cerebral blood flow changes associated with ethanol intoxication. *Stroke.*17(6) 1156-1159 [https://doi: 10.1161/01.str.17.6.1156](https://doi:10.1161/01.str.17.6.1156).
18. Matson L. M, Grahame N. J. (2013) Pharmacologically relevant intake during chronic, free-choice drinking rhythms in selectively bred high alcohol-preferring mice. *Addict Biol.* 18(6):921-9. [https://doi: 10.1111/j.1369-1600.2011.00412.x](https://doi:10.1111/j.1369-1600.2011.00412.x).
19. Matson L. M., Kasten C. R, Boehm S. L. 2nd, Grahame N. J. (2014) Selectively bred crossed high-alcohol-preferring mice drink to intoxication and develop functional tolerance, but not locomotor sensitization during free-choice ethanol access. *Alcohol Clin Exp Res.* 38(1):267-74. [https://doi: 10.1111/acer.12216](https://doi:10.1111/acer.12216).
20. Mostofsky, E., Burger, M. R., Schlaug, G., Mukamal, K. J., Rosamond, W. D., & Mittleman, M. A. (2010). Alcohol and acute ischemic stroke onset: the stroke onset study. *Stroke*, 41(9), 1845–1849. <https://doi.org/10.1161/STROKEAHA.110.580092>
21. Mulligan, M. K., Ponomarev, I., Hitzemann, R. J., Belknap, J. K., Tabakoff, B., Harris, R. A., Crabbe, J. C., Blednov, Y. A., Grahame, N. J., Phillips, T. J., Finn, D. A., Hoffman, P. L., Iyer, V. R., Koob, G. F., & Bergeson, S. E. (2006). Toward understanding the genetics of alcohol drinking through transcriptome meta-analysis. *Proceedings of the National Academy of Sciences of the United States of America*, 103(16), 6368–6373. <https://doi.org/10.1073/pnas.0510188103>

22. National Research Council (US) Committee for the Update of the Guide for the Care and Use of Laboratory Animals. Guide for the Care and Use of Laboratory Animals. 8th ed. Washington (DC): National Academies Press (US); 2011. PMID: 21595115.
23. Newlin D. B., Golden C. J., Quaife M., Graber B. (1982). Effect of alcohol ingestion on regional cerebral blood flow. *Int J Neurosci.* 17(3) 145-150 [https://doi: 10.3109/00207458208985916](https://doi.org/10.3109/00207458208985916).
24. Oberlin, B., Best, C., Matson, L., Henderson, A., & Grahame, N. (2011). Derivation and characterization of replicate high- and low-alcohol preferring lines of mice and a high-drinking crossed HAP line. *Behavior genetic*, 41(2), 288–302. <https://doi.org/10.1007/s10519-010-9394-5>
25. Oraevsky A. A., Karabutov A. A. (2014) Optoacoustic tomography- Biomedical photonics Handbook. 125, 34, pp1-34, CRC press Boca Raton, FL. <https://doi.org/10.1201/b17288>
26. Pedersen L., Grunkin M., Ersbüll B., Madsen K., Larsen M., Christofferson N., and Skands U. (2000) Quantitative measurement of change in retina vessels diameter in ocular fundus images. *Pattern Recognition Letters* 21(13), 1215. [https://doi.org/10.1016/S0167-8655\(00\)00084-2](https://doi.org/10.1016/S0167-8655(00)00084-2)
27. Pfefferbaum A., Sullivan E. V., Mathalon D. H., and Lim K. O., (1997) Frontal lobe volume loss observed with magnetic resonance imaging in older chronic alcoholics *Alcohol Clin. Exp. Res.* 21, 521. <https://doi.org/10.1111/j.1530-0277.1997.tb03798.x>
28. Roman H., Lu A., Paul C. B., Benjamin T. C., (2019). Estimating blood oxygenation from photoacoustic images: can a simple linear spectroscopic inversion ever work?. *J. Biomed. Opt* 24(12). <https://doi.org/10.1117/1.JBO.24.12.121914>
29. Shan T., Zhao Y., Jiang S., Jiang H. (2020). In-vivo hemodynamic imaging of acute prenatal ethanol exposure in fetal brain by photoacoustic tomography. *J. Biophotonics.* 13(5) <https://doi.org/10.1002/jbio.201960161>.
30. Spanagel R. (2017). Animal models of addiction. *Dialogues in clinical neuroscience*, 19(3), 247–258. <https://doi.org/10.31887/DCNS.2017.19.3/rspanagel>.
31. Sullivan, E. V., Rosenbloom, M. J., Lim, K. O., & Pfefferbaum, A. (2000). Longitudinal changes in cognition, gait, and balance in abstinent and relapsed alcoholic men: Relationships to changes in brain structure. *Neuropsychology*, 14(2), 178–188. <https://doi.org/10.1037/0894-4105.14.2.178>.
32. Sun Y, Jiang H. (2009). Quantitative three-dimensional photoacoustic tomography of the finger joints: phantom studies in a spherical scanning geometry. *Phys Med Biol.* 2009 Sep 21;54(18):5457-67. <https://doi.org/10.1088/0031-9155/54/18/007>.
33. Sun Y., Jiang H., and O'Neill B. E. (2011), Photoacoustic imaging- An emerging optical modality in diagnostic and Theranostic Medicine, *J. Biosens. bioelectronics* 2, 108. [https://doi:10.4172/2155-6210.1000108](https://doi.org/10.4172/2155-6210.1000108)

34. Varma J. K., Subramanyan K., Durgan J., (2004) Full width at half maximum as a measure of vessel diameter in computed Tomography Angiography, *Proc SPIE*. 5372. <https://doi.org/10.1117/12.535642>
35. Hoelen, Christoph GA, and Frits FM de Mul. "Image reconstruction for photoacoustic scanning of tissue structures." *Applied Optics* 39, no. 31 (2000): 5872-5883.
36. Vavilala, Monica S., Lorri A. Lee, and Arthur M. Lam. "Cerebral blood flow and vascular physiology." *Anesthesiology Clinics of North America* 20, no. 2 (2002): 247-264.

5.2 Photoacoustic Imaging Guided System for Repetitive Low Intensity Focused

Ultrasound Stimulation for the Treatment of Alcohol Use Disorder

5.2.1 Abstract

The interaction between alcohol and various neurotransmitter systems in the brain's reward and stress system results in changes in neuronal function that underline the development of sensitization, tolerance, withdrawal, dependence, and an eventual alcohol use disorder (AUD). The socioeconomic burden from AUD and the inability of existing medications to significantly improve the condition demonstrates a strong incentive for research towards identifying and implementing novel noninvasive, neural circuits-specific therapeutic treatments that would support and maintain alcohol abstinence and of associated strategies aiming at preventing or at least limiting AUD. Here, we describe a novel Photoacoustic imaging guided (PAI-LIFU) system for repetitive low intensity focused ultrasound stimulation for the treatment of AUD in crossed high alcohol preferring (c-HAP) mice. We demonstrate the effectiveness, safety, and repeatability of the system to precisely deliver LIFU to the nucleus accumbens (NAc) in crossed high alcohol preferring mice (cHAPs) with high resolution. Results from repetitive treatments using our system suggests that LIFU, targeted to the NAc in cHAPs, reduces ethanol consumptions with a marked increase in water consumption in a two-bottled choice paradigm. Furthermore, by analyzing the

ratio of volume of ethanol consumed to total volume of fluid consumed, we note a significant drop in ethanol preference ratios in favor of water, following treatments using our system.

5.2.2 Introduction

The Diagnostic and statistical manual of mental disorders, 5th edition (DSM-V), defines alcohol use disorder (AUD- alcohol abuse, alcohol dependence, alcohol addiction, and alcoholism) as a medical condition characterized by an impaired ability to stop or control alcohol use despite adverse social, occupational, or health consequences [1]. It is a chronically relapsing brain disorder characterized by the compulsion to seek and take alcohol, loss of control in limiting alcohol intake, and the emergence of a negative emotional state when access to alcohol is discontinued [2]. AUD is a major global risk factor for disability and premature loss of life [3], affecting an estimated 76 million people worldwide with huge health and socioeconomic burden [4]. In the USA alone, more than \$249 billion in economic costs is attributable to AUD [5]

Despite the socioeconomic menace, advancements in research towards underpinning the etiology and pathophysiology of AUD was impeded for a long time because AUD had been regarded as a punishable moral deficiency, rather than a chronically relapsing brain disease [6,7]. With advancements in technology and the development of animal models of alcohol addiction, more rigorous research is progressively unraveling the brain neural circuits, systems and processes involved with the development of an AUD. It is now clear that chronic alcohol exposure induces neuroadaptive changes on the brain neural circuits that control motivational processes such as reward, arousal, and stress. Such changes lead to a functional disruption in various brain systems utilizing signaling molecules like dopamine, opioid peptides, gamma-aminobutyric acid, glutamate, including systems that modulate the brain's response to stress [7-9]. The overall effect of these changes is the development of an incentive sensation to alcohol's effect

which motivates the individual to continually seek alcohol [8]. When alcohol is discontinued, they develop withdrawal symptoms characterized by dysphoria, extreme stress, and anxiety, which further motivates alcohol seeking. Thus, the individual is caught in a cycle where they want to continually seek alcohol to either keep getting the rewards (such as euphoria) associated with it or to avoid the negative withdrawal symptoms (stress, anxiety, dysphoria) associated with alcohol discontinuation.

An overview of the brain's reward system, its associated circuitry, and how chemical signals flow through it is crucial for a proper understanding of how chronic alcohol exposure induces neuroadaptive changes on brain neural circuits, and how novel treatment modalities for AUD could be approached. This system involves the mesolimbic and mesocortical dopamine pathways, including the medial forebrain and the extended amygdala [9,10]. It is the system that is activated in response to a rewarding stimulus, such as food, water, sex etc. and is responsible for complex cognitive processes such as incentive motivation, expectation, and emotions [9,11]. Its dopamine projections originate from the ventral tegmental area (VTA) to innervate neurons of the nucleus accumbens (NAc) (mesolimbic pathway) and neurons of the prefrontal cortex (mesocortical pathway) [10]. Brain neural circuits consists of a series of interconnected nerve cells each relaying information related to specific functions to the other through electrochemical signaling mediated by neurotransmitters. Dopamine, the main neurotransmitter of the reward system is stored in the presynaptic vesicles and is released when an action potential arrives the presynaptic dendrite. Its reception is the function of specialized ligand-gated receptors located on the post synaptic neuron, while its reuptake from the synaptic space is mediated by specialized transport proteins on the presynaptic neuronal dendrite. PET studies have confirmed that, unlike

most addictive drugs that target specific receptors and transporters, alcohol affects a wide range of targets and indirectly increases dopamine in the NAc.

Despite the negative consequences of AUD, current treatment modalities consisting of a combination of behavioral therapies and medications are associated with a low success rate, [13] with a 40%-70% relapse rate one to three years after standard treatment [14]. The three FDA-approved medications for AUD (Acamprosate, Disulfiram and Naltrexone) are either associated with unpleasant side effects (drowsiness, weakness, tiredness, dizziness etc.), or are ineffective in preventing withdrawal symptoms [15]. Also, existing therapeutic interventions require expensive long-term inpatient treatment, often afforded by a few addicts only, leaving the greater chunk of them untreated [13]. Given these drawbacks, it is imperative to expand treatment to novel, non-invasive, non-medication-based modalities that would support and maintain alcohol abstinence, prevent cravings and withdrawal symptoms. To this end, low intensity focused (LIFU) ultrasound-based neuromodulation-, the targeted alteration of nerve activity through the controlled delivery of LIFU neurostimulations to a specific region of interest (ROI) within the brain, - could potentially change this as it may offer a way of mechanically inducing neuroplasticity – The capacity of the nervous system to modify its structural and functional organization, adjusting itself to a changing environment [16] -, through the localized application of an ultrasound stimulus to a suitable ROI.

The concept of using neuromodulation-based treatment for AUD is not entirely new. In 2007, Kuhn et al [17]. reported the unintended remission of long-term comorbid alcohol consumption by a patient following deep brain stimulation of the nucleus accumbens for treating an anxiety disorder. Subsequently, data from both animal and human studies involving DBS of the NAc showed reduced alcohol consumption [18-21]. Repetitive transcranial magnetic stimulation (rTMS) to the dorsolateral prefrontal cortex (DLPFC) has been shown to reduce alcohol-related

cravings or consumption, post active rTMS treatment [22-27]. Transcranial direct current stimulation (tDCS) has equally shown promise in reducing alcohol related cravings and consumption [28-33]. DBS is pruned to risks of infection and neural immune system reactions [34]. TMS and tDCS fail to provide the required spatial resolution to target deep brain regions of interest and are unable to stimulate such regions without exerting undesired effects to surrounding tissues, even with the integration of H-coils into modern TMS machines in a bit to focus more precisely [35]. LIFU on the other hand combines exceptional millimeter scale spatial resolution with the potential to target subcortical structures (deeper than 10 cm) through intact skull [36]. It has already seen successful applications in promoting bone fracture healing [37], acceleration of soft tissue regeneration [38,39], opening ion channels and synaptic activation [40], suppression of induced epileptic behavior [41], preventing a rise in morphine place preference in opioid dependent rats [42] amongst several other application. The goal in neuroscience is to make brain stimulation noninvasive, inexpensive, user-friendly, direct, and safe; all features of which, LIFU has the capacity to provide.

A key feature in every LIFU stimulation is to use a suitable imaging modality to guide ultrasound to the neural target of interest. Imaging guidance typically has a dual role: - first to ensure that the ultrasound reaches the desired ROI and as a tool to evaluate the effect of the stimulation. Most previous studies have used variants of MRI for guiding LIFU stimulation [43]. However, MRI scanners still suffer from their perennial cost-ineffectiveness, bulkiness, coupled with a long scanning time. To overcome these limitations, an alternative imaging modality such as photoacoustic imaging (PAI) can be used for guidance. PAI has the advantage of being nonionizing, noninvasive, cost-effective and can generate both structural and functional

information [44-46]. PAI has been used for guidance in high intensity focused ultrasound tissue ablation [47] and as guidance for various surgical procedures [48].

In this work, we use photoacoustic imaging to guide the LIFU stimulation of the nucleus accumbens (NAc) in crossed high alcohol preferring (c-HAP) mice. We observe the effects of LIFU by monitoring the drinking behavior of the c-HAPs before and after stimulation. Our choice of the nucleus accumbens (NAc) stems from the strategic position it occupies along the brain's reward pathway and the role it plays in receiving dopaminergic innervations from the VTA and processing reward stimuli alike.

5.2.3 Method

5.2.3.1 System Description

A block diagram of the system is shown in Figure 5.6. It consists of two detachable subsystems.

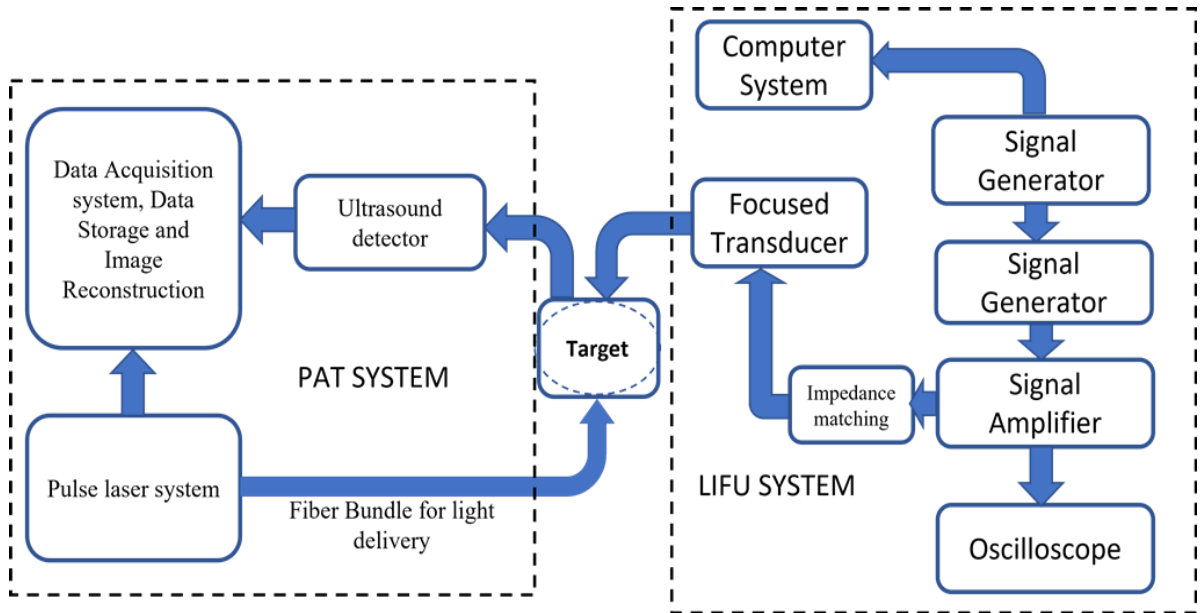


Figure 5.6 Block diagram of the photoacoustic imaging guided system for repetitive low intensity focus ultrasound stimulation for the treatment of alcohol use disorder in cross high alcohol preferring mice.

The photoacoustic imaging (PAT) subsystem and the low intensity focused ultrasound (LIFU) treatment subsystem. The LIFU subsystem consists of a single element focused ultrasound transducer (H101, Sonic Concepts, Bothell, WA) operating at a fundamental frequency of 1.3 MHz used to deliver short tone burst of pulse ultrasound to the target. The 64 mm piezo-electric element is coupled with an acoustic lens, having a 51 mm radius of curvature. The input electrical waveform to the transducer is generated by two serially connected function generators (Tektronix Technologies, Beaverton, OR), and amplified using a linear power amplifier (Tektronix Technologies, Beaverton, OR). An impedance matching device between the amplifier and transducer ensures that the signal to the transducer is always matched to the amplified signal.

The imaging subsystem is a 2 dimensional photoacoustic imaging setup. A short pulse laser beam is generated from a portable fast-tuning Phocus mobile OPO laser (OPOTEK LLC, Carlsbad, California; Pulse width 7ns, repetition rate: 20Hz). A custom-made fiber optic bundle (Ceram Optec GmbH, Germany) couples the laser beam through interlocked ports and delivers it to the target. The fiber bundle has an output end with a large circular numerical aperture (NA= 0.37) which covers and provides uniform illumination to the target's ROI. The photoacoustic signals generated are detected by a semi-circular cylindrically focused transducer array (ultrasound detector) with 256 elements (Japan probe Co. Ltd. Japan). The array has a radius of 65 mm with a center frequency of 4 MHz and a bandwidth greater than 80%. It is coupled with a custom-made 256 channel data acquisition system which has an integrated amplifier system with an adjustable gain of 40-91dB (Photosound Technologies Inc., Houston Texas, sampling rate = 40 MSP; resolution = 12 bits, frame rate 50Hz). A 3.0 USB cable transfers the signal to the computer in real time, for processing and image reconstruction. For a 20 Hz single pulse imaging, our system collects one complete frame of data in approximately 0.05 seconds.

5.2.3.2 System Testing

5.2.3.2.1 Ultrasound Field Characterization

To evaluate the system's compliance with its specified requirements, we used it to stimulate the nucleus accumbens (NAc) in a mouse model of alcohol use disorder, using set treatment parameters. For the set parameters, we first characterize the acoustic field of the LIFU transducer, by mapping its spatial profile (Figure. 5.7A) at the focal location in both free field and a tissue mimicking phantom, in a degassed water tank (Figure. 5.7 B), using a calibrated needle hydrophone (HNC1000, 2.4 mm tip diameter, ONDA Sunnyvale, CA). The hydrophone was mounted on a three-axis motorized linear stage controlled by a LabVIEW virtual instrument, as it moved around the focal region, laterally and axially to the transducer surface. The output voltage signals from the hydrophone were measured and converted to acoustic pressure using equations (5.7).

$$p(t) = \frac{V(t)}{G(f_{awf})} \quad 5.7$$

where $p(t)$ (MPa) is the temporal acoustic pressure, $V(t)$ (mV) is the voltage due to the acoustic pressure incident on the active element of the needle hydrophone. $G(f_{awf})$ (mV/MPa) is the hydrophone sensitivity at the acoustic working frequency f_{awf} .

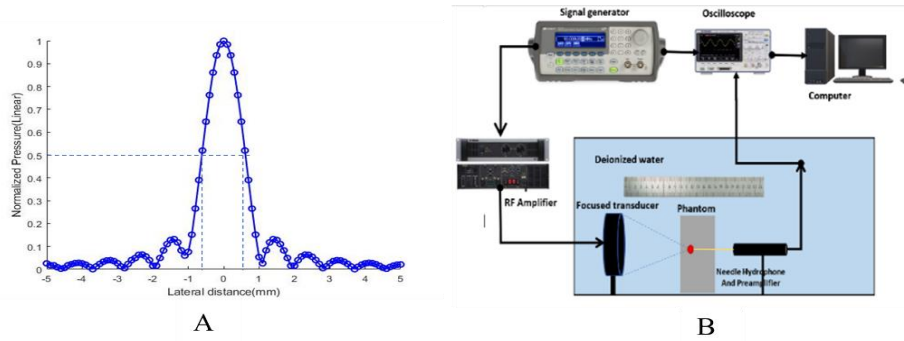


Figure 5.7 Characterization of the acoustic field of a low intensity focused ultrasound transducer.

The focal dimension, defined as the full width at half maximum of the resulting lateral and axial spatial profiles were respectively 1.24 mm in diameter and 5.71 mm in length (Figs 5.7A, 5.8A). Using equation (5.8) we converted pressure data from equation (5.7) to intensity data, from where we estimated the relevant in situ acoustic intensities at the transducer focus. The effective acoustic pressure (P_{eff}) is the root-mean square positive and negative pressures measured using the calibrated hydrophone. Here, ρ is the density of the water and c is the speed of sound in water.

$$I = \frac{P_{eff}^2}{\rho c} \quad 5.8$$

The *in-situ* intensity at the focus was estimated to be $I_{sppa} = 0.168 \text{ W/cm}^2$ (spatial peak pulse average intensity) and $I_{spta} = 0.062 \text{ W/cm}^2$, (spatial peak temporal average)

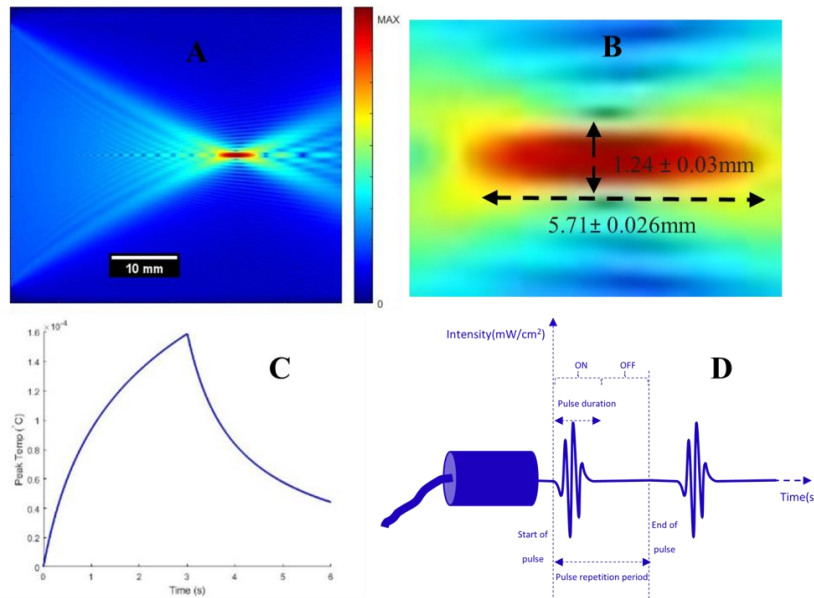


Figure 5.8 Modelling of low intensity focused ultrasound distribution through intact mouse brain. A. Modeled ultrasound field distribution. B. Close in on the ultrasound beam focus to highlight the simulated lateral and axial beam dimensions. C. Maximum temperature rise due to LIFU induced thermal effect. D. Key ultrasound pulse parameters definition.

To estimate the potential thermal effect of sonication and hence safety of the treatment, we carried out both measurements and simulations of the maximum temperature increase at the focus due to the thermal effect for our set treatment parameters. Our simulation indicated only a $0.08 \text{ }^\circ\text{C}$

rise in temperature above equilibrium body temperature of 37°C (Fig. 5.8 C), significantly small to cause damage. To measure the temperature rise, the hydrophone (Fig. 5.7 B) was replaced with a sensitive digital needle probe thermometer (-40°C – 155°C, Delta Trak, Pleasanton, CA), factory calibrated to NIST traceable standards. The maximum temperature rise indicated by the probe was 0.001°C.

5.2.3.2.2 Animal Model of Alcohol Use Disorder

Ten singly housed crossed high alcohol preferring mice (cHAP) were used in the study to test the efficacy of our system. The crossed replicate lines selectively bred to prefer 10% (v/v) ethanol over water were obtained from Indiana University Purdue University Indianapolis (IN, USA) [93,94]. Upon arrival at University of South Florida (USF), mice were housed at the USF Department of psychology (PSY) animal facility in a reversed 12:12 light-dark cycle colony room, with lights off at 8:00am. Each mouse had free access to two-bottle choice 10% ethanol (v/v), water and rodent chow *ad libitum*. Water and ethanol were provided using 50-ml graduated test tubes mounted on each cage. Prior to treatment, the mice were allowed to drink for two weeks to reach a baseline ethanol/water consumption. At the end of the second week, and prior to the first day of treatment, blood samples were drawn from the tail at midday when animals were expected to be at peak drinking [94,95]. After plasma supernatant extraction using a Pasteur pipette, baseline blood ethanol concentration (BEC) was measured by means of a benchtop Analox Alcohol Analyzer. This procedure was meant to check that the cHAPs were drinking to above pharmacological levels as the daily ethanol consumption data revealed. Details of the animal model generation and line selection can be seen in these works [93-97].

5.2.3.3 PAT Guided LIFU Stimulation of the Nucleus Accumbens

5.2.3.3.1 Animal Handling Procedures and PAT Imaging of NAc

The animal handling procedures were in accordance with a laboratory animal use protocol approved by the university of South Florida institutional animal care and use committee (USF-IACUC). All animal procedures were performed in conformity with the guidelines of the US National Institute of Health guide for the care and use of laboratory animals [61]. Because of potential interaction of anesthetic substances and psychoactive drugs like alcohol [59], no anesthesia was use in our animal procedures. A custom-made wrap was used to restraint and keep animal warm during LIFU stimulation [60]. While in a restrained position, hair was removed from the animal scalp using a rodent clipper, followed by hair removal cream to depilate any remaining hair. The bregma midline was identified and animal placed in a stereotaxic frame Figure 5.9 A.

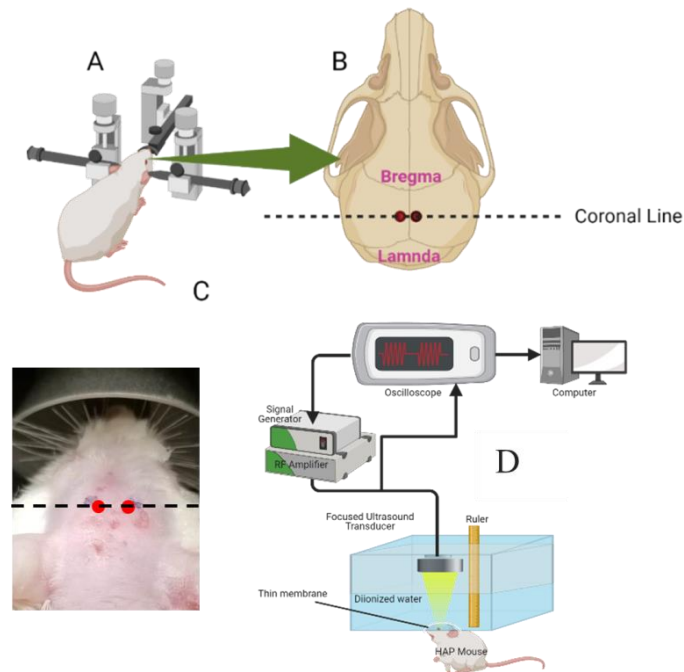


Figure 5.9 Animal preparation for LIFU stimulation. A.: Illustration of mouse in stereotaxic frame with B: Mouse scalp showing the bregma and lambda lines. C: Stimulation point for the lateral and medial NAc. D: LIFU stimulation setup. The mouse is wrapped with a custom wrap which restraints and keeps it warm and placed beneath the degassed water tank. A thin plastic membrane is used to cover mouse head as it protrudes beneath the water tank and ultrasound gel used for coupling (Created with BioRender.com).

Using a mouse brain atlas in stereotaxic coordinates, the stereotaxic coordinates of the medial and lateral NAc were marked on the scalp using an indelible marker. (Lateral NAc shell: AP 1.36; ML +/- 1.6; DV -4.1, For the medial NAc shell: AP 1.6; ML +/- 0.5; DV -4.3). A coronal line was then marked across these points to prepare the animal for PAT imaging. A coronal slice (Fig. 5.10 A) of the mouse brain was taken along a plane passing through the marked line to reveal the NAc (Fig. 5.10 C). We then analyzed the PAT image to determine the depth of the NAc. This depth was used to adjust the focal length of the LIFU transducer for accurately focusing the ultrasound to the NAc.

5.2.3.3.2 Choice of NAc for *In vivo* PAT Guided LIFU Stimulation

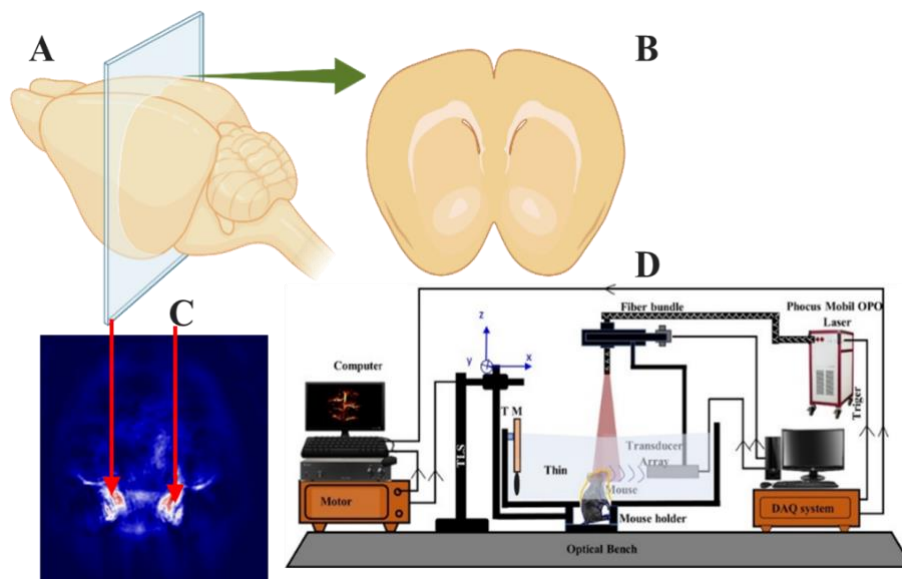


Figure 5.10 PAT setup for LIFU guidance. A: Coronal slice of mouse brain around the point of stimulation B: PAT coronal slice showing the NAc. C: PAT coronal slice showing the focus point at the NAc. This slice was taken using our 2D PAT system. D: Our 2 D photoacoustic imaging system used in low intensity focused ultrasound guidance. System is used to take coronal slices of the mouse brain around the point of stimulation. (A and B are Created with BioRender.com)

Our choice of the NAc as a region of interest for stimulation stems from the several bodies of evidence highlighting its role in alcohol reinforcement. Alcohol mediates its reinforcing

properties by targeting the mesocorticolimbic DA system [9-11]. This system originates in the VTA and projects to its major targets; the NAc and the medial prefrontal cortex (PFC). Besides being the primary target of dopaminergic innervations from the VTA, about 95% of the NAc is composed of medium spiny neurons (MSNs) [49,50]. With mainly excitatory synaptic interconnections within the NAc, these neurons receive extensive glutamatergic inputs from limbic areas, especially the medial prefrontal cortex (mPFC), ventral subiculum of the hippocampus and basolateral amygdala, while projecting widely to the ventral pallidum, substantia nigra and the VTA. Several bodies of evidence believe that alcohol activates or “hijacks” some of the synaptic plasticity mechanism in NAc excitatory neurons, leading to alterations in excitatory glutamatergic synaptic functions within the NAc. Such alterations cumulatively result in alcohol seeking behavioral adaptation. Just as this plasticity underlies experience-dependent learning, it produces a long-term shift in the activity of both reward and inhibitory control mechanisms, driving alcohol seeking behaviors [49-58].

5.2.3.3.3 *In vivo* PAT Guided LIFU Stimulation of The Nucleus Accumbens

A total of 10 cHAP mice (our best drinkers) were set aside for this study (5 LIFU and 5 controls). Prior to LIFU treatment, animals were observed for 14 days to ensure they stabilize in their drinking pattern. On the first day of the stimulation experiment, blood samples were drawn from tail vein for blood ethanol concentration measurements. The LIFU group received a dose of LIFU, while the control group received a sham LIFU. To LIFU stimulate the NAc, we first used our PAT system to obtain images of the mouse brain along several coronal planes around the target ROI to reveal the NAc (Fig. 5.10 C). From these PAT images, the location of the NAc was estimated and the LIFU transducer adjusted accordingly to place its focus at the NAc. Focused ultrasound was subsequently delivered in short tone bursts at a frequency of 1.3MHz. The pulse

repetition frequency was set at 1KHz and duty cycle at 50%. The pulse duration was set at 0.5ms and stimulation was done for 500ms. The *in situ* intensities at the focal point were estimated from the acoustic pressure profile prior to stimulation as described elsewhere. We proceeded with treatment for 14 days, while observing the drinking pattern for alcohol and water.

5.2.4 Results

5.2.4.1 Ethanol and Water Drinking Following LIFU Stimulation of the NAc

Figure 5.11 shows the drinking data (g/kg) and the blood ethanol concentration (BEC) before and after treatment.

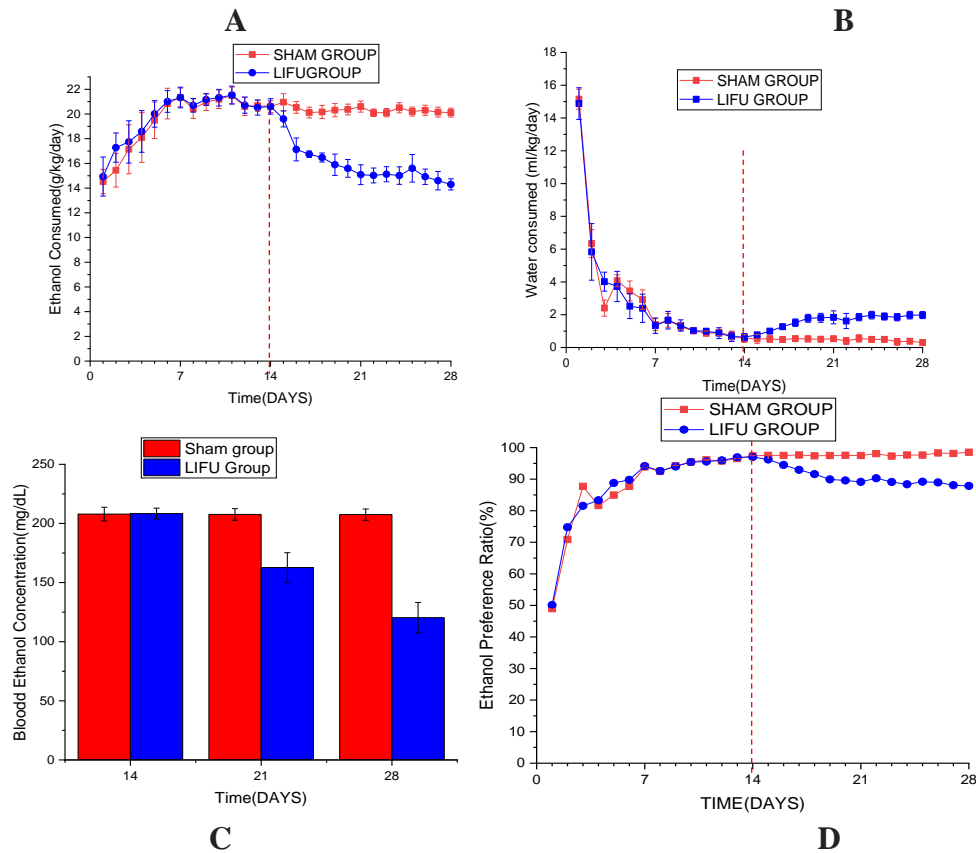


Figure 5.11 Fluid consumption and blood ethanol concentration. Ethanol (A) and water (B) consumptions. Blood ethanol concentration (C) and ethanol preference ratios before and after LIFU stimulation of NAc (D). LIFU treatment started at Day 14 (red dashed line in A, B and C). n=5 for each group, data represented as mean \pm SEM.

There was no significant difference in ethanol drinking between the sham and LIFU groups during the alcohol escalation period or at baseline (Fig. 5.11 A). A general linear model (GLM) repeated measures ($\alpha=0.05$) found a significant effect of LIFU treatment on alcohol intake ($F=297.35$; $p < 0.0001$), with lower alcohol intake in the LIFU-treated group from day 15 onward ($p < 0.05$; Fig. 5.11A). The reduction in ethanol consumption was further supported by a drop in BEC (Fig. 5.11 C). After treatment, there was a significant decrease in BEC in the LIFU group, compared to the sham group ($F=15.89$; $p = 0.004$). Ethanol preference is calculated as the percentage of ethanol consumed to total fluid (ethanol and water) intake. Figure 5.11 D shows that there was no significant difference in baseline ethanol preference but ethanol preference decreased significantly in the LIFU group following LIFU treatment ($F=113.5$; $p < 0.0001$).

5.2.4.2 Activation of the NAc Following LIFU Stimulation

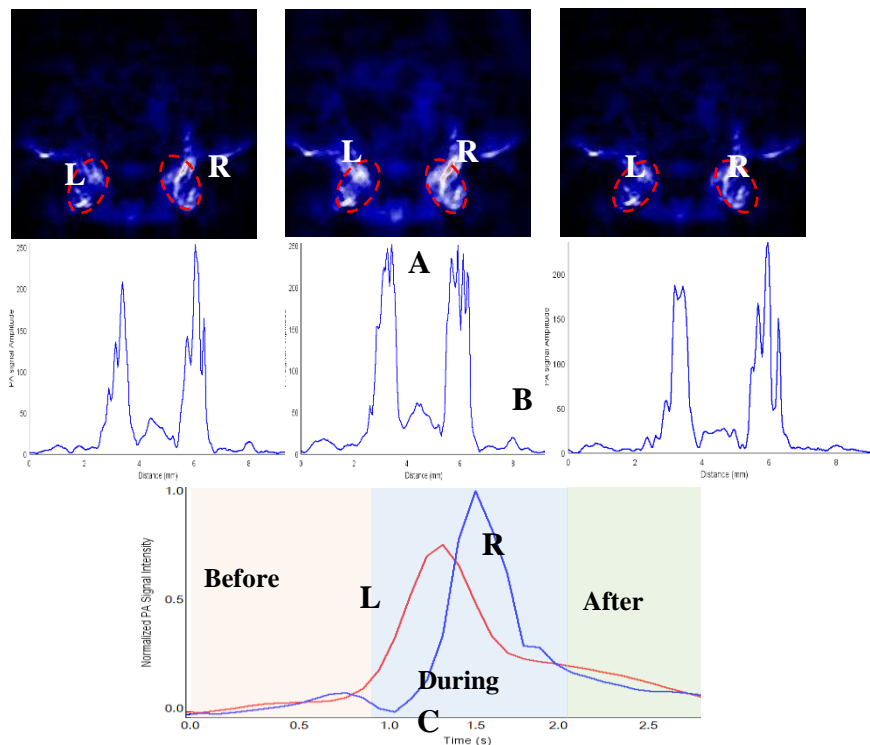


Figure 5.12 Change in PAT signal intensity before, during and after LIFU stimulation. A: PAT functional Images B: Signal Intensity at each NAc. C: Change in PAT signal intensity across each NAC.

For a 20-Hz single-pulse imaging, our system collected one complete frame of data in approximately 0.05 s (1/20Hz). We acquired PAT images for 1s each before, during and after LIFU stimulation, for a total of 3s. and averaged for each second. Figure 5.12 shows PAT images averaged for each second, the signal amplitude across the lateral and medial NAc (for left -L and right-R NAc) shell/core and the change in PAT signal during across each NAc.

5.2.5 Discussion

We have described a novel photoacoustic imaging guided system for low intensity focused ultrasound stimulation for the treatment of alcohol use disorder in crossed high alcohol preferring mice (c-HAP). Using our system to stimulate the NAc, we have found that, low intensity focused ultrasound targeted to the Nucleus Accumbens (NAc) produces a significant reduction in ethanol consumption, with a marked increase in water consumption in a two-bottle choice paradigm. The NAc, a key node of the mesolimbic dopamine circuitry has long been conceptualized as a critical functional connection between limbic system structures such as the amygdala and hippocampus, and motor system structures including the basal ganglia [62,63]. In fact, it is widely hypothesized that NAc dopamine release accounts for the addictive liability of drugs of abuse [64-66] and thus it remains a crucial convergence point of the brain's neurocircuitry shaping motivated response to salient rewarding and aversive stimuli [63]. Besides dopaminergic innervations from the VTA, GABAergic medium spiny neurons (MSNs) making up most of the NAc with their excitatory synaptic interconnections within it, receive extensive glutamatergic inputs from limbic areas, especially the medial prefrontal cortex (mPFC), ventral subiculum of the hippocampus and basolateral amygdala, while projecting widely to the ventral pallidum, substantia nigra and the VTA [49,50]. Ethanol exerts its effect by altering proteins (mainly Cys-loop and purinergic ligand-gated ion channels as well as neurotransmitter receptors and transporters) involved with synaptic

transmission within neurons of the brain. The end results of these alteration is some form of alcohol-induced synaptic plasticity, mainly long-term potentiation (a persistent increase in synaptic transmission) or long term-depression (Persistent decrease in synaptic transmission) [67-82].

The effects of ultrasound on tissue are strictly parameter-based and are broadly classified into thermal and nonthermal effects, with LIFU being under the nonthermal division [83]. Nonthermal effects are further divided into acoustic radiation force and cavitation effects. Cavitation refers to bubbles formed as a result of shock waves fluctuation, when a mechanical wave such as ultrasound propagates [84]. Low intensity Ultrasound stimulation results in only minimal rise in temperature, with no side effect on the surrounding tissue [85,86]. Thus, the results obtained here cannot be due to cavitation effects. Acoustic radiation forces result from momentum transfer between the ultrasound acoustic field and the brain tissue, as the wave interacts with tissue [84,87]. They are responsible for radiation torques and acoustic streaming and are capable of displacing small ions, molecules, and organelles as well as eliciting fluid movements around and along cell membranes [88]. In fact, Tyler et al [88-90] believed that LIFU may modulate neuronal excitability by either exerting mechanical stress which changes the viscoelastic properties of lipid bilayers or by mechano-sensitive transmembrane proteins modulating receptor channel gating kinetics. Recent studies [91,92] have indicated that LIFU could activate voltage gated sodium and calcium channels, thereby eliciting action potential and synaptic transmission. Thus, the results observed in this study are most likely due to mechanisms related to neuronal excitability at the NAc.

5.2.6 References

1. Stein, Dan J., Katharine A. Phillips, Derek Bolton, K. W. M. Fulford, John Z. Sadler, and Kenneth S. Kendler. "What is a mental/psychiatric disorder? From DSM-IV to DSM-V." *Psychological medicine* 40, no. 11 (2010): 1759-1765.
2. Koob, George F., and Michel Le Moal. "Drug abuse: hedonic homeostatic dysregulation." *Science* 278, no. 5335 (1997): 52-58.
3. Abuse, Substance. "Mental Health Services Administration (SAMHSA). 2001 National Household Survey on Drug Abuse Summary Findings." *Office of Applied Studies: Rockville, MD* (2002).
4. J. Rehm, C. Mathers, S. Popova, et al., Global burden of disease and injury and economic cost attributable to alcohol use and alcohol use disorders, *Lancet* 373 (2009) 2223–2233.
5. J. Rehm, K.D. Shield, Alcohol, and mortality: global alcohol-attributable deaths from cancer, liver cirrhosis and injury in 2010, *Alcohol Res. Curr. Rev.* 35 (2013) 174–183.
6. Klenowski, Paul M. "Addictive Behaviors Emerging role for the medial prefrontal cortex in alcohol-seeking behaviors."
7. Fibiger, H.C. and A.G. Phillips, *Mesocorticolimbic dopamine systems and reward*. *Ann N Y Acad Sci*, 1988. 537: p. 206-15.
8. Gardner, E.L., *Brain reward mechanisms*, in *Substance Abuse: a Comprehensive Textbook*, J. Lowinson, et al., Editors. 1997, Williams & Wilkins: Baltimore. p. 61-85.
9. Koob, George F., S. Barak Caine, Petri Hyytia, Athina Markou, Loren H. Parsons, Amanda J. Roberts, Gery Schulteis, and Friedbert Weiss. "Neurobiology of drug addiction." (1999).
10. Klenowski, Paul M. "Addictive Behaviors Emerging role for the medial prefrontal cortex in alcohol-seeking behaviors."
11. Fibiger, H.C. and A.G. Phillips, *Mesocorticolimbic dopamine systems and reward*. *Ann N Y Acad Sci*, 1988. 537: p. 206-15.
12. Moos, Rudolf H., and Bernice S. Moos. "Rates and predictors of relapse after natural and treated remission from alcohol use disorders." *Addiction* 101, no. 2 (2006): 212-222.
13. Tabakoff, Boris, and Paula L. Hoffman. "The neurobiology of alcohol consumption and alcoholism: an integrative history." *Pharmacology Biochemistry and Behavior* 113 (2013): 20-37.
14. Domi, Esi, Ana Domi, Louise Adermark, Markus Heilig, and Eric Augier. "Neurobiology of alcohol seeking behavior." *Journal of Neurochemistry* (2021).

15. Koob, G. F., and N. D. Volkow. "Neurobiology of addiction: a neurocircuitry analysis. *Lancet Psychiatry*. 2016; 3 (8): 760–73."
16. Koob, George F., S. Barak Caine, Petri Hyytia, Athina Markou, Loren H. Parsons, Amanda J. Roberts, Gery Schulteis, and Friedbert Weiss. "Neurobiology of drug addiction." (1999).
17. Kuhn, Jens, Doris Lenartz, Wolfgang Huff, SunHee Lee, Athanasios Koulousakis, Joachim Klosterkoetter, and Volker Sturm. "Remission of alcohol dependency following deep brain stimulation of the nucleus accumbens: valuable therapeutic implications" *Journal of Neurology, Neurosurgery & Psychiatry* 78, no. 10 (2007): 1152-1153.
18. Muller UJ, Sturm V, Voges J, Heinze HJ, Galazky I, Heldmann M, et al. Successful treatment of chronic resistant alcoholism by deep brain stimulation of nucleus accumbens: first experience with three cases. *Pharmacopsychiatry*. 2009;42(6):288-91.
19. Knapp, Clifford M., Lisa Tozier, Arlene Pak, Domenic A. Ciraulo, and Conan Kornetsky. "Deep brain stimulation of the nucleus accumbens reduces ethanol consumption in rats." *Pharmacology Biochemistry and Behavior* 92, no. 3 (2009): 474-479.
20. Henderson, Michael B., Alan I. Green, Perry S. Bradford, David T. Chau, David W. Roberts, and James C. Leiter. "Deep brain stimulation of the nucleus accumbens reduces alcohol intake in alcohol-preferring rats." *Neurosurgical focus* 29, no. 2 (2010): E12.
21. Wilden, Jessica A., Kurt Y. Qing, Sheketha R. Hauser, William J. McBride, Pedro P. Irazoqui, and Zachary A. Rodd. "Reduced ethanol consumption by alcohol-preferring (P) rats following pharmacological silencing and deep brain stimulation of the nucleus accumbens shell." *Journal of neurosurgery* 120, no. 4 (2014): 997-1005.
22. Hadar, R., V. Vengeliene, E. Barroeta Hlusicke, S. Canals, H. R. Noori, F. Wieske, J. Rummel et al. "Paradoxical augmented relapse in alcohol-dependent rats during deep-brain stimulation in the nucleus accumbens." *Translational psychiatry* 6, no. 6 (2016): e840-e840.
23. Höppner, Jacqueline, Thomas Broese, Lutz Wendler, Christoph Berger, and Johannes Thome. "Repetitive transcranial magnetic stimulation (rTMS) for treatment of alcohol dependence." *The World Journal of Biological Psychiatry* 12, no. sup1 (2011): 57-62.
24. Maatoug, Redwan, Kévin Bihan, Philibert Duriez, P. Podevin, L. Silveira-Reis-Brito, Amine Benyamina, Antoni Valero-Cabré, and Bruno Millet. "Non-invasive and invasive brain stimulation in alcohol use disorders: A critical review of selected human evidence and methodological considerations to guide future research." *Comprehensive psychiatry* 109 (2021): 152257.
25. Haaranen, Mia, Giulia Scuppa, Stefano Tambalo, Vilja Järvi, Sine M. Bertozzi, Andrea Armirotti, Wolfgang H. Sommer, Angelo Bifone, and Petri Hyytiä. "Anterior insula stimulation suppresses appetitive behavior while inducing forebrain activation in alcohol-preferring rats." *Translational psychiatry* 10, no. 1 (2020): 1-11.

26. Schluter, Renée S., Ruth J. van Holst, and Anna E. Goudriaan. "Effects of ten sessions of high frequency repetitive transcranial magnetic stimulation (HF-rTMS) add-on treatment on impulsivity in alcohol use disorder." *Frontiers in neuroscience* 13 (2019): 1257.
27. Pettorruso, Mauro, Massimo di Giannantonio, Luisa De Risio, Giovanni Martinotti, and George F. Koob. "A light in the darkness: repetitive transcranial magnetic stimulation (rTMS) to treat the hedonic dysregulation of addiction." *Journal of addiction medicine* 14, no. 4 (2020): 272-274.
28. Perini, Irene, Robin Kämpe, Theodor Arlestig, Hanna Karlsson, Andreas Löfberg, Michal Pietrzak, Abraham Zangen, and Markus Heilig. "Repetitive transcranial magnetic stimulation targeting the insular cortex for reduction of heavy drinking in treatment-seeking alcohol-dependent subjects: a randomized controlled trial." *Neuropsychopharmacology* 45, no. 5 (2020): 842-850.
29. Wietschorke, Katharina, Julian Lippold, Christian Jacob, Thomas Polak, and Martin J. Herrmann. "Transcranial direct current stimulation of the prefrontal cortex reduces cue-reactivity in alcohol-dependent patients." *Journal of neural transmission* 123, no. 10 (2016): 1173-1178.
30. den Uyl, Tess E., Thomas E. Gladwin, and Reinout W. Wiers. "Transcranial direct current stimulation, implicit alcohol associations and craving." *Biological psychology* 105 (2015): 37-42.
31. Trojak, Benoit, Agnès Soudry-Faure, Nicolas Abello, Maud Carpentier, Lysiane Jonval, Coralie Allard, Foroogh Sabsevari et al. "Efficacy of transcranial direct current stimulation (tDCS) in reducing consumption in patients with alcohol use disorders: study protocol for a randomized controlled trial." *Trials* 17, no. 1 (2016): 1-8.
32. Witkiewitz, Katie, Elena R. Stein, Victoria R. Votaw, Adam D. Wilson, Corey R. Roos, Stevi J. Gallegos, Vincent P. Clark, and Eric D. Claus. "Mindfulness-based relapse prevention and transcranial direct current stimulation to reduce heavy drinking: A double-blind sham-controlled randomized trial." *Alcoholism: Clinical and Experimental Research* 43, no. 6 (2019): 1296-1307.
33. Klauss, Jaisa, Quézia S. Anders, Luna V. Felipe, Michael A. Nitsche, and Ester M. Nakamura-Palacios. "Multiple sessions of transcranial direct current stimulation (tDCS) reduced craving and relapses for alcohol use: a randomized placebo-controlled trial in alcohol use disorder." *Frontiers in pharmacology* 9 (2018): 716.
34. Kim, Hyun Joon, and Nyeonju Kang. "Bilateral transcranial direct current stimulation attenuated symptoms of alcohol use disorder: A systematic review and meta-analysis." *Progress in Neuro-Psychopharmacology and Biological Psychiatry* 108 (2021): 110160.
35. Bronstein, Jeff M., Michele Tagliati, Ron L. Alterman, Andres M. Lozano, Jens Volkmann, Alessandro Stefani, Fay B. Horak et al. "Deep brain stimulation for Parkinson disease: an

- expert consensus and review of key issues." *Archives of neurology* 68, no. 2 (2011): 165-165.
36. Parasuraman, Raja, James Christensen, and Scott Grafton. "Neuroergonomics: The brain in action and at work." *Neuroimage* 59, no. 1 (2011): 1-3.
 37. Rezayat, Ehsan, and Iman Ghodrati Toostani. "A review on brain stimulation using low intensity focused ultrasound." *Basic and clinical neuroscience* 7, no. 3 (2016): 187.
 38. Pounder, Neill M., and Andrew J. Harrison. "Low intensity pulsed ultrasound for fracture healing: a review of the clinical evidence and the associated biological mechanism of action." *Ultrasonics* 48, no. 4 (2008): 330-338.
 39. Best, Thomas M., Kevin E. Wilk, Claude T. Moorman, and David O. Draper. "Low intensity ultrasound for promoting soft tissue healing: a systematic review of the literature and medical technology." *Internal medicine review (Washington, DC: Online)* 2, no. 11 (2016).
 40. Tyler, William J., Yusuf Tufail, Michael Finsterwald, Monica L. Tauchmann, Emily J. Olson, and Cassondra Majestic. "Remote excitation of neuronal circuits using low-intensity, low-frequency ultrasound." *PloS one* 3, no. 10 (2008): e3511.
 41. Li, Xin, Huifang Yang, Jiaqing Yan, Xingran Wang, Yi Yuan, and Xiaoli Li. "Seizure control by low-intensity ultrasound in mice with temporal lobe epilepsy." *Epilepsy research* 154 (2019): 1-7.
 42. Deveci, Erdem, Alperen Kılıç, Onur Yılmaz, Aynur Nabi, Arif Sanlı Ergün, Ayhan Bozkurt, Ayşe Kurtulmuş et al. "The effects of focused ultrasound pulsation of nucleus accumbens in opioid-dependent rats." *Psychiatry and Clinical Psychopharmacology* 29, no. 4 (2019): 748-759.
 43. Attia, Amalina Binte Ebrahim, Ghayathri Balasundaram, Mohesh Moothanchery, U. S. Dinish, Renzhe Bi, Vasilis Ntziachristos, and Malini Olivo. "A review of clinical photoacoustic imaging: Current and future trends." *Photoacoustics* 16 (2019): 100144.
 44. Zhao, Hongzhi, Xuejun Gu, and Huabei Jiang. "Model-based ultrasound tomography: Tissue phantom experiments." *Medical physics* 32, no. 8 (2005): 2659-2664.
 45. Xu, Minghua, and Lihong V. Wang. "Photoacoustic imaging in biomedicine." *Review of scientific instruments* 77, no. 4 (2006): 041101.
 46. Rosenthal, Amir, Vasilis Ntziachristos, and Daniel Razansky. "Acoustic inversion in optoacoustic tomography: A review." *Current Medical Imaging* 9, no. 4 (2013): 318-336.
 47. Wang, Bo, Liangzhong Xiang, Max S. Jiang, Jianjun Yang, Qizhi Zhang, Paul R. Carney, and Huabei Jiang. "Photoacoustic tomography system for noninvasive real-time three-dimensional imaging of epilepsy." *Biomedical optics express* 3, no. 6 (2012): 1427-1432.

48. Ntziachristos, Vasilis, and Daniel Razansky. "Molecular imaging by means of multispectral optoacoustic tomography (MSOT)." *Chemical reviews* 110, no. 5 (2010): 2783-2794.
49. Soares-Cunha, Carina, Nivaldo AP de Vasconcelos, Bárbara Coimbra, Ana Verónica Domingues, Joana M. Silva, Eduardo Loureiro-Campos, Rita Gaspar, Ioannis Sotiropoulos, Nuno Sousa, and Ana João Rodrigues. "Nucleus accumbens medium spiny neurons subtypes signal both reward and aversion." *Molecular psychiatry* 25, no. 12 (2020): 3241-3255.
50. Sneddon, Elizabeth A., Kristen M. Schuh, John W. Frankel, and Anna K. Radke. "The contribution of medium spiny neuron subtypes in the nucleus accumbens core to compulsive-like ethanol drinking." *Neuropharmacology* 187 (2021): 108497.
51. Spiga, S., G. Mulas, F. Piras, and M. Diana. "The "addicted" spine. *Front Neuroanat* 8: 110." (2014).
52. Spigelman, Igor, and Vincent N. Marty. "Long-lasting alterations in membrane properties, K⁺ currents, and glutamatergic synaptic currents of nucleus accumbens medium spiny neurons in a rat model of alcohol dependence." *Frontiers in neuroscience* 6 (2012): 86.
53. Gonzales, Rueben A., Martin O. Job, and William M. Doyon. "The role of mesolimbic dopamine in the development and maintenance of ethanol reinforcement." *Pharmacology & therapeutics* 103, no. 2 (2004): 121-146.
54. Volkow, N.D., et al., *Brain DA D2 receptors predict reinforcing effects of stimulants in humans: replication study*. *Synapse*, 2002. 46(2): p. 79-82.
55. Koob, G.F., *The neurobiology of addiction: a neuroadaptational view relevant for diagnosis*. *Addiction*, 2006. 101 Suppl 1: p. 23-30.
56. Koob, G.F. and M. Le Moal, *Drug abuse: hedonic homeostatic dysregulation*. *Science*, 1997. 278(5335): p. 52-8.
57. Morzorati, S.L. and R.L. Marunde, *Comparison of VTA dopamine neuron activity in lines of rats selectively bred to prefer or avoid alcohol*. *Alcohol Clin Exp Res*, 2006. 30(6): p. 991-7.
58. Morzorati, S.L., *VTA dopamine neuron activity distinguishes alcohol-preferring (P) rats from Wistar rats*. *Alcohol Clin Exp Res*, 1998. 22(4): p. 854-7.
59. Peck, Tom, Adrian Wong, and Emma Norman. "Anaesthetic implications of psychoactive drugs." *Continuing Education in Anaesthesia, Critical Care & Pain* 10, no. 6 (2010): 177-
60. Walker, Jennifer L., Brendan M. Walker, Fernanda Monjaraz Fuentes, and David M. Rector. "Rat psychomotor vigilance task with fast response times using a conditioned lick behavior." *Behavioural brain research* 216, no. 1 (2011): 229-237.

61. National Research Council. "Guide for the care and use of laboratory animals." (2010).
62. Mogenson, Gordon J., Douglas L. Jones, and Chi Yiu Yim. "From motivation to action: functional interface between the limbic system and the motor system." *Progress in neurobiology* 14, no. 2-3 (1980): 69-97.
63. Volkow, Nora D., Roy A. Wise, and Ruben Baler. "The dopamine motive system: implications for drug and food addiction." *Nature Reviews Neuroscience* 18, no. 12 (2017): 741-752.
64. Di Chiara, Gaetano, and Assunta Imperato. "Drugs abused by humans preferentially increase synaptic dopamine concentrations in the mesolimbic system of freely moving rats." *Proceedings of the National Academy of Sciences* 85, no. 14 (1988): 5274-5278.
65. Koob, George F., Pietro Paolo Sanna, and Floyd E. Bloom. "Neuroscience of addiction." *Neuron* 21, no. 3 (1998): 467-476.
66. Nestler, Eric J. "The neurobiology of cocaine addiction." *Science & practice perspectives* 3, no. 1 (2005): 4.
67. Vengeliene, V., A. Bilbao, A. Molander, and R. Spanagel. "Neuropharmacology of alcohol addiction." *British journal of pharmacology* 154, no. 2 (2008): 299-315.
68. Collingridge, Graham L., Richard W. Olsen, John Peters, and Michael Spedding. "A nomenclature for ligand-gated ion channels." *Neuropharmacology* 56, no. 1 (2009): 2-5.
69. Aguayo, Luis G., Robert W. Peoples, Hermes H. Yeh, and Gonzalo E. Yevenes. "GABA-A receptors as molecular sites of ethanol action. Direct or indirect actions?" *Current topics in medicinal chemistry* 2, no. 8 (2002): 869-885.
70. Nelson, A.M., G.A. Larson, and N.R. Zahniser, *Low or high cocaine responding rats differ in striatal extracellular dopamine levels and dopamine transporter number*. *J Pharmacol Exp Ther*, 2009. 331(3): p. 985-97.
71. You, Z.B., Y.Q. Chen, and R.A. Wise, *Dopamine and glutamate release in the nucleus accumbens and ventral tegmental area of rat following lateral hypothalamic self-stimulation*. *Neuroscience*, 2001. 107(4): p. 629-39.
72. Diana, M., M. Melis, and G.L. Gessa, *Increase in meso-prefrontal dopaminergic activity after stimulation of CB1 receptors by cannabinoids*. *Eur J Neurosci*, 1998. 10(9): p. 2825-30.
73. Hertel, P., et al., *Effects of D-amphetamine and phencyclidine on behavior and extracellular concentrations of neurotensin and dopamine in the ventral striatum and the medial prefrontal cortex of the rat*. *Behav Brain Res*, 1995. 72(1-2): p. 103-14.

74. Tanda, G., F.E. Pontieri, and G. Di Chiara, *Cannabinoid and heroin activation of mesolimbic dopamine transmission by a common mu1 opioid receptor mechanism.* *Science*, 1997. 276(5321): p. 2048-50.
75. Cami, J. and M. Farre, *Drug addiction.* *N Engl J Med*, 2003. 349(10): p. 975-86.
76. Vengeliene, V., et al., *Neuropharmacology of alcohol addiction.* *Br J Pharmacol*, 2008. 154(2): p. 299-315.
77. Kauer, Julie A., and Robert C. Malenka. "Synaptic plasticity and addiction." *Nature reviews neuroscience* 8, no. 11 (2007): 844-858.
78. Heilig, Markus, Mark Egli, John C. Crabbe, and Howard C. Becker. "Acute withdrawal, protracted abstinence and negative affect in alcoholism: are they linked?" *Addiction biology* 15, no. 2 (2010): 169-184.
79. Eckardt, Michael J., Sandra E. File, Gian Luigi Gessa, Kathleen A. Grant, Consuelo Guerri, Paula L. Hoffman, Harold Kalant, George F. Koob, Ting-Kai Li, and Boris Tabakoff. "Effects of moderate alcohol consumption on the central nervous system." *Alcoholism: Clinical and Experimental Research* 22, no. 5 (1998): 998-1040.
80. Grobin, A. Chistina, Douglas B. Matthews, Leslie L. Devaud, and A. Leslie Morrow. "The role of GABAA receptors in the acute and chronic effects of ethanol." *Psychopharmacology* 139, no. 1 (1998): 2-19.
81. Kumar, Ashok, and Thomas C. Foster. "Enhanced long-term potentiation during aging is masked by processes involving intracellular calcium stores." *Journal of neurophysiology* 91, no. 6 (2004): 2437-2444.
82. Kumar, Ashok, Karthik Bodhinathan, and Thomas C. Foster. "Susceptibility to calcium dysregulation during brain aging." *Frontiers in aging neuroscience* 1 (2009): 2.
83. Tsui, Po-Hsiang, Shyh-Hau Wang, and Chih-Chung Huang. "In vitro effects of ultrasound with different energies on the conduction properties of neural tissue." *Ultrasonics* 43, no. 7 (2005): 560-565.
84. O'Brien Jr, William D. "Ultrasound–biophysics mechanisms." *Progress in biophysics and molecular biology* 93, no. 1-3 (2007): 212-255.
85. Bystritsky, Alexander, Alex S. Korb, Pamela K. Douglas, Mark S. Cohen, William P. Melega, Amit P. Mulgaonkar, Antonio DeSalles, Byoung-Kyong Min, and Seung-Schik Yoo. "A review of low-intensity focused ultrasound pulsation." *Brain stimulation* 4, no. 3 (2011): 125-136.
86. Jolesz, Ferenc A. "MRI-guided focused ultrasound surgery." *Annual review of medicine* 60 (2009): 417-430.

87. Dalecki, Diane. "Mechanical bioeffects of ultrasound." *Annu. Rev. Biomed. Eng.* 6 (2004): 229-248.
88. Johns, Lennart D. "Nonthermal effects of therapeutic ultrasound: the frequency resonance hypothesis." *Journal of athletic training* 37, no. 3 (2002): 293.
89. Morris, Catherine E., and Peter F. Juranka. "Nav channel mechanosensitivity: activation and inactivation accelerate reversibly with stretch." *Biophysical journal* 93, no. 3 (2007):
90. Tyler, William J., Yusuf Tufail, Michael Finsterwald, Monica L. Tauchmann, Emily J. Olson, and Cassondra Majestic. "Remote excitation of neuronal circuits using low-intensity, low-frequency ultrasound." *PloS one* 3, no. 10 (2008): e3511.
91. Yoo, Sangjin, David R. Mittelstein, Robert Hurt, Jerome Lacroix, and Mikhail G. Shapiro. "Focused ultrasound excites neurons via mechanosensitive calcium accumulation and ion channel amplification." (2020).
92. Rezayat, Ehsan, and Iman Ghodrati Toostani. "A review on brain stimulation using low intensity focused ultrasound." *Basic and clinical neuroscience* 7, no. 3 (2016): 187.
93. Oberlin, Brandon, Christina Best, Liana Matson, Angela Henderson, and Nicholas Grahame. "Derivation and characterization of replicate high-and low-alcohol preferring lines of mice and a high-drinking crossed HAP line." *Behavior genetics* 41, no. 2 (2011):
94. Matson, Liana M., Chelsea R. Kasten, Stephen L. Boehm, and Nicholas J. Grahame. "Selectively bred crossed high-alcohol-preferring mice drink to intoxication and develop functional tolerance, but not locomotor sensitization during free-choice ethanol access." *Alcoholism: Clinical and Experimental Research* 38, no. 1 (2014): 267-274.
95. Matson, Liana M., and Nicholas J. Grahame. "Pharmacologically relevant intake during chronic, free-choice drinking rhythms in selectively bred high alcohol-preferring mice." *Addiction biology* 18, no. 6 (2013): 921-929.
96. Grahame, Nicholas J., T-K. Li, and Lawrence Lumeng. "Selective breeding for high and low alcohol preference in mice." *Behavior genetics* 29, no. 1 (1999): 47-57.
97. Mulligan, Megan K., Igor Ponomarev, Robert J. Hitzemann, John K. Belknap, Boris Tabakoff, R. Adron Harris, John C. Crabbe et al. "Toward understanding the genetics of alcohol drinking through transcriptome meta-analysis." *Proceedings of the National Academy of Sciences* 103, no. 16 (2006): 6368-6373.

Chapter 6: Conclusion

In this dissertation, we have demonstrated the structural and functional imaging capabilities of photoacoustic imaging and the possibility of using it for guided imaging in small animals. Due to the thickness of the human skull and the significant skull-induced acoustic aberration effects (Figure 6.1), significant modelling is required to account for the losses in optical and acoustic energy at the human skull before this technology can be translated to humans.

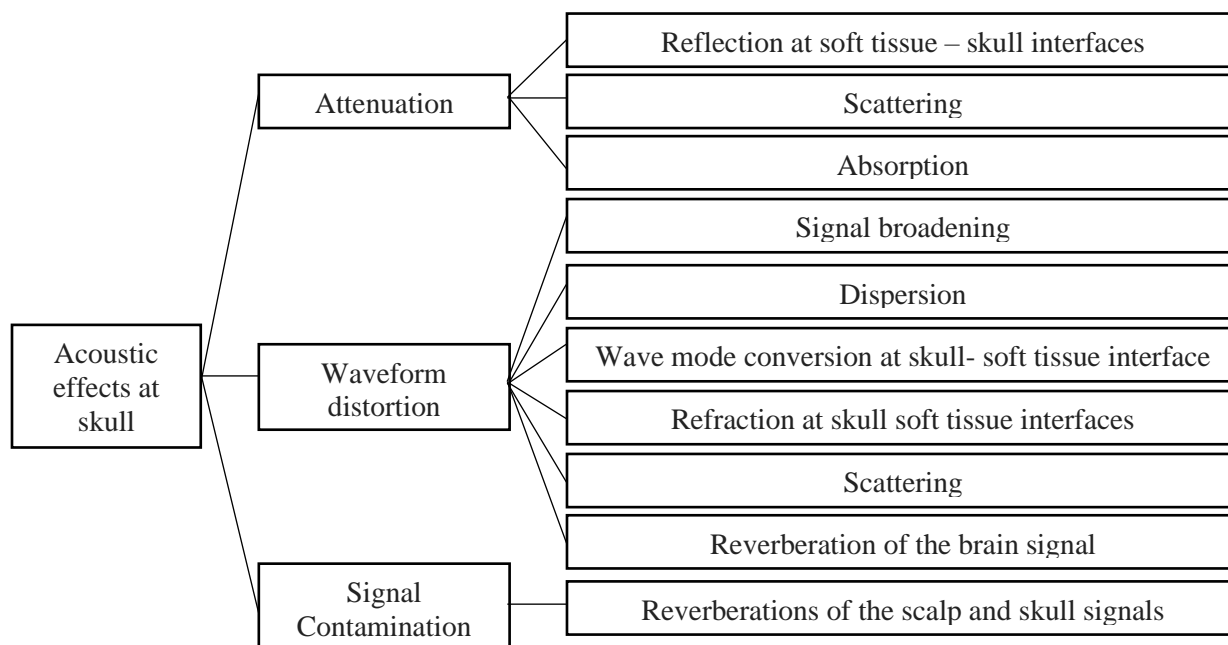


Figure 6.1 Acoustic effects of the skull

In the first part of the dissertation, we observed significant ethanol tolerance due to repeated binge drinking in HAPs, which resulted in the accumulation of the high blood ethanol concentration values (Figure 5.1). Such significant tolerance was not observed in the LAPs which did not repeatedly binge drink. We equally noted the response to a 20% v/v (3g/kg) ethanol binge

by both species. While both show cerebrovascular constriction and a drop in hemoglobin oxygen saturation, the response is more drastic in the LAPs, compared to the HAPs. These observations are quite significant. Current clinical diagnostic criteria for alcohol use disorder generally ignore alcohol tolerance. But as observed, repeated binge drinking results in tolerance and the drinker may need to consume huge amounts of alcohol thereby accumulating dangerously high and potentially fatal levels of blood alcohol concentration. Thus, this finding demonstrates the potential health benefits of identifying and intervening with individuals who binge drink and report tolerance, while they do not meet current AUD diagnostic criteria. We there propose the inclusion of questions related to tolerance as a key condition in AUD diagnosis.

The photoacoustic imaging guided system for low intensity focused ultrasound developed in the second part of this dissertation, though applied to the treatment of alcohol use disorder, can potentially be used in any situation requiring the noninvasive guided delivery of ultrasound or other substances to any deep brain region in small animals.

Appendix A: Copyright Permissions

The permission below is for the use of materials in Chapter 1 through Chapter 5. Some of the drawings were done in Biorender, with an academic subscription, which comes with publishing rights. Biorender is appropriately cites in these figures (Created with BioRender.com). The second permission is to reproduce materials published in Alcohol Elsevier journal.



Licensing and Usage

	Basic (Free) Account*	Academic Subscription	Industry Subscription
Educational Uses:			
Academic poster	✓	✓	✓
Thesis/dissertation (unpublished)	✓	✓	✓
Internal meetings (lab or team)	✓	✓	✓
Conference presentation	✓	✓	✓
Assignment/exam	✓	✓	✓
Teaching slides	✓	✓	✓
Personal blog/website posts	✓	✓	✓
Personal social media posts	✓	✓	✓
Publishing Uses:			
Journal publication		✓	✓
Textbook publication (< 5 figures)		✓	✓
Published thesis		✓	✓
Commercial Uses:			
Any uses that generate profit			✓
Textbook publication (5+ figures)			✓
Trade show materials (e.g. brochures)			✓
Information packages/user guides			✓

*Watermark must be included in exported figure
 *Free trial on a premium plan recommended for print uses
 For use cases not listed here, please go to biorender.com/contact

Conditions for Publication rights:

1. The figure was exported under a **paid subscription**.
2. Citation of "Created with BioRender.com" appears somewhere in the publication.



Photoacoustic imaging for in vivo quantification of alcohol-induced structural and functional changes in cerebral vasculature in high alcohol-preferring mice (HAP)

Author: Augustine Meombe Mbolle, Hao Yang, Huabei Jiang

Publication: Alcohol

Publisher: Elsevier

Date: May 2022

Published by Elsevier Inc.

Journal Author Rights

Please note that, as the author of this Elsevier article, you retain the right to include it in a thesis or dissertation, provided it is not published commercially. Permission is not required, but please ensure that you reference the journal as the original source. For more information on this and on your other retained rights, please visit: <https://www.elsevier.com/about/our-business/policies/copyright#Author-rights>

BACK

CLOSE WINDOW

Appendix B: Ethanol and Water Consumption for LIFU Group

Table B1 Week 1 drinking data

Wt of Feeding bottle = 60.0 g		7/2/2021		ETHANOL GROUP - Received actual LIFU to VTA												
Wt of bottle filled with water = 110.0 g																
Wt of bottle filled with 10% ethanol solution = 110.2g																
														Refill ethanol		
Week 1														Re-weigh		
CHAP COD	Weight	H2O wt/g	EtOH wt/g	H2O wt/g	EtOH wt/g	H2O wt/g	EtOH wt/g	Weight	H2O wt/g	EtOH wt/g	H2O wt/g	EtOH wt/g	H2O wt/g	EtOH wt/g	H2O wt/g	EtOH wt/g
M 8436	33.77	109.94	103.21	109.89	96.19	109.83	89.42	33.87	109.77	82.66	109.75	75.66	109.73	103.29	109.69	95.88
M 8824	33.80	109.94	103.12	109.90	95.72	109.85	89.13	33.89	109.81	82.33	109.77	75.24	109.73	103.31	109.7	96.43
M 8632	33.79	109.94	103.3	109.89	96.4	109.83	89.61	33.91	109.76	82.73	109.74	75.93	109.7	103.26	109.69	95.86
F 82719	33.76	109.99	102.83	109.97	95.49	109.93	88.25	33.96	109.87	81.02	109.85	73.6	109.81	102.76	109.77	95.48
F 86312	33.83	109.98	102.89	109.95	95.51	109.92	88.21	34.05	109.85	80.98	109.82	73.78	109.79	102.74	109.74	95.54
Water/ethanol g/kg/day																
	1.924785	20.69885	1.3325437	20.78768	1.776725	20.04738	1.771479	19.95867	0.590493	20.66726	0.590493	20.40154	1.180986	21.87777		
	1.775148	20.94675	1.183432	21.89349	1.47929	19.49704	1.180289	20.06492	1.180289	20.92063	1.180289	20.33048	0.885217	20.30097		
	1.775673	20.42024	1.5685114	20.42024	1.68689	20.0947	2.064288	20.289	0.589797	20.05308	1.179593	20.46594	0.294898	21.82247		
	0.296209	21.83057	0.7405213	21.74171	1.03673	21.4455	1.766784	21.28975	0.588928	21.84923	1.177856	21.90813	1.177856	21.43698		
	0.591156	21.60676	0.8571766	21.81367	1.064081	21.57721	1.908957	21.23348	0.881057	21.14537	0.881057	21.90896	1.468429	21.14537		
	1.272594	21.10063	1.136437	21.33136	1.408743	20.53237	1.73836	20.56716	0.766113	20.92711	1.001858	21.00301	1.001477	21.31671		
	0.766272	0.599379	0.3398861	0.678734	0.344579	0.925224	0.334918	0.64537	0.263666	0.657542	0.263731	0.828023	0.445575	0.641507		

Table B2 Week 2 and 3 drinking data

		Week 2			refill alcohol bottle and reverse ethanol and water											
CHAP COD	Weight	H2O wt/g	EtOH wt/g	H2O wt/g	EtOH wt/g	H2O wt/g	EtOH wt/g	Weight	H2O wt/g	EtOH wt/g	H2O wt/g	EtOH wt/g	H2O wt/g	EtOH wt/g	H2O wt/g	EtOH wt/g
M 8436	33.9	109.62	89.34	109.56	103.77	109.49	97.45	33.98	109.40	91.35	109.31	85.44	109.22	79.62	109.13	73.81
M 8824	33.91	109.63	89.75	109.56	103.58	109.49	96.98	34.00	109.40	91.14	109.31	85.41	109.22	79.53	109.13	73.71
M 8632	33.93	109.63	89.20	109.57	103.67	109.52	97.14	34.01	109.42	91.06	109.32	85.33	109.24	79.83	109.16	74.36
F 82719	33.99	109.70	88.72	109.64	103.65	109.58	96.89	34.08	109.46	90.23	109.37	83.57	109.27	77.02	109.18	70.85
F 86312	34.09	109.68	88.88	109.63	103.55	109.57	96.54	34.16	109.46	89.56	109.36	83.01	109.26	76.58	109.16	70.31
		Water/ethanol g/kg/day														
		2.064897	19.29204	1.8879056	18.96755	1.946903	18.64307		2.678046	17.95174	2.619188	17.39258	2.648617	17.12772	2.648617	17.09829
		1.975818	19.6992	2.1527573	19.52226	2.064288	19.46329		2.647059	17.17647	2.764706	16.85294	2.529412	17.29412	2.764706	17.11765
		1.915709	19.62865	1.6209844	19.24551	1.591512	19.24551		2.969715	17.87709	2.793296	16.84799	2.499265	16.17171	2.205234	16.0835
		2.059429	19.8882	1.7652251	19.27037	1.765225	19.8882		3.403756	19.54225	2.90493	19.54225	2.787559	19.21948	2.640845	18.10446
		1.818715	19.53652	1.4080375	19.50719	1.760047	20.56322		3.220141	20.43326	2.9274	19.17447	2.9274	18.82319	2.9274	18.3548
		1.966914	19.60892	1.766982	19.30258	1.825595	19.56066		2.983743	18.59616	2.801904	17.96205	2.678451	17.72724	2.63736	17.35174
		0.10347	0.219201	0.2800021	0.227302	0.183321	0.718189		0.331398	1.343304	0.1237	1.300247	0.179646	1.264374	0.267961	0.908319

		Week 3					Refill & Re-weigh									
CHAP COD	Weight	H2O wt/g	EtOH wt/g	H2O wt/g	EtOH wt/g	H2O wt/g	EtOH wt/g	Weight	H2O wt/g	EtOH wt/g	H2O wt/g	EtOH wt/g	H2O wt/g	EtOH wt/g	H2O wt/g	EtOH wt/g
M 8436	34.07	109.04	68.01	108.94	62.26	108.84	104.81	34.13	108.73	99.41	108.64	94.14	108.54	88.9	108.42	83.69
M 8824	34.08	109.04	68.01	108.94	62.33	108.88	104.65	34.13	108.79	99.21	108.69	94.11	108.63	89.02	108.53	83.94
M 8632	34.09	109.07	68.92	108.98	63.53	108.89	104.61	34.15	108.80	99.03	108.71	93.81	108.62	88.61	108.52	83.48
F 82719	34.16	109.10	64.94	108.99	59.12	108.93	104.61	34.21	108.83	98.98	108.74	93.15	108.64	87.61	108.54	82.18
F 86312	34.21	109.07	64.13	108.97	57.99	108.95	104.12	34.25	108.85	98.05	108.76	92.25	108.66	86.56	108.57	81.01
		Water/ethanol g/kg/day														
		2.64162	17.02377	2.9351335	16.87702	2.935134	15.82037		3.164372	15.82186	2.842074	15.44096	2.783475	15.35306	3.515968	15.26516
		2.58216	16.72535	3.0223005	16.66667	1.61385	16.28521		2.783475	15.93906	2.783475	14.94287	1.757984	14.91357	2.929974	14.88427
		2.552068	15.95776	2.8160751	15.81109	2.464066	16.39777		2.72328	16.33968	2.781845	15.28551	2.489019	15.22694	2.928258	15.02196
		2.34192	17.30094	3.1615925	17.03747	1.814988	16.36417		2.923122	16.45718	2.63081	17.0418	2.923122	16.1941	2.923122	15.87255
		2.63081	18.06489	2.9231219	17.94797	0.584624	17.77258		2.919708	17.72263	2.773723	16.93431	2.773723	16.61314	2.627737	16.20438
		2.549716	17.01454	2.9716447	16.86804	1.882532	16.52802		2.902791	16.45608	2.762385	15.92909	2.545465	15.66016	2.985012	15.44966
		0.121717	0.772296	0.1289725	0.766931	0.89547	0.733565		0.169989	0.756182	0.078445	0.984085	0.467624	0.712855	0.323898	0.566806

Table B3 Week 4 drinking data

cHAP COD	Week4																			
	Weight	H2O wt/g	EtOH wt/g	H2O wt/g	EtOH wt/g	H2O wt/g	EtOH wt/g	Weight	H2O wt/g	EtOH wt/g	H2O wt/g	EtOH wt/g	H2O wt/g	EtOH wt/g	H2O wt/g	EtOH wt/g				
M 8436	34.19	108.31	78.53	108.22	73.4	108.11	105.11	34.13	108.02	100.06	107.91	95.14	107.80	90.32	107.7	85.58				
M 8824	34.2	108.43	78.96	108.36	74.01	108.25	105.26	34.13	108.16	100.41	108.06	95.61	107.96	90.83	107.86	85.94				
M 8632	34.23	108.43	78.38	108.34	73.53	108.23	105.41	34.15	108.14	100.71	108.05	96.11	107.92	91.55	107.81	87.01				
F 82719	34.26	108.45	76.94	108.37	71.78	108.27	105.09	34.21	108.16	100.01	108.07	95.07	107.97	90.61	107.87	86.18				
F 86312	34.31	108.47	75.56	108.38	70.19	108.28	104.88	34.25	108.19	99.95	108.07	95.21	107.98	90.51	107.89	86.03				
	Water/ethanol g/kg/day																			
	3.100322	15.09213		2.7493419	15.00439		3.12957	14.88739		2.871374	14.79637		3.076472	14.41547		3.222971	14.12247		2.929974	13.88808
	2.923977	14.5614		2.0467836	14.47368		3.099415	14.44444		2.754175	14.21037		2.929974	14.06387		2.929974	14.00527		2.929974	14.32757
	2.629273	14.89921		2.6292726	14.16886		3.213555	13.99357		2.781845	13.76281		2.635432	13.46999		3.660322	13.35286		3.221083	13.29429
	2.62697	15.2948		2.3350846	15.0613		2.860479	14.91535		3.420053	14.84946		2.63081	14.44022		2.776966	13.03712		2.923122	12.94943
	2.914602	15.88458		2.6231419	15.65141		2.914602	15.50568		2.773723	14.39416		3.240876	13.83942		2.744526	13.72263		2.627737	13.08029
	2.839029	15.14643		2.4767249	14.87193		3.043524	14.74929		2.920234	14.40263		2.902713	14.04579		3.066952	13.64807		2.926378	13.50793
	0.206257	0.493256		0.2845787	0.573129		0.149637	0.566308		0.283019	0.447518		0.269565	0.408261		0.381852	0.452388		0.209806	0.5824

Appendix C: IACUC Approvals

This appendix contains the USF Institutional Animal Care and Use Commission (IACUC) protocols under which the animal procedures in this dissertation were carried out. The various approval certificates and procedural changes are shown.



MEMORANDUM

TO: Hao Yang,

FROM: [REDACTED]
Farah Moulvi, MSPH, IACUC Coordinator
Institutional Animal Care & Use Committee
Research Integrity & Compliance

DATE: 5/5/2020

PROJECT TITLE: Non-invasive, in vivo imaging of alcohol relapse using Photoacoustic Tomography.

FUNDING SOURCE: USF department, institute, center, etc.

IACUC PROTOCOL #: R IS00005147

PROTOCOL STATUS: **APPROVED**

Your request for continuation of this study was received and will be reported to the Institutional Animal Care and Use Committee (IACUC). The IACUC acknowledges that this study is currently on going as previously approved. Please be advised that **continuation of this study is in effect for a one-year period beginning 7/31/2020:**

Please take note of the following:

• **IACUC approval is granted for a one-year period at the end of which, an annual renewal form must be submitted for years two (2) and three (3) of the protocol through the eIACUC system.** After three years all continuing studies must be completely re-described in a new electronic application and submitted to IACUC for review.

• **All modifications to the IACUC-Approved Protocol must be approved by the IACUC prior to initiating the modification.** Modifications can be submitted to the IACUC for review and approval as an Amendment or Procedural Change through the eIACUC system. These changes must be within the scope of the original research hypothesis, involve the original species and justified in writing. Any change in the IACUC-approved protocol that does not meet the latter definition is considered a major protocol change and requires the submission of a new application.

INSTITUTIONAL ANIMAL CARE AND USE COMMITTEE
PHS No. A4100-01, AAALAC No. 000434, USDA No. 58-R-0015
University of South Florida • 12901 Bruce B. Downs Blvd., MDC35 • Tampa, FL 33612-4799
(813) 974-7106 • FAX (813) 974-7091




UNIVERSITY OF
SOUTH FLORIDA
USF RESEARCH & INNOVATION

RESEARCH INTEGRITY & COMPLIANCE
INSTITUTIONAL ANIMAL CARE & USE COMMITTEE

MEMORANDUM

TO: Hao Yang,

FROM: 
Farah Moulvi, MSPH, IACUC Coordinator
Institutional Animal Care & Use Committee
Research Integrity & Compliance

DATE: 2/28/2020

PROJECT TITLE: Non-invasive, in vivo imaging of alcohol relapse using Photoacoustic Tomography.

FUNDING SOURCE: USF department, institute, center, etc.

IACUC PROTOCOL #: R IS00005147

PROTOCOL STATUS: **Procedural Change APPROVED**

The Institutional Animal Care and Use Committee (IACUC) received your Modification concerning the above referenced IACUC protocol.

On **2/28/2020** the IACUC reviewed and approved your Modification for the following:

Modifications: Characteristics of Animals and Pain Category of Research 5.1.1

Changed: Mouse: BALB/c (6-8 weeks/23-26g/male/female)

New Value: 100

Modifications: Statistical Analysis and Rationale 9.1

Changed: Mouse: BALB/c (6-8 weeks/23-26g/male/female)

New Value: 100


Modifications: Statistical Analysis and Rationale 9.1.1



RESEARCH INTEGRITY AND COMPLIANCE
INSTITUTIONAL ANIMAL CARE & USE COMMITTEE

MEMORANDUM

TO: Hao Yang,

FROM: 
Farah Moulvi, MSPH, IACUC Coordinator
Institutional Animal Care & Use Committee
Research Integrity & Compliance

DATE: 6/3/2019

PROJECT TITLE: Non-invasive, in vivo imaging of alcohol relapse using Photoacoustic Tomography.

FUNDING SOURCE: USF department, institute, center, etc.

IACUC PROTOCOL #: R IS00005147

PROTOCOL STATUS: **APPROVED**

Your request for continuation of this study was received and will be reported to the Institutional Animal Care and Use Committee (IACUC). The IACUC acknowledges that this study is currently on going as previously approved. Please be advised that **continuation of this study is in effect for a one-year period beginning 8/1/2019:**

Please take note of the following:

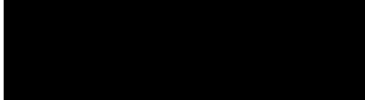
- **IACUC approval is granted for a one-year period at the end of which, an annual renewal form must be submitted for years two (2) and three (3) of the protocol through the eIACUC system.** After three years all continuing studies must be completely re-described in a new electronic application and submitted to IACUC for review.
- **All modifications to the IACUC-Approved Protocol must be approved by the IACUC prior to initiating the modification.** Modifications can be submitted to the IACUC for review and approval as an Amendment or Procedural Change through the eIACUC system. These changes must be within the scope of the original research hypothesis, involve the original species and justified in writing. Any change in the IACUC-approved protocol that does not meet the latter definition is considered a major protocol change and requires the submission of a new application.



RESEARCH INTEGRITY AND COMPLIANCE
INSTITUTIONAL ANIMAL CARE & USE COMMITTEE

MEMORANDUM

TO: Hao Yang,

FROM: 
Farah Moulvi, MSPH, IACUC Coordinator
Institutional Animal Care & Use Committee
Research Integrity & Compliance

DATE: 1/9/2019

PROJECT TITLE: Non-invasive, in vivo imaging of alcohol relapse using Photoacoustic Tomography.

FUNDING SOURCE: USF department, institute, center, etc.

IACUC PROTOCOL #: R IS00005147

PROTOCOL STATUS: **Procedural Change APPROVED**

The Institutional Animal Care and Use Committee (IACUC) received your Modification concerning the above referenced IACUC protocol.

On **1/9/2019** the IACUC reviewed and approved your Modification for the following:

Modifications: Characteristics of Animals and Pain Category of Research 5.1.1

Changed: Mouse: BALB/c (6-8 weeks/23-26g/male/female)

Modifications: Housing Facilities 6.2.1

Changed: ID00006537

New Value: PSY – Psychology

Modifications: Outside Housing and Use Sites 6.3.1

Added: ID00002284

New Value: Interdisciplinary Science Building (ISA)- 7030D- The photoacoustic system we have built is bulky and attached to specialized optical tables in our laboratory. It is therefore not convenient to move the system back and forth during the imaging experiment. It will be easier to transport the animal to the laboratory for imaging. After the experiment, the animal will be euthanized- Animals will be transported to the building by golf cart in sanitized, reinforced disposable shipping containers that completely conceals contents and contains filter protected ventilation openings

Modifications: Experimental Design 8.1.1